Differential Regulation of Dendritic Structures by NOMA-GAP

Dissertation to obtain the academic degree
Doctor rerum naturalium (Dr. rer. nat.)

submitted to the Department of Biology, Chemistry and Pharmacy
of the Freie Universität Berlin

by
Steffen Schuster
from Frankfurt an der Oder
2015

1st reviewer: Dr. Marta Rosário

2nd reviewer: Prof. Dr. Stephan Sigrist

Date of Disputation: 21.12.2015

In memory of Klaus-Jürgen, Evelin and Maik

Table of Contents

List of Figures

List of Acronyms

AMPAR	α-amino-3-hydroxy-5-methyl-4-isoxazole propionic acid receptor
ASD	Autism spectrum disorder
BDNF	brain-derived neurotrophic factor
CA	constitutively active
Cdc42	cell division cycle 42
DIV	days *in vitro*
DN	dominant negative
F-actin	filamentous actin
GAP	GTPase activating protein
GEF	guanine nucleotide exchange factor
GDI	guanine nucleotide exchange inhibitor
GDP	guanosine diphosphate
GK	guanylate kinase
GTP	guanosine triphosphate
IUE	*in utero* electroporation
LTD	long-term depression
LTP	long-term potentiation
MAGUK	membrane associated guanylate kinase
NLGN	neuroligins
NMDAR	N-methyl-D-aspartate receptor
NOMA-GAP	neurite outgrowth multiadaptor GTPase - activating protein
NLGN	neuroligin
NRXN	neurexin
NT-3	neurotrophin-3
PAK	p21 protein (Cdc42/Rac) activated kinase
PDZ	PSD-95, Dlg (disc large homolog), and ZO-1 (zona occludens or tight junctions))
PX	Phox
PSD	postsynaptic density
Rac1	Ras-related C3 botulinum toxin substrate 1
RhoA	Ras homologous member A
Trk	Tropomyosin receptor kinase
SH3	Src homology 3

Abstract

Dendritic structures are thought to determine the function of morphologically distinct and specialized neuronal subclasses. Abnormalities in dendritic structures are commonly associated with neuropsychiatric developmental disorders. However, little is known about the molecular mechanisms instructing layer- and compartment-specific maturation of dendrites. This work reveals that the Cdc42-specific GAP, NOMA-GAP, selectively regulates dendritic development of cortical pyramidal neurons. First, I show that NOMA-GAP is not required for the generation, migration, cell fate determination and axonal connectivity of excitatory neurons in the neocortex. After pyramidal neurons have reached their final position in the neocortex, NOMA-GAP initiates dendritic complexity of layer II-III pyramidal neurons, but not layer V pyramidal neurons. Furthermore, NOMA-GAP regulates the maturation of dendritic spines specifically in basal dendrites of layer II-III pyramidal neurons, but not in their apical dendrites. In addition, I show that NOMA-GAP directly interacts with several MAGUK family proteins and regulates the surface expression of AMPARs. Importantly, I provide evidence for a cross-regulation of NOMA-GAP and PSD-95 during development. NOMA-GAP regulates the subcellular localization and phosphorylation state of PSD-95, while PSD-95 inhibits Cdc42-GAP activity of NOMA-GAP. Finally, I show that NOMA-GAP regulates dendritic complexity and dendritic spine maturation respectively by a Cdc42-dependent and a Cdc42-independent mechanism. Loss of NOMA-GAP leads to hyperactivation of Cdc42 in the neocortex that reduces dendritic complexity of layer II-III neurons. Genetic reduction of post-mitotic Cdc42 levels partially restored dendritic complexity in NOMA-GAP-deficient mice. Moreover, NOMA-GAP mediates the inhibition of Cdc42 signaling that subsequently enables activation of the actin regulator cofilin. Remarkably, expression of a constitutively active cofilin mutant in NOMA-GAP-deficient neurons is sufficient to restores dendritic complexity in the neocortex. In contrast, reduction of post-mitotic Cdc42 levels fails to restore dendritic spine morphology. However, overexpression of a RhoGAP deletion mutant of NOMA-GAP restores dendritic spine morphology in NOMA-GAP-deficient mice. My findings demonstrate a critical role for NOMA-GAP in layer- and compartment-specific development of dendritic structures. NOMA-GAP specifies cortical upper layer connectivity by the combination of Cdc42-GAP-dependent and Cdc42-GAP-independent mechanisms that contributes to the establishment of cognitive circuits.

Kurzfassung

Es wird angenommen, dass dendritische Strukturen die Funktion von morphologisch unterscheidbaren neuronalen Unterklassen determinieren. Anomalien in den dendritischen Strukturen werden häufig mit neuropsychiatrischen Entwicklungsstörungen assoziiert. Allerdings ist wenig über die molekularen Mechanismen bekannt, die Schichten- und Kompartiment-spezifische Reifung von Dendriten instruieren. Diese Arbeit zeigt, dass die Cdc42-spezische GAP, NOMA-GAP, die dendritische Entwicklung in cortikalen Pyramidenzellen selektiv reguliert. Als erstes zeige ich, dass NOMA-GAP nicht für die Generierung, Migration, genetische Bestimmtheit und axonale Konnektivität von erregenden Neuronen im Neocortex erforderlich ist. Nachdem die Pyramidenzellen ihre finale Position im Neocortex erreicht haben, initiiert NOMA-GAP die dendritische Verzweigung spezifisch von Pyramidenzellen in Lamina II-III, aber nicht von Pyramidenzellen in Lamina V. Darüber hinaus reguliert NOMA-GAP die Reifung dendritischer Dornenfortsätze spezifisch in den basalen Dendriten von Pyramidenzellen in Lamina II-III, aber nicht in deren apikalen Dendriten. Außerdem zeige ich, dass NOMA-GAP direkt mit mehreren MAGUK Proteinen interagiert und die Oberflächenexpression von AMPARs reguliert. Interessanterweise ergeben sich Hinweise auf eine wechselseitige Regulierung von NOMA-GAP und PSD-95 während der Entwicklung. NOMA-GAP reguliert die subzelluläre Lokalisation und Phosphorylierung von PSD-95, während PSD-95 die Cdc42-GAP Aktivität von NOMA-GAP inhibiert. Schließlich zeige ich, dass NOMA-GAP die dendritische Komplexität und die Reifung von dendritischen Dornenfortsätzen durch einen Cdc42-abhängigen beziehungsweise Cdc42-unabhängigen Mechanismus reguliert. Der Verlust von NOMA-GAP führt zu einer Hyperaktivierung von Cdc42 im Neocortex, welche die dendritische Komplexität von Pyramidenzellen in Lamina II-III beeinträchtigt. Die genetische Reduktion der post-mitotischen Cdc42 Konzentration ermöglicht eine partielle Wiederherstellung der dendritischen Komplexität in NOMA-GAP-defizienten Mäusen. Zudem inhibiert NOMA-GAP die Cdc42 Signalkaskade, welche die Aktivierung des Aktin-Regulators cofilin ermöglicht. Bemerkenswerterweise ermöglicht die Expression von konstitutiv aktiven cofilin in NOMA-GAP-defizienten Neuronen die Wiederherstellung der dendritischen Komplexität im Neocortex. Im Gegensatz dazu führt nicht die genetische Reduktion des post-mitotischen Cdc42 Konzentration, sondern die Expression einer RhoGAP Deletionsmutante von NOMA-GAP zu einer Wiederherstellung der Morphologie von

dendritischen Dornenfortsätzen in NOMA-GAP-defizienten Mäusen. Meine Ergebnisse demonstrieren eine entscheidende Rolle von NOMA-GAP während der Typ-spezifischen Entwicklung dendritischer Strukturen. NOMA-GAP spezifiziert die Konnektivität von cortikalen Pyramidenzellen der oberen Schichten durch die Kombination von Cdc42-abhängigen und Cdc42-unabhängigen Mechanismen, die zur Etablierung von kognitiven Verbindungen beiträgt.

1 Introduction

1.1 Cortical Development

The mammalian six-layered neocortex is a network of billions of interconnected neurons that is thought to be responsible for higher cognitive abilities in humans. The generation and connectivity of cortical neurons is a tightly regulated developmental process, which is critical for receiving, processing and responding to complex stimuli. Disturbances in the pattern of connectivity are linked to neuropsychiatric developmental disorders like autism spectrum disorder (ASD) and schizophrenia (Penzes et al., 2011; Zoghbi and Bear, 2012).

The principal cell types in the neocortex are neurons that can be further classified into projection neurons and interneurons. Neocortical interneurons are GABAergic inhibitory neurons which are generated in the ganglionic eminences of the ventral telencephalon, before migrating tangentially into the neocortex (Marín, 2013). In contrast, projection neurons are glutamatergic excitatory neurons, which are sequentially generated from progenitors lining the dorsal part of the lateral ventricles (Greig et al., 2013; Rakic, 1972).

After neural tube closure, undifferentiated neuroepithelial cells form the telencephalic wall. Some of these neuroepithelial cells differentiate into radial glia cells and thereby establish the ventricular zone. Radial glia progenitors either divide symmetrically or asymmetrically (Lui et al., 2011). Symmetric divisions give rise to two progenitors to expand the progenitor pool. In contrast, asymmetric divisions give rise to a progenitor and a neuron. In addition to its progenitor function, radial glia cells provide a scaffold for neurons to migrate on. Radial glia cell processes span the cortex from the ventricular (apical) surface to the pial (basal) surface and the soma of Radial glia cells is located in the ventricular zone. Newborn neurons undergo axo-dendritic polarization and form a leading process and a trailing process (Polleux and Snider, 2010). The leading process faces the pial surface and attaches to the basal process of the clonally related radial glia cell (Valiente and Marín, 2010). Thus, neurons derived from radial glia cells establish radial units in the neocortex (Noctor et al., 2001).

The sequential birth of projection neurons builds the six-layered neocortex in an inside-out fashion. Early-born projection neurons occupy deep cortical layers V-VI and later-born neurons migrate past them to populate the upper cortical layers II-IV

(Molyneaux et al., 2007). Neurons in the different layers have different molecular and cellular characteristics as well as different targets. Deep layer neurons are predominantly corticofugal neurons that project from the neocortex to subcortical targets. Most layer VI neurons form cortico-thalamic connections, whereas layer V neurons form connections to basal ganglia, midbrain, hindbrain and spinal cord (Figure 1). Layer IV spiny stellate neurons project locally within a neocortical column and receive input from the thalamus. Layer II-III neurons are mostly intracortical neurons that project locally or to the contralateral hemisphere across the corpus callosom and receive input from other cortical areas (Franco and Müller, 2013). Layer I, the molecular layer, is a largely cell free layer. This is the only layer that develops outside the cortex. It consists mainly of apical dendrites from pyramidal neurons from deeper layers and axons. However, some Cajal-Retzius cells can be found here that secrete Reelin, which plays an pivotal role during neuronal migration (D'Arcangelo et al., 1995).

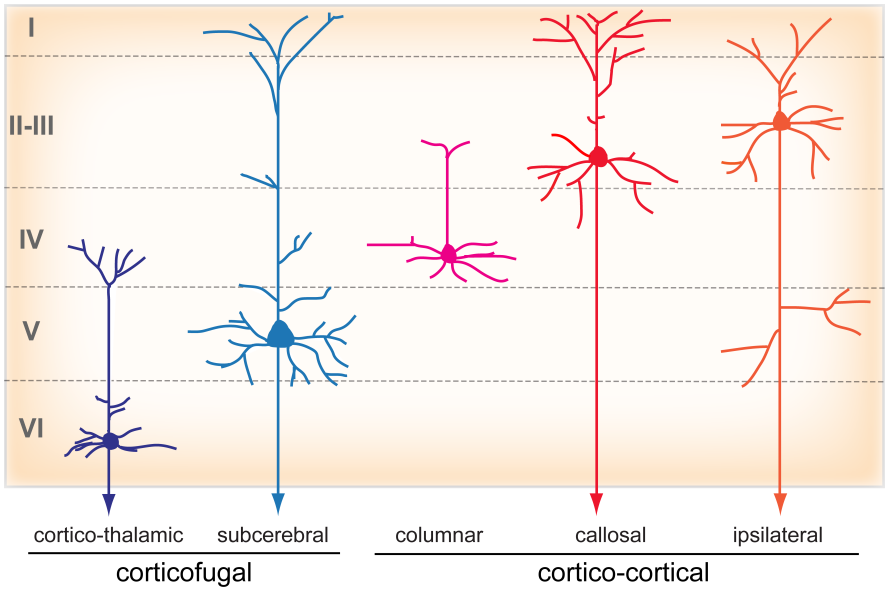

Figure 1: Neocortical projection neurons classified by their laminar position and projection pattern. Modified after Franco and Müller, 2013.

1.2 Dendritic Trees

Neurons are highly polarized cells that comprise axons and dendrites. The distinct axonal and dendritic compartments can be defined by functional as well as structural differences (Baas and Lin, 2011). Axons transmit information from one neuron to another and have unidirectional plus-end-distal microtubules. Dendrites receive and process incoming information and have both plus- and minus-end-distal microtubules.

Microtubules build the core of dendrites providing structural integrity, while filamentous actin (F-actin) is located in the periphery (Tahirovic and Bradke, 2009).

Different types of neurons show a distinctive and stereotyped dendritic branching pattern, which correlates with their function (Wong and Ghosh, 2002). The architecture of dendrites determines the extent and distribution of sensory or synaptic inputs on the neuron and are therefore critical for the establishment of neuronal networks (Parrish et al., 2007; Spruston, 2008). It is therefore important to understand how neurons acquire their type-specific dendritic morphology and cover their dendritic field. Pyramidal neurons are characterized by a distinct apical and basal dendritic tree, and by the pyramidal shape of the soma. However, there are considerable differences between pyramidal neurons (Figure 3). Cortical layer V pyramidal neurons, for example, have longer apical dendrites with fewer secondary dendrites than cortical layer II-III pyramidal neurons. The apical dendrites of hippocampal CA3 pyramidal neurons branch more proximal to the soma compared to those of hippocampal CA1 pyramidal neurons. The differences in dendritic patterning may reflect the requirement to receive and process information from different brain areas. The basal and proximal apical dendrite of layer II-III neurons receive local excitatory inputs and inputs from layer IV, whereas distal apical tufts receives inputs from more distant cortical and thalamic locations (Spruston, 2008).

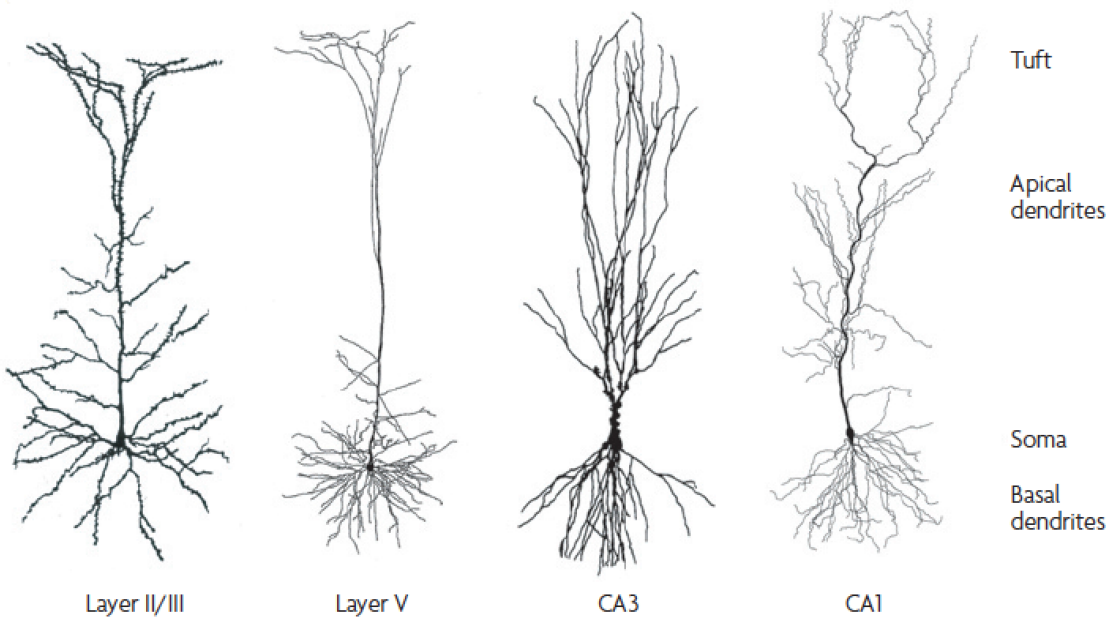

Figure 2: Morphology of pyramidal neurons from different cortical areas. Taken from Spruston, 2008.

During the migration of neocortical pyramidal neurons towards the pial surface the leading process becomes the apical dendrites and the trailing process the axon. The axon grows rapidly during migration while dendritic growth and branching is inhibited. After cortical projection neurons have reached their final position in the cortical plate the apical dendrite extends. Filopodia-like actin-rich protrusions that are prerequisite for the formation of neurites are formed *de novo* from the cell body to build primary basal dendrites (Dent et al., 2007). Dendrites can branch multiple times and consequently generate higher order dendrites. During this process, highly dynamic filopodial branches are continually added and retracted along the shaft of primary dendrites. Some of these newly formed filopodial branches stabilize and extend, building the basis for new dendritic branches (Dailey and Smith, 1996). Finally, dendrite growth is restrained by repulsive interaction between dendrites or molecular boundaries to enable non-redundant coverage of distinct areas (Puram and Bonni, 2013).

1.3 Dendritic Spines

Dendritic spines start to be formed along dendrites of pyramidal neurons during early postnatal stages (Yuste and Bonhoeffer, 2004). Ramón y Cajal first described dendritic spines in the late 19th century as small protrusions emerging from the dendritic shaft of a neuron that could form contact sites between neurons. Today it is known that dendritic spines receive most of the excitatory synaptic input on pyramidal neurons and many other principle neurons (Yuste, 2011). The primary function of dendritic spines is thought to compartmentalize local synaptic signaling pathways and to serve as a diffusion barrier for postsynaptic molecules (Newpher and Ehlers, 2008).

Dendritic spines emerge from the dendritic shaft via a thin neck and end with a bulbous enlargement, which is defined as the spine head. They differ in shape and size and can be classified into stubby, thin and mushroom spines (Yuste and Bonhoeffer, 2004) (Figure 3). Immature neurons possess more long filopodia-like protrusions whereas mature neurons show more mushroom-shaped spines (Dailey and Smith, 1996). Most spines are thought to arise from dendritic filopodia during early postnatal development, although *de novo* formation in adult mice has been observed (Holtmaat and Svoboda, 2009). Dendritic spines are highly dynamic structures, changing their morphology and appearance throughout the lifetime of the neuron. Thick mushroom shaped spines seem to be more stable than thinner spines and filopodia that have very short life spans (Trachtenberg et al., 2002). As the brain matures and thereby neuronal circuits are established, turnover rate decreases and more spines become stable over longer time-periods (Holtmaat and Svoboda, 2009).

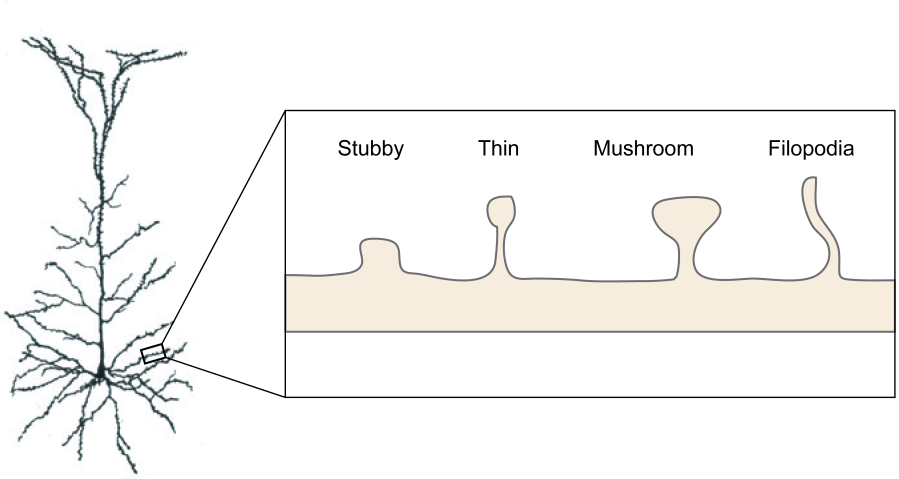

Figure 3: Different shapes of dendritic spines. Morphological classification into stubby, thin and mushroom shaped dendritic spines. In addition, filopodia can be found along dendritic segments. Modified after Spruston, 2008 and Yuste and Bonhoeffer, 2004

1.4 The Postsynaptic Density

Chemical synapses are highly specialized compartments within the neuron. They consist of a pre- and postsynaptic site separated by the intermediate synaptic cleft. Synapses are highly dynamic throughout the lifetime of a neuron. Dynamic changes in synaptic transmission, termed synaptic plasticity, are thought to underlie learning and memory. The precise apposition between the region of synaptic vesicle release, called active zone, and the postsynaptic receptor field is required for rapid and efficient synaptic transmission (Oliva et al., 2012). Inhibitory synapses are formed on the dendritic shaft, soma and axon initial segment, whereas excitatory synapses of pyramidal neurons are mainly formed at the tips of dendritic spine heads (Sheng and Kim, 2011). The morphological and functional specialization of the excitatory postsynaptic membrane is called the postsynaptic density (PSD), a specialized signaling domain composed of adhesion molecules, receptors, channels, structural proteins and signaling molecules (Figure 4).

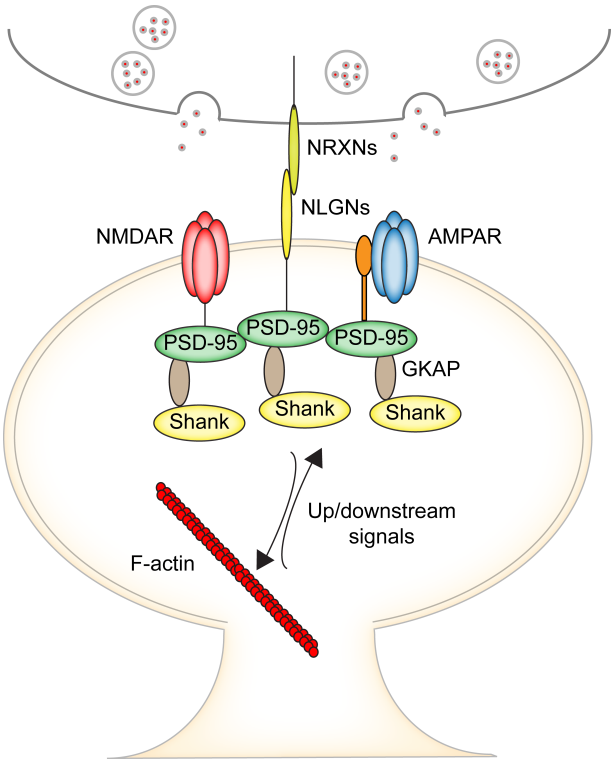

Figure 4: The postsynaptic density (PSD). The PSD contains adhesion molecules (e.g. Neuroligins (NLGNs)), receptors (e.g. AMPAR and NMDAR) and scaffold proteins (e.g. PSD-95 and Shank). Various signaling molecules connect the PSD with the actin cytoskeleton.

Synaptic cell adhesion molecules bridge presynaptic and postsynaptic neurons and are significantly involved in the formation, maturation and function of synaptic connections (Dalva et al., 2007). Postsynaptic neuroligins (NLGNs) and presynaptic neurexins (NRXNs) are the best characterized synaptic cell-adhesion molecules that mediate trans-synaptic signaling and modulate synaptic function of excitatory and inhibitory synapses (Südhof, 2008). The PDZ (**P**SD-95, **D**lg (disc large homolog), and **Z**O-1 (*zona occludens* or tight junction)) - interacting motif in NLGNs was shown to interact with PSD-95, which recruits ionotropic glutamate receptors (Irie et al., 1997).

The main neurotransmitter receptors at excitatory synapses in the mammalian brain are ionotropic and metabotropic glutamate receptors. The ionotropic glutamate receptors α-amino-3-hydroxy-5-methyl-4-isoxazole propionic acid (AMPA)-type receptors (AMPAR) and N-methyl-D-aspartate (NMDA)-type receptors (NMDAR) are essential for depolarization of the postsynaptic cell. AMPARs mediate the majority of fast excitatory postsynaptic current in the mammalian brain. They are tetrameric assemblies of four homologous subunits, namely GluR1-4 (also called GluA1-4). GluR1-4 consists of homologous extracellular and transmembrane regions, but vary in their intracellular C-terminal domains. The AMPAR composition is dynamic during development and differs between different brain regions (Schwenk et al., 2014). Native

AMPARs in the mammalian brain are macromolecular complexes assembled from the pore-forming units (GluR1-4), auxiliary subunits of the inner core (e.g. transmembrane AMPA receptor regulatory proteins) and constituents of the periphery (e.g. membrane associated guanylate kinases (MAGUKs)). The distinct composition of AMPAR complexes defines the function and trafficking. The number of AMPARs at the plasma membrane is dependent on relative rates of exocytosis and endocytosis (Anggono and Huganir, 2012). Enhanced AMPAR exocytosis occurs during synaptic activation whereas endocytosis is increased during synaptic depression (Collingridge et al., 2004). Exocytotic and endocytotic recycling of AMPARs occur mostly at extrasynaptic sites and travel into dendritic spines by lateral diffusion (Krugers et al., 2010; Lin et al., 2009). NMDARs are heterotetramers composed of two NR1, two NR2 subunits (NR2A-D), and occasionally an NR3 subunit (NR3A-B) (Newpher and Ehlers, 2008). The activity of NMDARs is dependent on glycine and glutamate binding to the NR1 and NR2 subunits respectively, but channel opening requires coincident postsynaptic depolarization to release the Mg^{2+} block in the channel pore. Thus, excitatory synapses solely comprising NMDAR remain silent synapses (Hanse et al., 2013). Influx of Ca^{2+} through NMDARs is essential for synaptic plasticity such as long-term potentiation (LTP) and long-term depression (LTD), a cellular mechanism involved in learning and memory (Bliss and Collingridge, 1993; Mayford et al., 2012). Each NMDAR subunit contains a large N-terminal extracellular domain, three membrane-spanning domains, a pore-lining region and an intracellular C-terminal domain. Like AMPARs, native NMDARs in the mammalian brain are organized in macromolecular complexes of synaptic scaffolding and adaptor proteins which links the receptors to downstream signaling proteins (Lau and Zukin, 2007). The subunit composition and localization of NMDARs affect channel activity and downstream signaling (Köhr, 2006). Each NR2 subunit has a different intracellular domain that can bind different sets of signaling proteins (Ryan and Grant, 2009). In addition, NR2 subunits affect electrophysiological properties of the NMDAR and show a developmentally and spatially restricted expression in the brain (Liu et al., 2004; Wenzel et al., 1997).

Scaffold proteins anchor the PSD at the postsynaptic membrane and orchestrate the assembly of postsynaptic signaling complexes at glutamatergic synapses. The main postsynaptic scaffold is formed by two groups of PDZ domain-containing proteins, those with proline-rich domains, such as Shank proteins and those with a guanylate kinase (GK) domain, called the MAGUKs. PDZ proteins often contain additional domains, which mediates binding to each other and to signaling molecules. The Shank family of proteins (Shank1-3) is a group of synaptic scaffold proteins that organize protein complex at the PSD of excitatory glutamatergic synapses (Jiang and Ehlers,

2013). Shank proteins directly bind guanylate kinase-associated protein (GKAP) to form the PSD-95-GKAP-Shank complex. MAGUKs are key scaffold proteins for receptors, adhesion proteins and various signaling proteins. They comprise *DLG1-4* or SAP97, PSD-93, SAP102 and PSD-95 as well as calcium/calmodulin-dependent protein kinase (CASK) and membrane associated guanylate kinase inverted (MAGI). MAGUKs contain PDZ, GK and various combinations of additional protein domains, like Src homology 3 (SH3), two tryptophan residues, MAGUK LIN2 + LIN7 (L27) and calcium/calmodulin-dependent proteins kinase (CaMK). During development, MAGUKs helps to organize the postsynaptic density via association with other scaffold proteins, such as Shank and Homer, and the actin cytoskeleton. MAGUKs cluster glutamate receptors and other receptors at the postsynaptic membrane. SAP97 and SAP102 are highly expressed in newborn rodents and then decrease, whereas PSD-93 and PSD-95 expression increases during postnatal development (Oliva et al., 2012). The switch from SAP102 to PSD-95 during synaptic development is associated with changes in NMDA receptor composition. Similar to the pattern of SAP102, NR2B is the dominant NR2 subunit in newborns, while PSD-95 has a similar pattern to NR2A (Sans et al., 2000). It has been shown, that PSD-95 directly binds to NR2 subunits (Kornau et al., 1995). However, there is supporting evidence that MAGUKs mainly regulate postsynaptic clustering and function of AMPAR (Béïque and Andrade, 2003; Béïque et al., 2006; El-Husseini et al., 2000).

1.5 Regulation of Dendritic Structures

Dendritic patterning is regulated by intrinsic and extrinsic factors as well as activity-dependent mechanisms (Jan and Jan, 2010). Cell-intrinsic mechanisms do not depend on external cues, although they may influence them. In this chapter, I want to describe how intrinsic and extrinsic signals can regulate the morphology of dendrites.

1.5.1 Transcriptional Regulators

Transcription factors can positively and negatively regulate distinct aspects of dendritic morphogenesis. The transcription factor Foxo6 induces the expression of p21 protein (Cdc42/Rac) activated kinase 1 (PAK1), which promotes axo-dendritic polarization and at later stages inhibits the growth of differentiated dendrites in the mammalian brain (De La Torre-Ubieta et al., 2010). The basic helix-loop-helix transcription factor NeuroD1 was shown to stimulate dendrite growth and branching (Gao et al., 2009; Gaudillière et al., 2004).

The layer-restricted expression of transcription factors has been shown to contribute to the distinct dendritic tree of pyramidal neurons. For example, the zinc finger transcription factor *Fezf2* is expressed in subcortical projection neurons of layer V and in cortico-thalamic projection neurons of layer VI (Chen et al., 2005). Knockdown and knockout experiments showed that *Fezf2* controls dendritic branching and dendritic spine number of layer V pyramidal neurons (Chen et al., 2008, 2005). The homeobox transcription factors *Cux1* and *Cux2* are expressed by layer II-III pyramidal neurons and control their dendritic growth and branching (Cubelos et al., 2010). In addition, Cux genes intrinsically regulate the number and differentiation of dendritic spines by binding and regulating the expression of the chromatin remodeling genes X-linked lymphocyte regulate (*Xlr*) *3b* and *Xlr4b* (Cubelos et al., 2010).

Several studies suggest that at least some transcription factors that mediate dendritic morphogenesis are evolutionarily conserved. The *Drosophila* transcription factor *Cut*, the invertebrate homolog of *Cux1* and *Cux2*, induces dendritic complexity of *Drosophila* sensory neurons (Grueber et al., 2003). Similarly, the zinc finger transcription factor *BTBD3* and the *Drosophila* homolog *Abrubt* control dendritic patterning (Li et al., 2004; Matsui et al., 2013; Sugimura et al., 2004).

1.5.2 Actin dynamics

Actin is one of the major components of the cellular scaffold that is essential for the architecture of cells. The formation, remodeling and stabilization of dendritic structures require dynamic assembly and disassembly of the actin cytoskeleton (Hotulainen and Hoogenraad, 2010; Simó and Cooper, 2012). Actin exists in two states, as monomeric globular actin (G-actin) and as an asymmetric two-stranded helical filament (F-actin) composed of G-actin (Cingolani and Goda, 2008). F-actin preferentially polymerizes at the barbed end of the filament while G-actin monomers are lost on the pointed end. Actin-binding proteins can modify actin-filament dynamics while others link F-actin to cytoskeletal networks (Pollard and Borisy, 2003)

Rho family of GTPases are key regulators of cytoskeletal dynamics and are required for the formation and maturation of dendritic structures (Govek et al., 2005; Newey et al., 2005). RhoGTPases cycle between an active guanosine triphosphate (GTP) bound state and an inactive guanosine diphosphate (GDP) bound state (Etienne-Manneville and Hall, 2002) (Figure 5). The cycling is mediated by Guanine nucleotide exchange factors (GEFs), which mediate the exchange of GDP to GTP and therefore activating RhoGTPases. On the other hand, GTPase activating proteins (GAPs) promote the hydrolysis of GTP to GDP and inactivate RhoGTPase. Guanine nucleotide exchange

inhibitors (GDIs) prevent activation of RhoGTPases and sequester inactive RhoGTPases in specific subcellular locations.

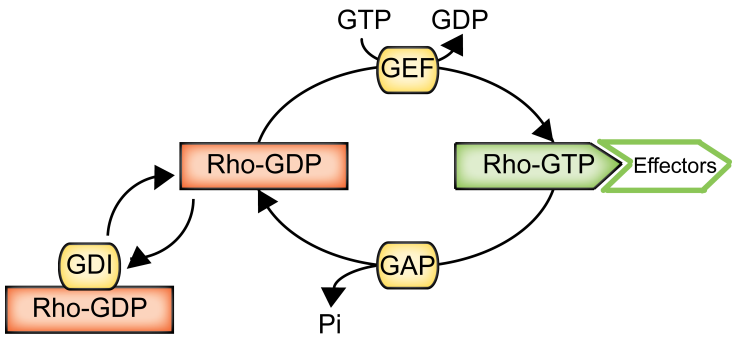

Figure 5: The RhoGTPAse cycle. RhoGTPases cycle between active GTP-bound and inactive GDP-bound conformations. In the active state, they interact with effectors. The cycle is highly regulated by three classes of protein. GEFs catalyze nucleotide exchange and mediate activation. GAPs stimulate GTP hydrolysis, leading to inactivation. GDIs prevent activation by RhoGEFs. Modified after Etienne-Manneville and Hall, 2002.

The most studied members of this large family of RhoGTPases are Ras homologous member A (RhoA), Ras-related C3 botulinum toxin substrate 1 (Rac1) and cell division cycle 42 (Cdc42). Studies using neuronal cell lines that can undergo initial steps of neuronal differentiation showed that Cdc42 and Rac1 commonly induce neurite growth and branching, while RhoA inhibits this process (Govek et al., 2005). Further, *in vivo* studies verified that Rac1 stimulates and RhoA inhibits dendrite growth and branching (Lee et al., 2000; Li et al., 2000; Luo et al., 1994; Ng et al., 2002; Ruchhoeft et al., 1999). However, the *in vivo* role of Cdc42 during dendritic development remained less clear and controversial. Overexpression of dominant-negative (DN) Cdc42 has been reported to reduce dendritic complexity in mouse cortical pyramidal neurons (Hayashi, 2002) and decrease the number and length of dendrites in *Xenopus* retinal ganglion cells (Hayashi, 2002). Loss of Cdc42 in *Drosophila* vertical system neurons has been shown to increase dendritic length but not the number of branch points (Scott et al., 2003). The overexpression of constitutively active (CA) Cdc42 increases the amount of dendritic branches in *Xenopus* optic tectal neurons (Li et al., 2000) and stimulates dendritic outgrowth in chick primary spinal neurons (Brown et al., 2000). In contrast, overexpression of CA-Cdc42 in *Drosophila* peripheral nervous system neurons was reported to lead to abnormal or absent dendrites, reduction in dendrite length on

mouse hippocampal pyramidal neurons and dendrite number and length in *Xenopus* retinal ganglion cells (Luo et al., 1994; Ruchhoeft et al., 1999; Tashiro et al., 2000).

The emergence and maintenance of dendritic spines is controlled by rearrangements of the actin cytoskeleton, of which RhoGTPases are prime regulators. Several studies indicate that Rac1 stimulates and RhoA inhibits dendritic spine formation and maintenance (Luo et al., 1996; Nakayama et al., 2000; Pilpel and Segal, 2004; Tashiro et al., 2000). The role of Cdc42 is again less clear. Tashiro and colleagues reported that overexpression of CA-Cdc42 or DN-Cdc42 does not have a significant effect on spine density or length in murine cortical pyramidal cells in organotypic slices (Tashiro et al., 2000). In contrast, Irie and Yamaguchi reported that overexpression of DN-Cdc42 in murine hippocampal neurons inhibits dendritic spine formation (Irie and Yamaguchi, 2002). Furthermore, they showed that Cdc42 is locally activated by the association of the EphB2 receptor with the Cdc42 specific GEF intersectin-1, resulting in the expansion of dendritic spine heads. Loss of Cdc42 in vertical system neurons in *Drosophila* was reported to reduce the number of dendritic spines (Scott et al., 2003).

1.5.3 Trafficking of cargo

The growth, stabilization and maintenance of dendritic structures are dependent on polarized trafficking of cargo into dendrites (Hanus and Ehlers, 2008). This process requires a highly orchestrated transport of cargo over long distances. Golgi outposts are compartmentalized Golgi organelles that localize selectively to dendritic branch points of apical dendrites and are excluded from axons (Horton and Ehlers, 2003; Horton et al., 2005). Local laser damaging of Golgi outposts was shown to reduce dendritic branch dynamics in *Drosophila* neurons (Ye et al., 2007). Another study suggests that Golgi outpost function in addition as an acentrosomal microtubules nucleation site within dendritic arbors (Ori-McKenney et al., 2012).

The endoplasmatic reticulum exists as a continuous network in dendrites (Spacek and Harris, 1997). Membrane proteins rapidly diffuse within this continuous network but are confined by increased endoplasmatic reticulum complexity at dendritic branch points (Cui-Wang et al., 2012). This indicates that local endoplasmatic reticulum complexity spatially scales secretory trafficking within dendrites.

The vesicular transport of cargo along microtubules is essential for dendritic development and function (Hirokawa et al., 2010). The dynein superfamily proteins mediate the retrograde minus-end-directed transport, while kinesin superfamily proteins (Kifs) mediate the anterograde plus-end-directed transport (Poulain and Sobel, 2010). The glutamate receptor interacting protein 1 (GRIP1) promotes dendritic complexity by

serving as an adaptor protein for the kinesin-dependent transport of dendritic cargo (Geiger et al., 2014; Hoogenraad et al., 2005). The kinesin-related motor protein CHO1 is enriched in dendrites and was found to be essential for dendritic differentiation (Sharp et al., 1997; Yu et al., 2000). Microtubule regulatory proteins, including microtubule associated proteins (MAPs), cytoplasmatic linker proteins (CLIPs) and end-binding proteins (EBs) regulate microtubule dynamics (Conde and Cáceres, 2009). Interestingly, PSD-95 alters dendrite branching patterns in cultured rat hippocampal neurons by altering microtubule dynamics via an association with EB3 (Sweet et al., 2011).

1.5.4 Extracellular Signals

Dendritic development of cortical neurons requires the coordinated action of several ligand-receptor pairs to guide dendritic orientation, growth, branching, stabilization and maturation (Dong et al., 2014; Whitford et al., 2002a).

The secreted protein Semaphorin-3a acts as a chemoattractant for the growing apical dendrite towards the pial surface (Polleux et al., 2000). Polleux and colleagues found that Semaphorin-3a forms a concentration gradient form upper to deeper cortical layers and demonstrated that apical dendrites grow towards high Semaphorin-3a concentrations. In addition, Semaphorin-3a induces clustering of both PSD-95 and presynaptic synapsin-1 in cultured cortical neurons without changing the density of spines or filopodia (Morita et al., 2006).

Slits family proteins are diffusible chemotropic ligands that bind to Roundabout (Robo) family of receptors. Slit proteins were first identified as chemorepellants that prevent the recrossing of commissural axons in vertebrates and invertebrates (Bagri et al., 2002; Brose et al., 1999; Kidd et al., 1999; Plump et al., 2002). However, out of the three vertebrate slit and three robo genes, *slit1*, *robo1*, and *robo2* are highly expressed in the developing neocortex during dendritic development. Studies using primary cultures and slice overlay assays indicate that endogenous Slit1 may control dendritic growth and branching of pyramidal neurons in the neocortex (Whitford et al., 2002b).

Multiple neurotrophic factors, including nerve growth factor, brain-derived nerve growth factor (BDNF), neurotrophin-3 (NT-3) and neurotrophin-4 (NT-4), have been shown to influence the morphology of dendrites through binding to Trk family of tyrosine receptors (Park and Poo, 2013). Studies in slice cultures showed that pyramidal neurons in each cortical layer respond to a subset of neurotrophins with distinct effects on apical or basal dendrites (McAllister et al., 1995). Moreover, BDNF was demonstrated to increase dendritic complexity in layers IV, while NT-3 inhibits BDNF-

dependent growth. Reciprocally, NT-3 induce dendritic complexity in layer VI and BDNF inhibits its action (McAllister et al., 1997). This suggests that a distinct expression pattern of receptor and signaling complexes in each cortical layer or dendritic compartment could result in a differential response to the same extrinsic factor. Moreover, several studies indicate that BDNF-TrkB signaling regulates the formation and morphology of dendritic spines. Exogenous BDNF was reported to increase spine density in cultured cerebellar Purkinje neurons without altering dendritic complexity and spine morphology, while inhibition of TrkB signaling result in longer spine necks (Shimada et al., 1998). In rat hippocampal slices, the repetitive pairing of postsynaptic spikes and two-photon glutamate uncaging at single dendritic spines result in increased spine head volume in CA1 pyramidal neurons, while inhibition of BDNF-TrkB signaling abolished the persistent enlargement of spine heads (Tanaka et al., 2008).

Dendritic growth becomes markedly reduced as cortical neurons mature. Growing dendrites get in contact with dendrites of neighboring neurons, which enables the activation of the cell surface receptor Notch by its ligands, Delta and Jagged (Sestan et al., 1999). This activation mediates the cleavage of the intracellular domain of Notch and subsequently the translocation into the nucleus, where it functions as a transcriptional regulator that inhibits dendritic growth (Artavanis-Tsakonas et al., 1999). Overexpression of the CA-Notch intracellular domain in cultured neurons mediates premature inhibition of dendritic growth (Sestan et al., 1999). Knockdown of Notch signaling in cultured neurons was shown to result in abnormally long but less branched dendrites (Redmond et al., 2000).

1.5.5 Activity-dependent mechanisms

Several studies indicate that dendritic complexity can be regulated in response to neuronal activity (Wong and Ghosh, 2002). Ghosh and colleagues showed that the transcription factor cAMP responsive element binding protein (CREB) and the SYTr-related nuclear protein calcium-responsive transactivator (CREST) are required for calcium-induced dendritic growth and complexity of cortical neurons in the mammalian brain (Aizawa et al., 2004; Redmond et al., 2002). Others showed that the activity-regulated protein kinase CaMKIIα stimulates phosphorylation of NeuroD1 and thereby activates NeuroD1-dependent transcription and dendritic branching (Gaudillière et al., 2004). Moreover, afferent input from thalamocortical axons seem to be necessary for oriented dendritic growth and stabilization of layer IV spiny stellate neurons (Iwasato et al., 2000).

1.6 The Known Function of NOMA-GAP

The neurite outgrowth multiadaptor GTPase- activating protein (NOMA-GAP) identified as a neuronal enriched regulator of Rho family GTPases containing an incomplete Phox (PX) domain, an SH3 domain and a RhoGAP domain (Rosário et al., 2007). Our group found that NOMA-GAP interacts directly with the cytoplasmatic domain of TrkA receptor through an N-terminal region that includes the SH3 and the RhoGAP domain. Activation of TrkA by NGF stimulates the interaction of the tyrosine enriched C-terminus of NOMA-GAP with the SH2 domain of the tyrosine phosphatase SHP2. Binding of SHP2 to NOMA-GAP is necessary for the sustained activation of Erk5 Mitogen-activated protein kinase (MAPK) and neurite extension in PC12 cells. Furthermore our group demonstrated that the RhoGAP domain of NOMA-GAP specifically inactivates Cdc42 after stimulation by NGF, which is also critical for neurite extension in PC12 cells. Loss of NOMA-GAP in PC12 cells leads to increased phosphorylation of the Cdc42 downstream effector serine/threonine kinase PAK1/2. Thus NOMA-GAP is essential for NGF-induced neurite extension in PC12 cells by recruitment of SHP2 and inactivation of Cdc42 (Rosário et al., 2007). An alternative spliced isoform of the murine NOMA-GAP homolog, named TCGAP (**T**C10/**C**dc42 **G**TPase **a**ctivating **p**rotein), has been reported to play an important role in the regulation of insulin-stimulated glucose transport (Chiang et al., 2003).

Recently, our group generated NOMA-GAP-deficient mice by replacing exons 7-12 of the *ARHGAP33* gene with a nuclear localized β-galactosidase gene, followed by stop codons (Rosário et al., 2012). This insertion results in a frame-shift and subsequently loss of NOMA-GAP. The expression of *ARHGAP33* in mice was found to be restricted to the nervous system, at E8.5 in the neural tube and at E14.5 onwards in the cortical plate. *ARHGAP33* expression can also found in the hippocampus, striatum, cerebellum, olfactory bulb and distinct regions of the brain, but no expression is seen in proliferative zones. NOMA-GAP-deficient mice are born at the expected Mendelian ratio and have the same body weight at birth. Magnetic resonance imaging scans of living animals and Nissl-staining of brain sections show that the brain structure is conserved. However, loss of NOMA-GAP results in a reduction in total brain volume and especially cortical volume (Rosário et al., 2012).

1.7 Aim of this Thesis

The aim of my thesis was to explore the role of NOMA-GAP during cortical development in mice, using knockout and overexpression studies combined with molecular and morphological analysis. First, I analyzed NOMA-GAP-deficient mice during early stages of neuronal differentiation, namely the generation, migration, fate determination and axonal connectivity of excitatory neurons in the neocortex. Furthermore, I shed light on the differential maturation of dendritic structures. More specifically, I studied the role of NOMA-GAP during layer-specific dendritic branching and compartment-specific maturation of dendritic spines. Finally, I identified the mechanisms how NOMA-GAP regulates the maturation of dendritic structures.

2 Material and Methods

2.1 Animals

All mouse experiments were carried out according to German law and were approved by Landesamt für Gesundheit und Soziales Berlin. NOMA-GAP-deficient mice were generated by replacing exons 7-12 of the NOMA-GAP gene *ARHGAP33* with a nuclear-localized *LacZ* reporter gene using homologous recombination in embryonic stem cells. Floxed Cdc42 and Nex1-cre recombinase mouse lines were obtained from Cord Brakebusch (University of Copenhagen) and Klaus Armin Nave (Max Planck Institut für Experimentelle Medizin), respectively. All mice are C57Bl/6 background. In order to generate Cdc42 conditional mutant, where Cdc42 has been heterozygous deleted from postmitotic cells within the cortex, Cdc42fl/fl mice were mated with Nex1-cre mice. The day of vaginal plug was considered as E0.5.

2.2 List of antibodies

Antigen	Host	Company	Cat number	Dilution
Cdc42	Mouse	BD Biosciences	610929	1:500 WB
cofilin (D59)	Rabbit	Cell Signaling	3318	1:1000 WB
p-cofilin (Ser3)	Rabbit	Cell Signaling	3311	1:1000 WB
Ctip2	Rat	Abcam	18465	1:250 IF
ephrin-B1/2/3	Rabbit	Santa Cruz	910	1:500 WB
p-Erk 1/2	Mouse	Cell signaling	9106	1:2000 WB
FLAG	Rabbit	Sigma	F7425	1:1000 WB
GluR1	Mouse	NeuroMab	75-327	1:250 IF, 1:500 WB
GFP	Goat	Rockland	600-101-215	1:1000 IF, 1:2000 WB
LIMK1	Rabbit	Cell signaling	3842	1:1000 WB
p-LIMK1/LIMK2	Rabbit	Cell signaling	3841	1:1000 WB
Myc-tag	Mouse	Cell signaling	2276	1:500 IF, 1:2000 WB

Myc-tag	Rabbit	Cell signaling	2278	1:1000 WB
NMDAR1	Rabbit	Millipore	AB9864R	1:1000 WB
NMDAR2B	Rabbit	Millipore	06-600	1:1000 WB
NOMA-GAP (N)	Goat	Abcam	4154	1:500 WB
NOMA-GAP (C)	Goat	Abcam	53513	1:500 WB
PAK	Mouse	Santa Cruz	Sc-166887	1:500 WB
p-PAK1/PAK2	Rabbit	Cell signaling	2605	1:500 WB
PSD-95	Mouse	Thermo Scientific	MA1-045	1:400 IF, 1:2000 WB
p-S295 PSD-95	Rabbit	Abcam	76108	1:500 WB
RFP/DsRed	Rabbit	Clontech	632496	1:250 IF
Satb2	Rabbit	Tarabykin lab		1:300 IF
synaptophysin1	Rabbit	Synaptic systems	101002	1:300 IF
Trk (C-14)	Rabbit	Santa Cruz	11	1:500 WB
α-tubulin	Mouse	Sigma	T9026	1:50000 WB

Dylight (Jackson Immunoresearch) or Alexa (Molecular probes) coupled secondary antibodies were used at a dilution by 1:600 for immunofluorescence. Horseradish peroxidase (HRP) linked secondary antbodies (Jackson Immunoresearch) were used for western blot analysis at a dilution of 1:5000.

2.3 Plasmids

The membrane-targeted GFP expression construct is a myristoylated Venus-GFP driven by a CAG promoter was a gift from Anna-Katerina Hadjantonakis (Addgene plasmid #32602). The eGFP expression construct is driven by a CAG promoter and was generated in the lab of Victor Tarabykin. Tagged wtNOMA-GAP and delRhoGAP constructs have been generated by Marta Rosario and have been described previously (Rosário et al., 2007). Tagged full length *DLG1*/SAP97, *DLG2*/PSD-93, *DLG3*/SAP102 and *DLG4*/PSD-95 were kindly provided by Nils Rademacher and Sarah A. Shoichet (Charité Universitätsmedizin Berlin). Our group subcloned V12 Cdc42 into the multiple cloning site of the NeuroD1 promoter-driven IRES-mCherry pA vector (kindly provided by Goichi Miyoshi and Gordon Fishell, New York University). S3A and wild type cofilin

expression constructs were kindly provided by Jun-Lin Gaun (University of Michigan) and have been described previously (Yoo et al., 2010).

To overexpress NOMA-GAP, PSD-95 and eGFP in primary cortical neurons, a GFP N-terminal tagged NOMA-GAP construct and a mCherry C-terminal tagged PSD-95 construct were subcloned by Thorsten Trimbuch (Charité Universitätsmedizin Berlin) into the lenti-viral shuttle vector FUGW in which the ubiquitin promoter was exchanged for a neuronal human synapsin-1 promoter. A double synapsin-1 promoter plasmid expressing eGFP served as a cytosolic reporter. Lentiviruses were produced by Bettina Brokowski and Thorsten Trimbuch as previously described (Lois et al., 2002).

2.4 Software

ImageJ and Adobe Photoshop were used for image processing and quantification. Figures were assembled in Adobe Illustrator. Microsoft office was used for writing and calculations. Graphs and statistical analysis were performed with GraphPad Prism 5.0.

2.5 Genotyping

Embryonal tailcuts were digested in 150 µl Lysis buffer (100 mM Tris pH 8.5, 10 mM EDTA, 200 mM NaCl, 0.2% SDS, 100 µg/ml Proteinase K) at 57°C for 2 hours to overnight. Samples were centrifugated at 14000 rpm for 5 min. The DNA in the supernatant was precipitated by adding 150 µl of isopropanol, followed by inverting the tube several times and centrifugation at 14000 rpm for 15 min. The DNA precipitate was washed in 80% ethanol, air-dried and re-suspended in 100 µl sterile distilled water. Tailcuts or ear punches from postnatal animals were digested as described for embryonal animals. Hairs or cartilages were removed by centrifugation at 14000 rpm for 2 min. The supernatant was removed and diluted tenfold. All PCR reactions were prepared in a final volume of 25 µl containing 1x GoTaq buffer (Promega), 0.2 mM dNTPs (Invitrogen), 0.5 µM forward primer, 0.5 µM reverse primer, 1 µl GoTaq polymerase (Promega), 1 µl template DNA and 15 µl ddH_2O. The following primer sequences and amplification programs were used.

1. NOMA-GAP wild type allele

Forward – 5' CATGAGCTGCCTTGTGCATGTTGA 3'
Reverse – 5' ACAGGTAGAGTCCATTCCTGCCAA 3'
37 amplification cycles – 95°C - 30'', 65°C - 15'', 72°C - 30''

2. NOMA-GAP knockout allele

Forward – 5' TGTGCTGCAAGGCGATTAAGTTGG 3'
Reverse – 5' ACAGGTAGAGTCCATTCCTGCCAA 3'
37 amplification cycles – 95°C- 30'', 65°C- 15'', 72°C- 30''

3. Cdc42 wild type and floxed alleles

Forward – 5' TCTGCCATCTACACATACAC3'
Reverse – 5' ATG TAG TGT CTG TCC ATT GG3'
41 amplification cycles – 95°C- 30'', 60°C- 30'', 72°C- 30''

4. Nex1 wild type allele

Forward- 5' AGA ATG TGG AGT AGG GTG AC 3'
Reverse- 5' GAG TCC TGG AAT CAG TCT TTT TC 3'
40 amplification cycles – 95°C- 30'', 54°C- 30'', 72°C- 30''

5. Nex1-Cre allele

Forward- 5' CCG CAT AAC CAG TGA AAC AG 3'
Reverse- 5' GAG TCC TGG AAT CAG TCT TTT TC 3'
40 amplification cycles – 95°C- 30'', 54°C- 30'', 72°C- 30''

PCR products were separated by SDS-PAGE using a 2% agarose gel and 1x TAE running buffer 40 mM Tris pH 7.6, 20 mM acetic acid, 1 mM EDTA).

2.6 HEK 293 cell culture

Human embryonic kidney cells (HEK 293) were grown in DMEM (Gibco) supplemented with 10% FBS (Biochrom) and antibiotics (Gibco) at 37°C with 5% CO_2. Every 3 days they were split and plated 1:10 in fresh medium. Transfections were carried out using Lipofectamine 2000 (Thermo Fisher Scientific) transfection reagent according to the manufacturer's instructions.

2.7 Primary cortical neuron culture

Primary cortical neurons were prepared from littermate E16.5 embryos for single cell studies for the biotinylation assay. Coverslips and plates were coated with 200 µg/ml poly-D-lysine hydrobromide (Sigma-Aldrich) and 2 µg/ml laminine (Sigma-Aldrich) dissolved in water overnight at 37°C and washed three times with sterile distilled water. Coverslips (Glaswarenfabrik Karl Hecht) were washed in 70% ethanol with gentle agitation overnight, three times for 1 hour in distilled water, two times in 100% ethanol

for 90 min, ones in 70% ethanol for 15 min, stored in 100% ethanol and finally baked at 200°C for 4 hours. Embryos were collected in cold HBSS+/+ (Gibco). Tail cuts of each embryo were taken for genotyping and the cortices were separately isolated and collected. The tissue was washed two times with HBSS-/- (Gibco) and incubated with 2.5% trypsine (Gibco) at 37°C for 30 min. Trypsinisation was blocked by two washes in plating media (DMEM (Gibco), 10% FBS (Gibco) and antibiotics (Gibco)) supplemented with 1% DNase (New England Biolabs). The tissue was resuspended in plating media and centrifuged at 100xg for 5min. The supernatant was removed and neurons resuspended in plating media. Neurons were counted in a Neubauer chamber and $5x10^4$ primary neurons were plated in 24-well plates on 12 mm coverslip plates and $5x10^5$ primary neurons in 12-well plates. After 3 hours incubation at 37°C in 5% CO_2, the plating media was changed to Neurobasal media (Gibco) supplemented with 1x B27 (Gibco), 1x Glutamax (Gibco), 25 µM β-Mercaptoethanol and 1x Penicillin/Streptomycin (Gibco) and grown at 37°C in 5% CO_2. After 7 days and 14 days *in vitro* half of the culture media was replaced with fresh media supplemented with 5-Fluoro-5´-deoxyuridine (Sigma-Aldrich) at a final concentration of 5 µM to limit glia proliferation. Cultured neurons were transfected using Effectene Transfection Reagent (Qiagen) according to the manufacturer's protocol. Overexpression of NOMA-GAP in mature primary cortical cultures was achieved by infection with lentivirus. Primary cortical neuron cultures were infected with 10 µL of the viral solution ($0.5\text{-}1x10^6$ IU/ml) after DIV7 and analyzed at DIV20.

2.8 Perfusion of mouse brains

Mice were anaesthetized with a mixture of ketamine/xylacine dissolved in 0.9% NaCl (up to 100 mg/kg body weight ketamine and 10 mg/kg body weight xylacine) that was injected intraperitoneally. Deeply asleep animals were intracardiac perfused first with PBS till the blood was washed out and then with 4% PFA/PBS. Perfused brains were isolated and incubated overnight in 4% PFA/PBS and stored in PBS before vibratome sectioning.

2.9 Vibratome sectioning

Fixed brains were embedded in melted 4% agarose (Applichem) dissolved in PBS. After the agarose was hardened, a block with the embedded brain in the middle was cut out of the agarose and glued with rapid glue (Marston-Domsel) onto the object holder of the vibratome (Leica VT1200). Brains were sliced coronal at 100 µm for

analysis of dendritic complexity in Venus-GFP expressing neurons and 50 µm for analysis of dendritic spine morphology as free-floating sections in PBS, which were collected with a brush and stored in 24-well plates filled with PBS.

2.10 Immunostaining

Cultured neurons were permeabilized and blocked in 0.1% Triton-X100, 5% FCS, 1% BSA in PBS for 30 min and vibratome sections in 0.2% Triton-X100, 10% FCS, 1% BSA in PBS for 1 hour. Primary antibody incubations were carried out overnight at 4°C in a dark humid chamber. Antibodies were diluted in PBS for cultured neurons and in 0.1% Triton-X100, 5% FCS, 1% BSA in PBS for brain sections. The next day, samples were incubated with appropriate fluorochrome-coupled secondary antibody in darkness for 2 hours at room temperature. All antibody incubations were followed by 3 washes in PBS for 10 min. Finally, samples were mounted using anti-fading reagent (DAKO or Thermo Fisher Scientific). In order to label surface GluR1, cultured neurons were only blocked in 5% FCS, 1% BSA in PBS for 30 min, followed by incubation with primary antibody diluted in PBS overnight at 4°C. Neurons were then washed three times with PBS and permeabilized and blocked in 0.1% Triton-X100, 5% FCS, 1% BSA in PBS for 30 min, followed by incubation with the appropriate fluorochrome-coupled secondary antibody and phalloidin-TRITC (Sigma-Aldrich). Fluorescent images were captured on a confocal Leica SL using the same settings across compared samples.

2.11 Axonal Tracing

For anterograde cortical axon tracing, 1,1'-dioctadecyl-3,3,3',3'-tetramethylindocarbocyanine-perchlorate (DiI) crystals (Molecular Probes) were placed in the presumptive primary motor cortex, somatosensory cortex and visual cortex of fixed and isolated brains with the help of a tungsten needle. In order to back-label projection neurons in the neocortex, DiI crystals were placed in the cerebral peduncle of unfixed brains. After DiI placement, brains were kept in the dark for 3 weeks for E18.5 brains or 5 weeks for P6 brains at 37°C immersed in PBS with 0.1% Sodium Azide to allow DiI diffusion. After incubation, brains were embedded in 4% agarose (Applichem) and coronal sectioned at 60 µm on a vibratome (Leica VT1200). The sections were counterstained with DAPI for 30 min at 37°C and mounted in PBS. Fluorescence was captured on an Olympus BX51 epifluorescent microscope and digitalized with MagnaFire software. At least 2 animals were used per phenotype.

2.12 Cytochrome C oxidase staining

P7 mice were anaesthetized with ketamine/xylacine cocktail injected intraperitoneally. Deeply asleep mice were intracardiac perfused first with 5 ml 10% sucrose dissolved in PBS and subsequently with 5 ml 4% formalin/ 20% sucrose dissolved in PBS. Perfused brains were isolated and incubated overnight in 30% sucrose dissolved in PBS. Cortical hemispheres were flatten between glas slides and embedded in 4% agarose (Applichem) dissolved in PBS. Brains were sagittal sectioned at 80 µm using a vibratome (Leica VT1200). Sagittal sections were transferred on slides and incubated with filtered staining solution (0.5 mg DAB, 0.3 mg Cytochrome C, 0.04 g sucrose dissolved in 1 ml of 0.1 M phosphate buffer) for around 2 hours. Cytochrome C oxidase staining was checked in between using a light microscope. Stained sections were rinsed in ddH_2O and mounted with mounting media (Thermo Fisher Scientific).

2.13 Sholl Analysis

Dendritic complexity of layer II-III and layer V cortical neurons was analyzed using the Sholl analysis (Sholl, 1953). The dendritic tree of Golgi-stained or Venus-GFP expressing cortical neurons were imaged using an Olympus IX81 inverted fluorescence microscope and Cell Sense Dimension software taking 3 mm spaced z-stacks. 30 concentric circles with a 10 µm distance where centered on the soma using the concentric circle plugin for ImageJ. The number of dendritic intersections for each circle through the z-stack was counted blindly to the genotype using the cell counter plugin for ImageJ. The intersection curve was plotted by the number of dendritic intersections for each circle versus the circle radius using GraphPad Prism software. Venus-GFP expressing neurons were imaged with a Zeiss LSM5 confocal microscope running on ZEN2009 software for representative examples. At least 3 animals were used per genotype.

2.14 Morphometric analysis of dendritic spines

Dendritic spines of secondary dendrites from primary cultured neurons and apical or basal secondary dendrites from pyramidal neurons in brain sections were imaged using a confocal Leica SL microscope running on LCS software taking 0.2 µm spaced z-stacks with a 60x oil objective and 4x zoom and 6x zoom respectively. Morphology of dendritic spines along dendritic segments with an approximately length of 60 µm in primary neurons and 40 µm in brain sections were blindly analyzed on z-projections using ImageJ software. Neck length was measured from the dendritic shaft to the

beginning of the spine head. When the neck was not clearly visible it was considered to be the shortest distance between spine head and dendritic shaft. Head width was defined as the widest length perpendicular to the neck. Spine density was defined as the number of spines divided by the length of the analyzed dendritic segment. Dendritic processes were classified as filopodia, stubby spines and mushroom/thin spines by their morphological characteristics. No distinction was made between mushroom spines and thin spines. Filopodia do not have a clear head-like structure, stubby spines show a head but no neck and mushroom/thin spines show a head and neck.

2.15 Quantification of excitatory synapse density

Synapse density was determined by blindly counting aligned presynaptic and postsynaptic proteins in GFP transfected neurons using the cell counter plugin for ImageJ divided by the length of the analyzed dendritic segment.

2.16 Subcellular fractionation

Adult mouse cortices were homogenized (Wheaton, Potter-Elvejhem) in ice-cold homogenization buffer (320 mM sucrose, 4 mM HEPES/KOH pH 7.4 and inhibitors (1x Protease inhibitor cocktail (Sigma-Aldrich), 1x PhosStop (Roche), 1 mM PMSF, 10 mM Benzamidine (Sigma-Aldrich), 1 mM Na_3VO_4 (Sigma-Aldrich), 10 µg/ml Leupeptin (Sigma-Aldrich) and 5 µg/ml Pepstatin (Sigma-Aldrich)) and centrifuged for 10 min at 4°C and 1300 x g (Beckman rotor TLA-100.4). The resulting supernatant 1 (S1) was centrifuged at 14000xg for 15 min to obtain the pellet 2 (P2, crude synaptosomes). P2 was resuspended in ice-cold homogenization buffer. Protein concentrations were measured using the BCA Protein Assay Kit (Thermo Fisher Scientific) and finally boiled in sample buffer at 95°C for 5 min.

2.17 Biotinylation of surface proteins

Primary cortical neurons (DIV20-22) were washed in cold rinsing solution (1x PBS pH 7.5 containing 0.1 mM $CaCl_2$ and 1 mM $MgCl_2$) to remove amines. Surface proteins were labeled with gentle agitation for 30 min at 4°C in rinsing solution containing 1 mg/ml Sulfo-NHS-SS-Biotin (Pierce Protein Research Products). The reaction was quenched using rinsing solution containing 100 mM glycine followed by washing in rinsing solution.

2.18 Pull-down assays

Lysates of endogenous proteins from the neocortex of adult mice and biotinylated proteins were prepared in cold RIPA buffer (50 mM Tris, 150mM NaCl, 1% vol/vol NP-40, 0.1% wt/vol SDS, 0.5% wt/vol deoxycholate, pH 7.4) containing protease and phosphatase inhibitors (1x Protease inhibitor cocktail (Sigma-Aldrich), 1x PhosStop (Roche), 1 mM Na_3VO_4 (Sigma-Aldrich), 10 µg/ml Leupeptin (Sigma-Aldrich) and 5 µg/ml Pepstatin (Sigma-Aldrich)). Protein lysates were clarified by centrifugation at 13500 rpm at 4°C for 15 min. Protein concentrations were measured using the BCA Protein Assay Kit (Thermo Fisher Scientific). All precipitations were carried out at 4°C from lysates containing equal amounts of protein. Lysates of endogenous proteins were incubated with the indicated antibodies for 2 hours and then captured with protein G sepharose beads (GE Healthcare) for 1 hour. Precipitation of biotinylated proteins were carried out using avidin agarose beads (Thermo Fisher Scientific for 1 hour at 4°C. All precipitates were washed once in RIPA buffer and three times in TBS buffer (50 mM Tris pH 7.4, 100 mM NaCl) and finally boiled in sample buffer at 95°C for 5 min.

For analysis of protein-protein interactions *in vitro*, HEK 293 cells were transfected and harvested 24 hours after transfection. Cells were lysed in cold FLAG buffer (50 mM Tris pH 7.5, 100 mM NaCl, 1 mM EDTA, 1% v/v Triton X-100) containing inhibitors (1x Protease inhibitor cocktail (Sigma-Aldrich), 1x PhosStop (Roche) 1 mM Na_3VO_4 (Sigma-Aldrich), 10 µg/ml Leupeptin (Sigma-Aldrich), 5 µg/ml Pepstatin (Sigma-Aldrich)) and collected in an Eppendorf tube using a cell scraper. Protein lysates were cleared by centrifugation at 14000 rpm 4°C for 20 min. Myc-tagged proteins were immunoprecipitated using anti-Myc 9B11 antibody for 2 hours and then captured on protein G Sepharose beads for 1 hour (GE Healthcare). Beads were washed once in FLAG lysis buffer and three times in TBS buffer (50 mM Tris pH7.4, 150 mM NaCl) and finally boiled in sample buffer at 95°C for 5 min.

2.19 Preparation of cortical lysates

Freshly dissected cortices from embryonic mice were lysed in FLAG buffer containing protease inhibitors and phosphatase inhibitors and centrifuged at 13500 rpm at 4°C for 15 min. Protein concentrations were measured using the BCA Protein Assay Kit (Thermo Fisher Scientific).

2.20 Western blotting

Immunoprecipitates or equal amounts of proteins were separated by SDS polyacrylamide gel electrophoresis (SDS-PAGE) using a Mini PROTEAN electrophoresis system (Bio-Rad). The percentage of acrylamid/bis-acrylamid in the running gel was determined by the size of the protein of interest and the stacking gel contained 4% acrylamid/bis-acrylamid. Equal amounts of proteins were loaded and separated by 60 V in the stacking gel and up to 90 V in the running gel. Prior transfer of separated proteins to Immobilon-P transfer membranes (Millipore) using a Mini Trans-Blot system (Bio-Rad) for 90 min at 100 V. Prior transfer, the membranes were activated with Methanol for 20 sec, washed 2 min in H_2O and soaked in transfer buffer (25 mM Tris-Base, 192 mM Glycine, 10% Methanol in H_2O). The membranes were blocked with 3% BSA (SERVA) dissolved in TBST (150 mM NaCl, 10 mM Tris pH 8.0, 0.05 vol/vol Tween20) for at least 30 min. Membranes were incubated with the indicated primary antibodies dissolved in 1% BSA/TBST overnight at 4°C. After three washes in TBST the membranes were incubated with the appropriate peroxidse-coupled secondary antibody (Jackson Laboratory) at room temperature for 2 hours and finally washed three times with TBST. Visualization of the proteins was achieved by using enhanced chemiluminescence substrate (PerkinElmer). Chemiluminescence signal was captured and quantified using the Image Lab Software on a ChemiDoc XRS+ detector (Bio-Rad).

If necessary, stripping of transfer membranes was performed using glycine stripping buffer (0.15 M glycine, 0.4% SDS in H_2O). Enhanced chemiluminescence substrates were washed off with TBST and incubated twice 10 min with glycine stripping buffer with gentle shaking. The membrane was neutralized with a quick wash in 1 M Tris pH 6.8 followed by washing in TBST. Harsher stripping of transfer membranes was performed using 2-mercaptoethanol stripping buffer (100 mM 2-mercaptoethanol, 2% SDS, 62.5 mM Tris-HCl pH 6.8) at 50°C for 30 min with occasional agitation.

3 Results

3.1 NOMA-GAP is dispensable for early corticogenesis

3.1.1 NOMA-GAP does not affect cell number, migration or cell fate of neurons in the neocortex

To address whether migration, cell number and fate determination of neurons in the neocortex were affected by loss of NOMA-GAP, 5-bromo-2´-deoxyuridin (BrdU) pulse-labeling experiments combined with immunostaining were performed (Figure 6A). Our group injected pregnant females with BrdU at E14.5 and stained cryosections for BrdU, Satb2 and Ctip2. I then imaged and analyzed the distribution of BrdU positive (BrdU+) cells in the somatosensory region of the neocortex of NOMA-GAP-deficient and control brain sections at E18.5. To assess the extent of migration of cells born at E14.5, I divided the neocortex into 10 bins and quantified the percentage of BrdU+ cells in each bin. There were no differences in the percentage of BrdU+ cells in each bin between NOMA-GAP-deficient and control brains, indicating that radial migration of pyramidal neurons born at E14.5 is not affected by the loss of NOMA-GAP (Figure 6B).

Possible alterations in cell number and fate specification were analyzed in E18.5 littermate brains by staining for 4', 6-diamidino-2-phenylindole (DAPI), the upper layer marker Satb2 and the deep layer marker Ctip2 (Figure 6A). My quantification revealed no difference in the relative number of DAPI-positive cells (DAPI+) (Figure 6C), in the percentage of Satb2-positive (Satb2+) cells (Figure 6D) or in the percentage of Ctip2-positive (Ctip2+) cells (Figure 6E) in the somatosensory cortex of NOMA-GAP-deficient brain sections compared to control at E18.5. These results indicate that deletion of NOMA-GAP does not affect the number of cells or fate determination of neurons in the neocortex of mice.

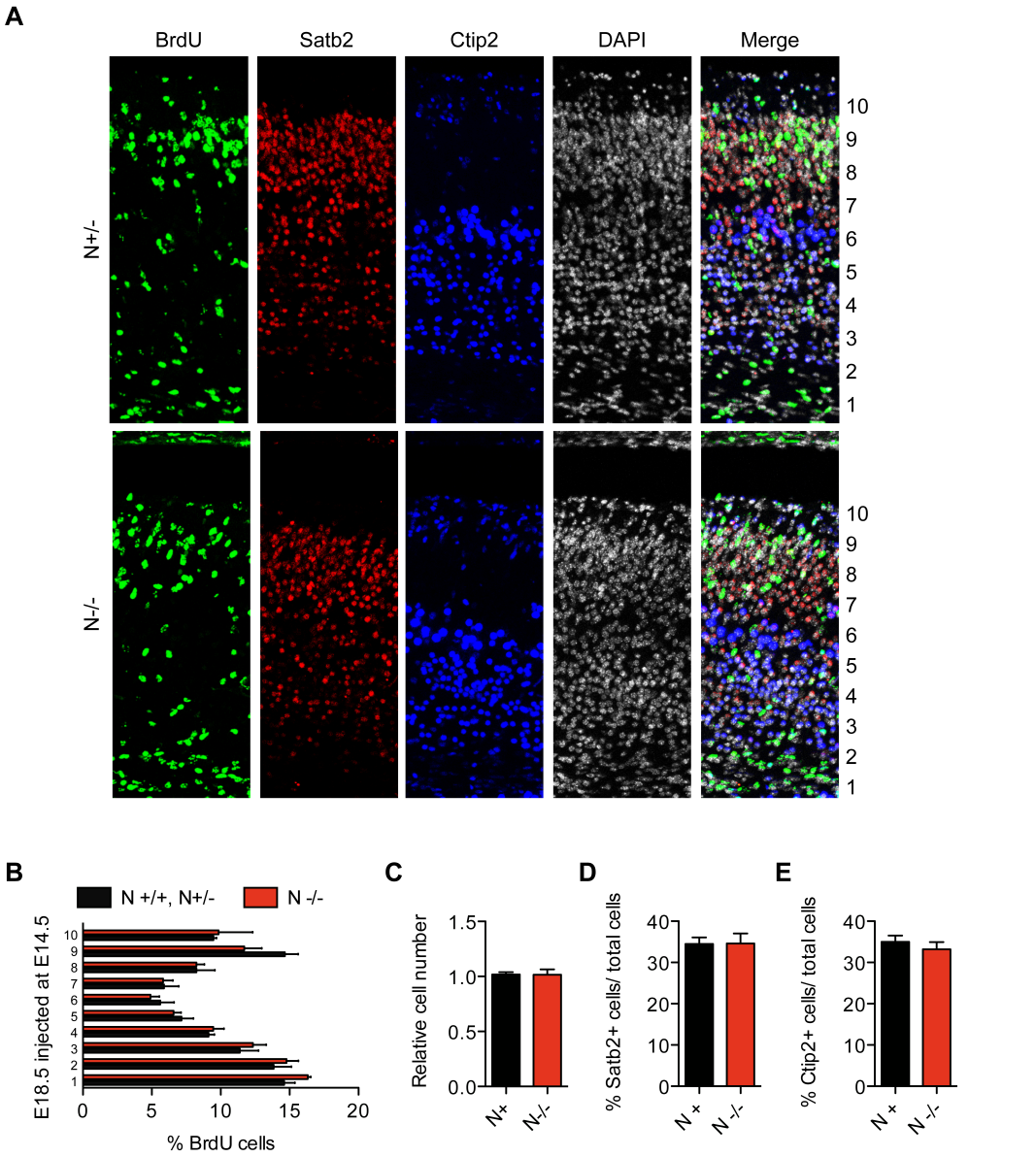

Figure 6: Migration, cell number and cell fate determination of cortical neurons is not affected by loss of NOMA-GAP. (A) BrdU was injected into pregnant females at E14.5 and brain sections of E18.5 NOMA-GAP-deficient and control embryos were stained for BrdU, Satb2, Ctip2 and DAPI. (B) Quantification of the distribution of BrdU+ cells across the neocortex. The neocortex was divided into 10 bins and the percentage of BrdU+ cells in each domain was quantified. Cells born at E14.5 migrate similarly in NOMA-GAP-deficient and control animals. (C) Quantification of the relative number of total cells achieved by counting DAPI+ cells in the neocortex of E18.5 embryos. Student´s t test, p = 0.9450. (D) Quantification of the percentage of Satb2+ cells normalized to total cells of E18.5 embryos. Student´s t test, p = 0.9702 (D) Quantification of the percentage of Ctip2+ cells normalized to total cells of E18.5 embryos. Student´s t test, p = 0.4348. n = 3 N+ and 3 N-/- animals. Modified after Rosario et al., 2012.

3.1.2 NOMA-GAP is dispensable for major axonal projections in the neocortex

Previously, Rosário and colleagues demonstrated that NOMA-GAP promotes the extension of the longest neurite in pheochromocytoma 12 (PC12) cells which in neurons becomes the axon (Rosário et al., 2007). In addition, they reported that overexpression of human wild type NOMA-GAP in the chick spinal cord promotes premature neuronal differentiation and axonal process extension. We therefore hypothesized that axonal projections may be disturbed in NOMA-GAP-deficient animals. I used the fluorescent lipophilic cationic indocarbocyanine dye DiI to map the major axonal projections from the cortex and thalamus in NOMA-GAP-deficient mice at late embryonic (E18.5) and early postnatal (P6) stages (Figures 7-10).

In order to analyze axonal projections in the neocortex, DiI crystals were placed in the presumptive primary motor (M1), primar somatosensory (S1) and primary visual cortex (V1) to anterogradely label corticofugal projections and retrogradely label thalamo-cortical axons of thalamic projection neurons at E18.5 (Figure 7). I observed no abnormalities in descending corticofugal axons and ascending thalamo-cortical axons via the internal capsule in NOMA-GAP-deficient compared to wild type brains at E18.5 (Figure 7A). Cells of the ventrobasal complex of the thalamus were retrogradely labeled in NOMA-GAP-deficient brains comparable to wild type brains, confirming that thalamo-cortical connections are not affected by the loss of NOMA-GAP at E18.5 (Figure 7B).

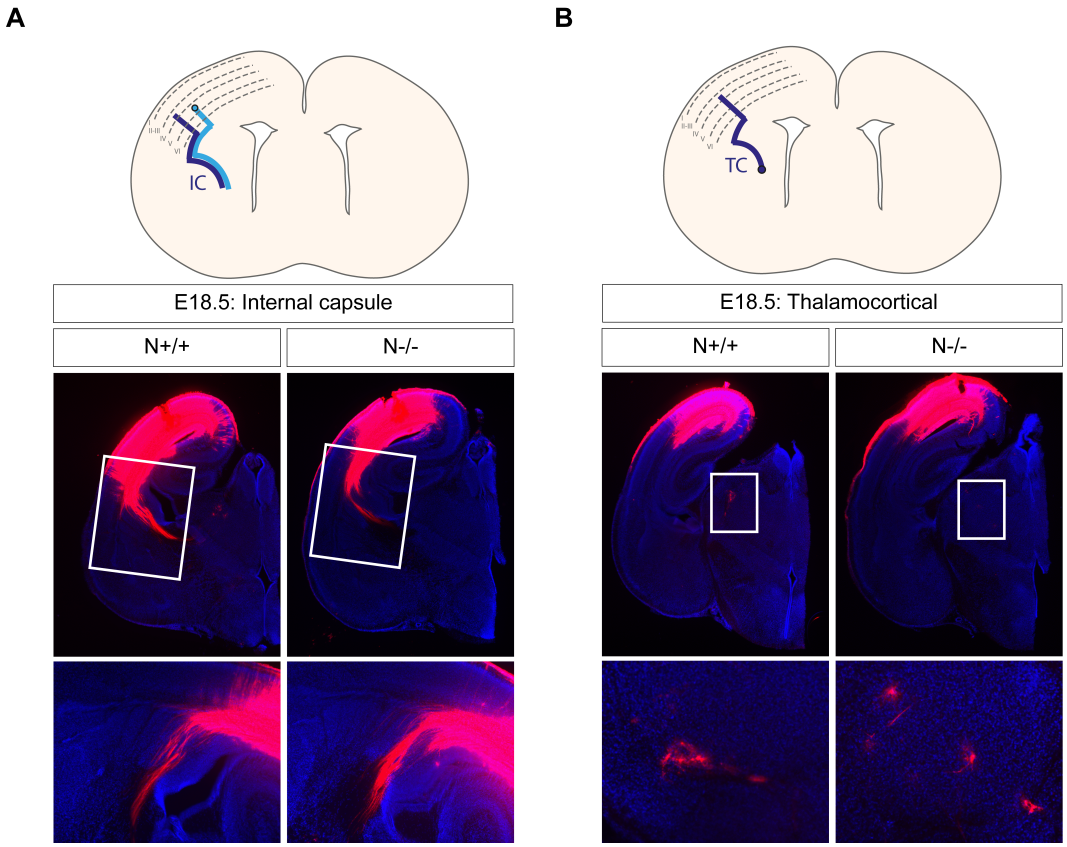

Figure 7: Normal corticofugal and thalamocortical projections via the internal capsule in NOMA-GAP-deficient animals at E18.5. DiI crystals were placed in the presumptive motor (M1), somatosensory (S1) and visual cortex (V1) of NOMA-GAP-deficient and wild type brains to label corticofugal and thalamo-cortical projections. (A) Normal corticofugal projections via the internal capsule to various targets in NOMA-GAP-deficient mice at E18.5. (B) Back-labeled cells in the ventrobasal Thalamus show normal thalamo-cortical innervation in NOMA-GAP-deficient mice at E18.5. Modified after Rosario et al., 2012.

In order to retrogradely label subcerebral layer V projection neurons, DiI was placed in the cerebral peduncle at E18.5 (Figure 8). In wild type brains, DiI placement in the cerebral peduncle back-labeled several layer V projection neurons in the neocortex, whereas only few back-labeled neurons were observed in NOMA-GAP-deficient brains (Figure 8).

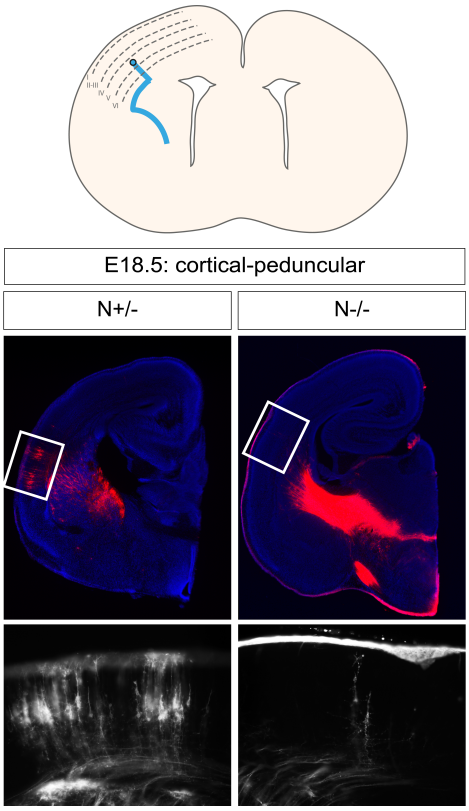

Figure 8: Reduced subcerebral projections from the neocortex to the cerebral peduncle in NOMA-GAP-deficient mice at E18.5. Dramatic reduction in the number of back-labeled layer V projection neurons in the neocortex in NOMA-GAP-deficient mice at E18.5 after DiI placement in the cerebral peduncle compared to wild type control. Modified after Rosario et al., 2012.

At P6, DiI crystals were placed in the presumptive M1, S1 and V1 to retrogradely label thalamo-cortical axons of thalamic projection neurons and callosal projections to the contralateral hemisphere (Figure 9). As seen already at E18.5, thalamo-cortical innervations do not seem to be affected in NOMA-GAP-deficient animals at P6 (Figure 9i). In addition, axonal projections through the corpus callosum are normal in NOMA-GAP-deficient animals (Figure 9ii).

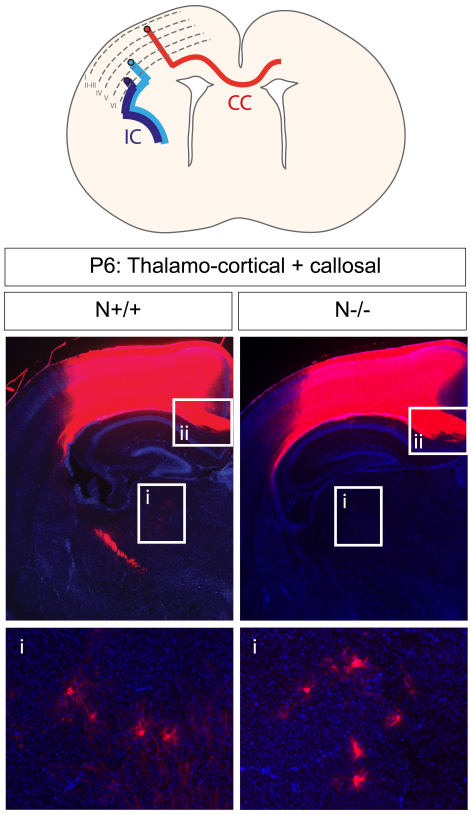

Figure 9: Normal thalamo-cortical and callosal connectivity in NOMA-GAP-deficient mice at P6. (i) Back-labeled thalamic projection neurons indicate that thalamo-cortical innervations are not affected in NOMA-GAP-deficient animals at P6. (ii) Axonal projections through the Corpus callosum are normal in NOMA-GAP-deficient animals at P6. Modified after Rosario et al., 2012.

To analyze if corticofugal connections are formed at P6 in NOMA-GAP-deficient mice, DiI was placed in the presumptive M1, S1 and V1 to anterogradely label subcerebral projections to the cerebral peduncle (Figure 10A) and in the cerebral peduncle to retrogradely label layer V projection neurons in the neocortex (Figure 10B). Placement of DiI crystals in the neocortex at P6 showed that corticofugal fibers reaching the cerebral peduncle in NOMA-GAP-deficient brains were comparable to control brains (Figure 10A). Moreover, DiI placement in the cerebral peduncle showed at this development stage the same amount of back-labeled projection neurons in the neocortex of NOMA-GAP-deficient brains, as the wild type controls (Figure 10B). This indicates that there is a delay in the outgrowth of corticofugal fibers through the cerebral peduncle in NOMA-GAP-deficient animals at E18.5, which is overcome by P6. Together the data suggest that NOMA-GAP is not essential for cortical axonal connectivity or other molecules are able to compensate for NOMA-GAP in these events.

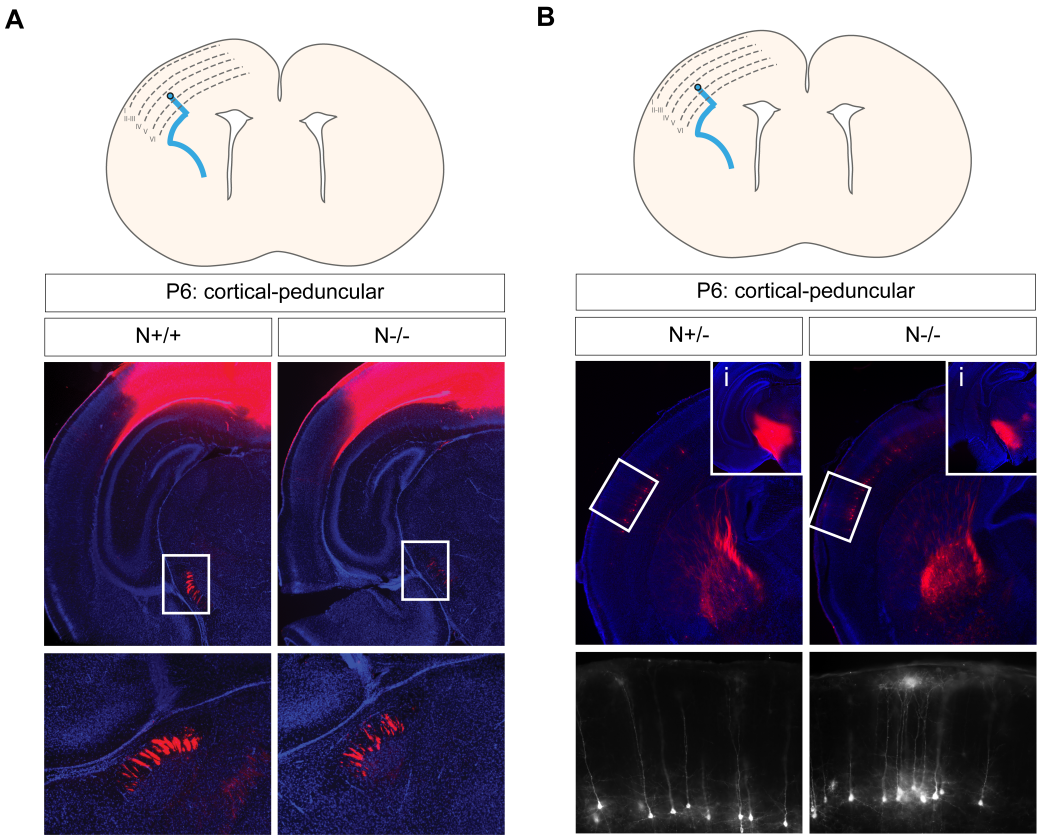

Figure 10: Normal subcerebral projections from the neocortex to the cerebral peduncle in NOMA-GAP-deficient mice at P6. (A) Normal corticofugal projections to the cerebral peduncle in NOMA-GAP-deficient mice at P6. (B) Back-labeled cells in the neocortex from the cerebral peduncle at P6 confirm normal cortical-pendicular innervations in NOMA-GAP-deficient animals at P6. (i) DiI placement in the cerebral peduncle. Modified after Rosario et al., 2012.

3.1.3 NOMA-GAP is dispensable for barrel cortex formation

Axons of thalamic neurons project to the primary somatosensory neocortex, forming the basis for discrete and well-defined cell clusters in layer IV, which in rodents are called barrels (Feldman and Brecht, 2005). These layer IV barrels are separated from each other by areas called septa and are arranged in an almost identical pattern to whiskers on the snout (Figure 11A). The barrel cortex forms early in development and the basic somatotopic map is established within the first days after birth (Petersen, 2007).

To investigate if the organization of the barrel cortex is affected in NOMA-GAP-deficient mice, I performed cytochrome oxidase histochemistry in NOMA-GAP-deficient and heterozygous control cortices at P7 (Figure 11B). Cytochrome oxidase reactivity is commonly used to visualize the morphology of the barrel map. In addition, cytochrome oxidase activity can also indicate changes in the relative levels of neuronal reactivity. The organization of the barrel cortex was not obviously affected in NOMA-GAP-

deficient mice at P7 (Figure 11B). However, I observed a slight increase in the cytochrome-oxidase reactivity in the barrels of NOMA-GAP-deficient mice compared to heterozygous controls. This result indicates that NOMA-GAP is not important for the convergence and ordering of thalamo-cortical afferents in layer IV of the primary somatosensory cortex and thus somatotopic map formation.

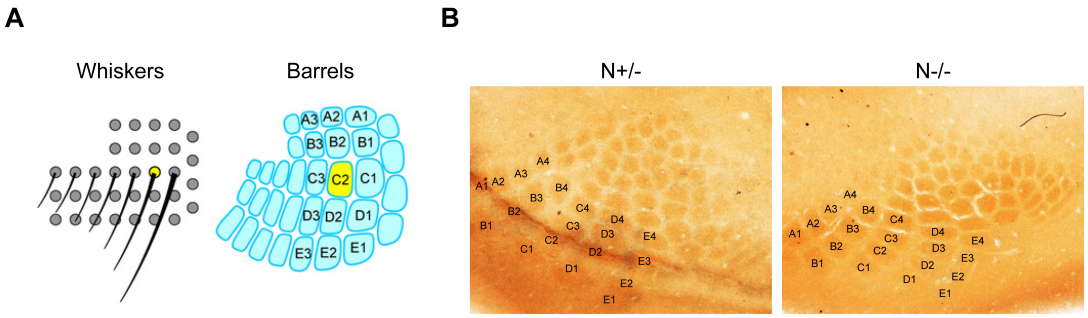

Figure 11: Normal organization of the barrel cortex in NOMA-GAP-deficient mice at P7. (A) The layout of whisker follicles on the snout of the rodent is highly conserved. Anatomical structures termed barrels in layer IV of the primary somatosensory neocortex, which are arranged in a nearly identical pattern to the whiskers (Taken from Petersen, 2007). (B) Representative examples of cytochrome oxidase histochemistry of the barrel cortex at P7 in NOMA-GAP-deficient and heterozygous control cortices. No obvious difference in the pattern of the barrel cortex was detected, but cytochrome oxidase reactivity seems to be slightly increased in NOMA-GAP-deficient primary somatosensory cortices.

3.2 NOMA-GAP regulates dendritic morphology

3.2.1 NOMA-GAP preferentially targets into dendrites

To gain insight into the role of NOMA-GAP during cortical development, I investigated the subcellular localization of NOMA-GAP *in vivo* and *in vitro* (Figures 12-14). To characterize the subcellular localization of NOMA-GAP *in vivo,* a GFP-tagged NOMA-GAP and DsRed expression construct were *in utero* co-electroporated at E15.5. I analyzed the subcellular localization of NOMA-GAP in layer II-III pyramidal neurons in P23 brain slices by imaging fluorescence signals (Figure 12). While fluorescence of DsRed was detected in both, dendrites and callosal axons, GFP-NOMA-GAP was only observed in dendrites and not in axons. As seen *in vitro*, tagged NOMA-GAP accumulates in dendritic spine heads (Figure 12, magnified panel). Thus, NOMA-GAP preferentially targets into dendrites and accumulates in dendritic spine head.

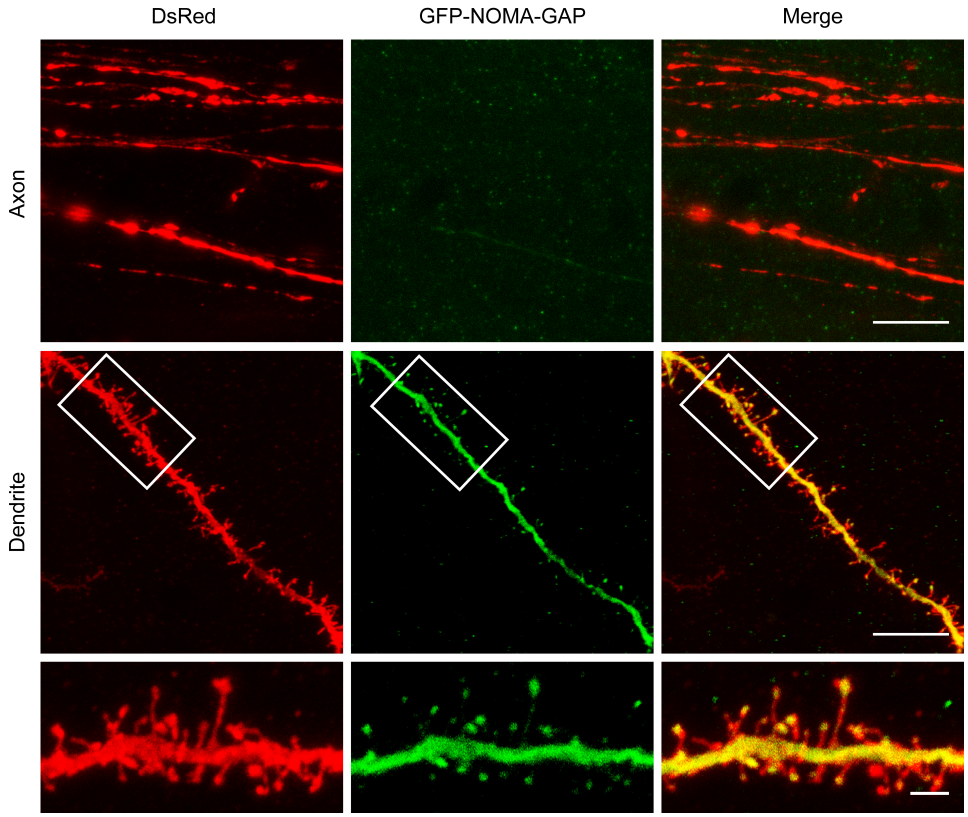

Figure 12: NOMA-GAP preferentially targets into dendrites. Expression of GFP-tagged NOMA-GAP together with DsRed in layer II-III pyramidal neurons in the neocortex following *in utero* electroporation at E15.5. Fluorescence signals in callosal axons and basal dendrites were imaged at P23. Scale bars = 10 µm for upper panels and 2 µm for magnified panel. Modified after Schuster et al., 2015.

Since we were not able to detect endogenous NOMA-GAP by immunofluorescence, I expressed Myc-tagged NOMA-GAP in primary cortical neurons at DIV5 and analyzed its subcellular localization at DIV7 (Figure 13). The morphology of neurons was visualized by staining for F-actin with phalloidin coupled to the fluorescent dye Tetramethylrhodamineisothiocyanate (TRITC). In addition to a strong somal expression in particular in the Golgi apparatus, Myc-tagged NOMA-GAP showed a punctuate pattern along dendrites and accumulated at dendritic branch points (Figure 13, arrows).

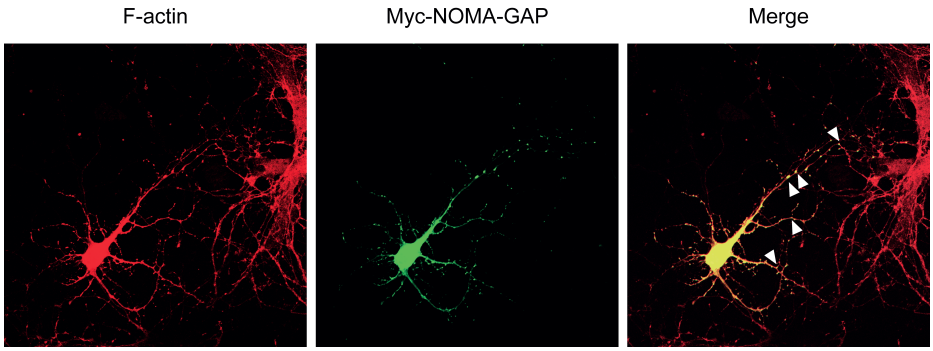

Figure 13: NOMA-GAP accumulates at dendritic branch points at DIV7. Myc-tagged NOMA-GAP (shown in green) was expressed in primary cortical neurons at DIV5 and the subcellular localization analyzed at DIV7. Neuronal morphology was visualized by F-actin staining with TRITC-phalloidin (shown in red).

Next I addressed the subcellular localization of NOMA-GAP in mature neurons at DIV20, by transfection of cultured mouse cortical neurons with Myc-tagged NOMA-GAP at DIV14. An eGFP expression construct was co-transfected to visualize the morphology of transfected neurons (Figure 14). As seen already at DIV7, Myc-tagged NOMA-GAP showed a punctuated staining along the dendritic shaft at DIV20. Interestingly, in mature cortical neurons Myc-tagged NOMA-GAP accumulated in dendritic spine heads (Figure 14, arrows).

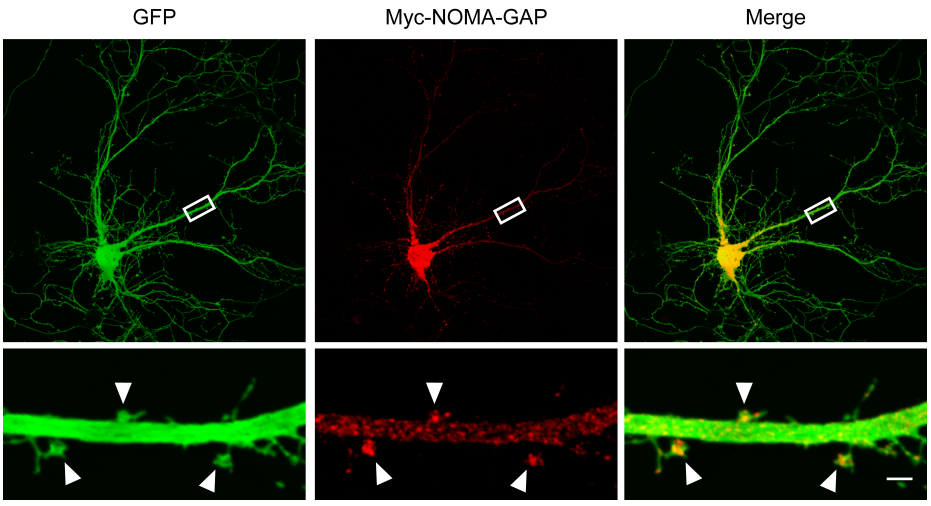

Figure 14: NOMA-GAP accumulates in dendritic spine heads at DIV20. Myc-tagged NOMA-GAP and eGFP were expressed in primary cortical neurons at DIV14 and the subcellular localization analyzed at DIV20. Arrows indicate dendritic spines. Scale bar = 2 µm. Modified after Schuster et al., 2015.

3.2.2 NOMA-GAP regulates dendritic complexity of layer II-III but not layer V cortical neurons

The accumulation at dendritic branch points suggested that NOMA-GAP might regulate dendritic branching of cortical neurons. To address the role of NOMA-GAP in dendritic complexity, I performed Sholl analysis on layer II-III and layer V pyramidal neurons on adult mouse brain sections (P25-26) that had previously been stained by René Jüttner using the Golgi method (Figures 15 and 16). Sholl analysis is a commonly used method to quantify the complexity of the dendritic tree by counting the number of dendritic intersections for concentric circles centered at the soma with a gradually increasing radius (Sholl, 1953).

First, I imaged and subsequently analyzed the complexity of layer II-III pyramidal neurons in the somatosensory cortex in NOMA-GAP-deficient and wild type animals (Figure 15A). I observed that loss of NOMA-GAP does not affect the number of primary dendrites, which directly emerge from the soma (Figure 15B). However, Sholl analysis of NOMA-GAP-deficient layer II-III neurons showed a downward shifted intersection curve that reflects reduced dendritic complexity in these animals (Figure 15C). Quantification of the average number of total dendritic intersections with concentric circles per neuron revealed a significant reduction in NOMA-GAP-deficient layer II-III neurons compared to wild type control (Figure 15D). These results demonstrate that NOMA-GAP regulates dendritic complexity of layer II-III pyramidal neurons in the somatosensory cortex.

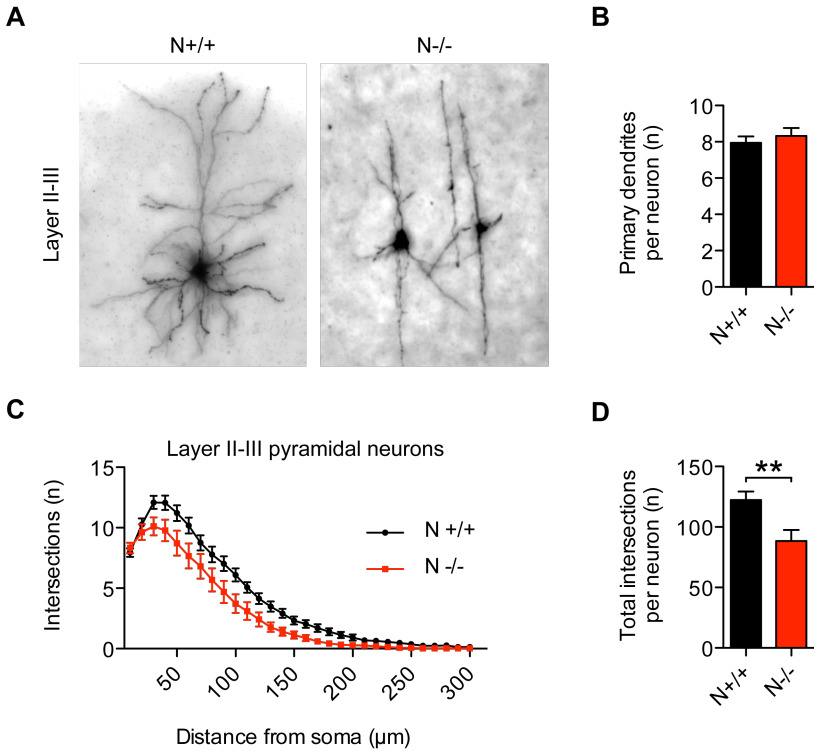

Figure 15: Loss of NOMA-GAP leads to a reduction in dendritic branching of layer II-III pyramidal neurons. (A) Representative average projections of z-stacks from Golgi-stained layer II-III neurons in the somatosensory cortex of NOMA-GAP-deficient and wild type animals at P25-26. (B) Quantification of the average number of primary dendrites of layer II-III neurons. Mann-Whitney U test, p = 0.3879. (C) Sholl profile of layer II-III neurons from NOMA-GAP-deficient and wild type animals. (D) Quantification of the average number of total dendritic intersections with concentric circles per layer II-III neuron. Mann-Whitney U test, $^{**}p$ = 0.0024. n = 62 N+/+ and 36 N-/- layer II-III pyramidal neurons in the somatosensory cortex from five and four animals, respectively. Modified after Rosario et al., 2012.

Since NOMA-GAP is expressed in all cortical layers, we assumed that loss of NOMA-GAP might also lead to a reduction in dendritic complexity of layer V pyramidal neurons. Therefore I performed Sholl analysis on previously Golgi-stained layer V neurons in the somatosensory cortex of NOMA-GAP-deficient and wild type mice (Figure 16A). In contrast to layer II-III pyramidal neurons, loss of NOMA-GAP did not affect the dendritic complexity of layer V pyramidal neurons up to a distance of 300 µm, which excludes in these large neurons the apical dendritic tuft (Figures 16B-16D). This suggests that NOMA-GAP differentially regulates dendritic complexity of pyramidal neurons in the neocortex. While dendritic complexity of layer II-III pyramidal neurons is reduced upon loss of NOMA-GAP, layer V pyramidal neurons appears to be unaffected.

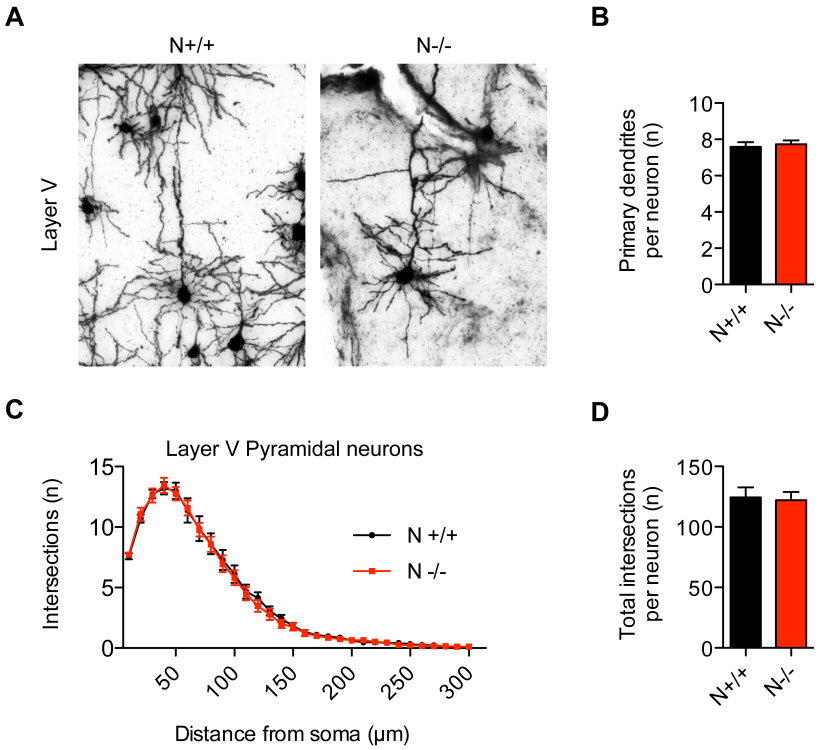

Figure 16: Layer V pyramidal neurons show no difference in the dendritic complexity of NOMA-GAP-deficient and wild type animals up to a distance of 300 µm. (A) Representative average projections of z-stacks from Golgi-stained layer V neurons in the somatosensory cortex of NOMA-GAP-deficient and wild type animals at P25-26. (B) Quantification of the average number of primary dendrites of layer V pyramidal neurons. Mann-Whitney U test, $p = 0.6468$. (C) Sholl profile of NOMA-GAP-deficient and wild type layer V pyramidal neurons. (D) Quantification of the average number of total intersections with concentric circles per layer V neuron. Student´s t test, $p = 0.8320$. n = 37 N+/+ and 33 N-/- layer V pyramidal neurons from four and three animals, respectively. Modified after Rosario et al., 2012.

NOMA-GAP has a N-terminal region with similarity to a PX domain. Previously, PX domains have been reported to negatively regulate activity in proteins with tandem PX-SH3 domains (Yuzawa et al., 2004). In agreement with this observation, Rosário and colleagues demonstrated that the PX domain of NOMA-GAP can negatively regulate its function, as deletion of the PX domain in NOMA-GAP (delPX NOMA-GAP) stimulates NOMA-GAP-induced neurite outgrowth in PC12 cells (Rosário et al., 2007). To investigate if overexpression of NOMA-GAP could lead to increased dendritic complexity in layer II-III pyramidal neurons, the delPX mutant of NOMA-GAP was expressed in cortical neurons together with membrane targeted GFP by *in utero* electroporation of wild type NMRI animals at E15.5, the birth date of layer II-III neurons. All *in utero* electroporations of my thesis were performed by our collaborator Srinivas Parthasarathy. I harvested electroporated brains at P23, imaged GFP fluorescence signals and carried out Sholl analysis as described in Figure 15 (Figure 17A). Overexpression of delPX NOMA-GAP does not affect the number of primary dendrites

compared to GFP control layer II-III neurons (Figure 17B). In addition, Sholl analysis showed that overexpression of delPX NOMA-GAP does not affect dendritic complexity of layer II-III neurons compared to GFP control neurons, as seen by a similar Sholl profile and in the average number total dendritic intersections with concentric circles per neuron (Figures 17C and 17D).

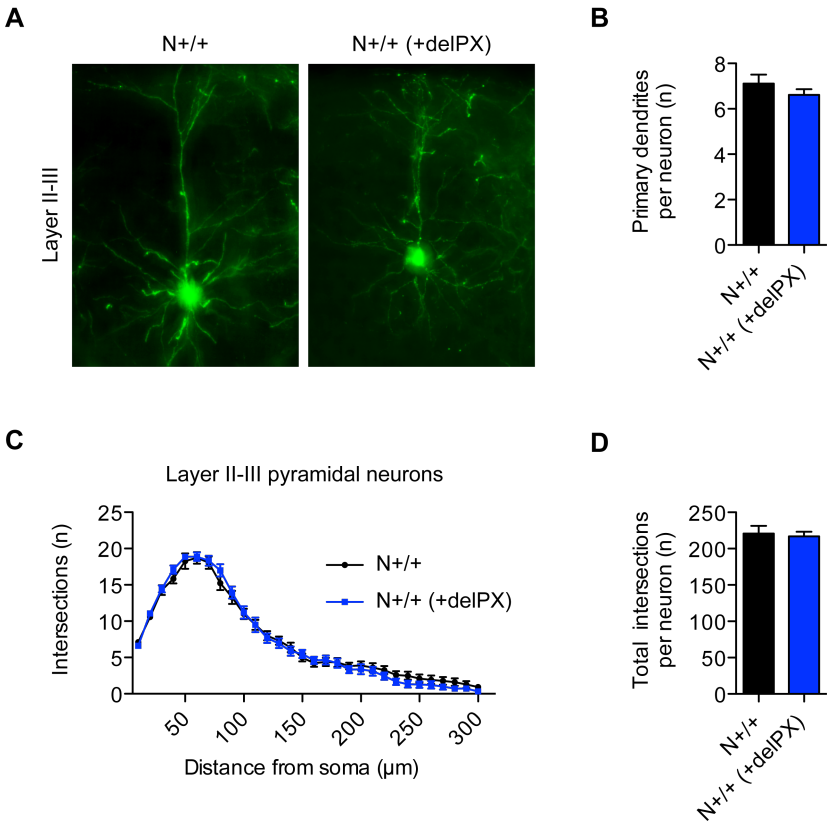

Figure 17: Overexpression of delPX NOMA-GAP does not increase dendritic complexity of wild type layer II-III pyramidal neurons. The NOMA-GAP mutant construct lacking the PX domain (delPX) was expressed in layer II-III neurons by *in utero* electroporation at E15.5 in wild type NMRI brains. For visualization and as control membrane targeted GFP was co-electroporated. Dendritic morphology of pyramidal neurons for GFP fluorescence was analyzed in of P23 brain sections. (A) Representative average projections of z-stack images of GFP fluorescence in layer II-III neurons with or without delPX NOMA-GAP expression. (B) Quantification of the average number of primary dendrites of layer II-III neurons. Student´s t test, p = 0.2965. (C) Sholl profile of layer II-III pyramidal neurons expressing GFP alone as a control or GFP together with delPX NOMA-GAP. (D) Quantification of the average number of total dendritic intersections with concentric circles per neuron. Student´s t test, p = 0.7599. n = 30 N+/+ and 30 N+/+ (+delPX) layer II-III pyramidal neurons in the somatosensory cortex from three animals per condition.

3.2.3 NOMA-GAP regulates dendritic spine development in basal but not apical dendrites

NOMA-GAP is expressed in the mouse neocortex during the first weeks after birth, that is a time period critical for formation and maturation of dendritic spines and synapses (Rosário et al., 2012). Previously, Liu and colleagues detected an alternatively spliced isoform of NOMA-GAP, which is not present in humans, in the postsynaptic fraction of adult mouse brain lysates (Liu et al., 2006). I observed that tagged NOMA-GAP accumulates in dendritic spine heads in mature cortical neurons (Figure 14). Therefore, we hypothesized that NOMA-GAP might be involved in dendritic spine development.

First, I evaluated dendritic spine morphology of cultured cortical neurons by measuring protrusion density, distribution of protrusion types, dendritic spine neck length and spine head width (Figure 18). I transfected NOMA-GAP-deficient and heterozygous primary cortical neurons with eGFP at DIV14 for visualization of dendritic protrusions and subsequently imaged dendritic segments at DIV20 (Figure 18A). Quantification of NOMA-GAP-deficient cortical neurons compared to heterozygous controls showed no significantly difference in protrusion density (Figure 18B), distribution of mushroom/thin, stubby, atypical dendritic spines and filopodia along dendritic segments (Figures 16C) and spine head width (Figures 18F and 18G). However, NOMA-GAP-deficient neurons possess dendritic spines with significant longer spine necks (1.171 ± 0.066 µm) compared to heterozygous control neurons (0.958 ± 0.049 µm) (Figure 18D). A cumulative frequency plot of spine neck lengths illustrates a shift towards longer spine necks in NOMA-GAP-deficient primary neurons compared to heterozygous controls (Figure 18E). This indicates that the loss of NOMA-GAP in cultured cortical neurons leads to immature looking dendritic spines with significantly longer spine necks.

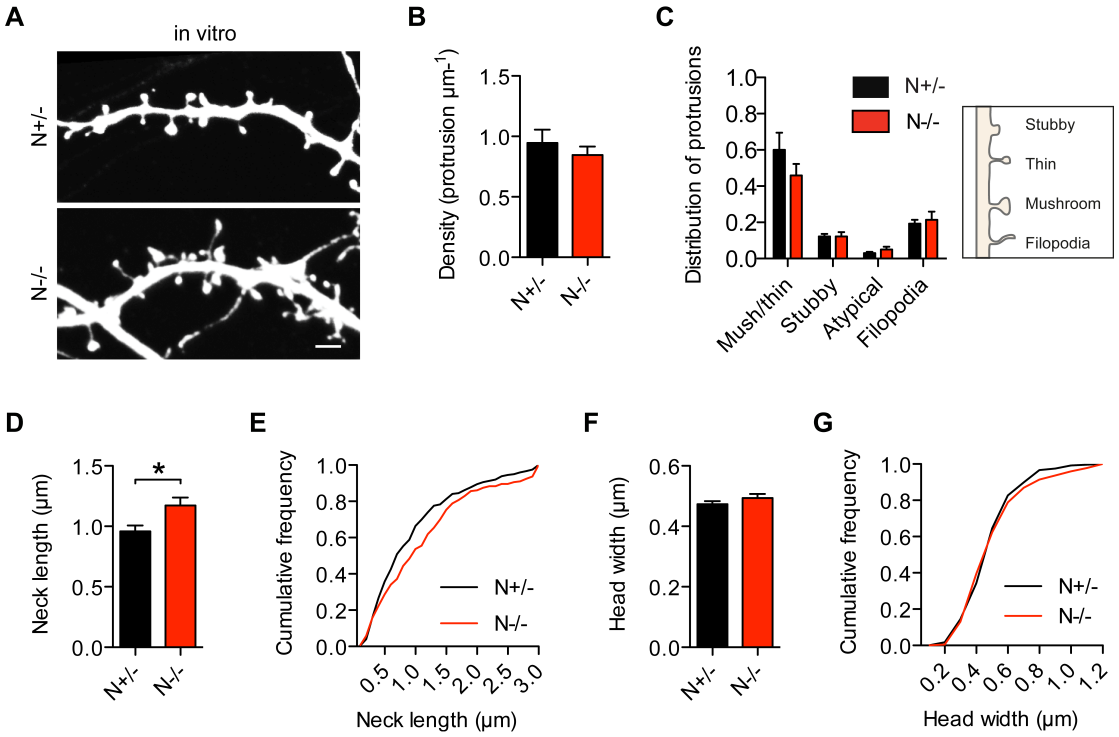

Figure 18: Cultured cortical neurons without NOMA-GAP showed longer dendritic spine necks. (A) Representative dendritic segments of NOMA-GAP-deficient and heterozygous control neurons, which were transfected with eGFP at DIV14 and visualized at DIV20. Scale bar = 2 µm. (B) Mean protrusion density. n = 7 N+/- and 7 N-/- dendritic segments of approximate length of 60 µm. Student´s t test, $p = 0.4570$. (C) Distribution of dendritic protrusion from dendrites between mushroom/thin, stubby, atypical spines and filopodia. Student´s t test, $p = 0.238$ for mush/thin; $p = 0.995$ for stubby. Mann-Whitney U test, $p = 0.295$ for atypical; $p = 0.671$ filopodia. (D) Mean spine neck length. n = 277 N+/- and 223 N-/-. Mann-Whitney U test, $*p = 0.0160$. (E) Cumulative frequency plot of spine neck length. (F) Mean spine head width. n = 277 N+/- and 223 N-/-. Mann-Whitney U test, $p = 0.8640$. (G) Cumulative frequency plot of spine head width. Modified after Schuster et al., 2015.

In order to investigate the influence of NOMA-GAP on the development of dendritic spines *in vivo*, eGFP was expressed in layer II-III pyramidal neurons by *in utero* electroporation of NOMA-GAP-deficient and heterozygous control littermate animals at E15.5. I harvested electroporated animals at P23 and imaged dendritic spines along basal dendrites of layer II-III pyramidal neurons in the somatosensory cortex (Figure 19A). Dendritic spine density along basal dendrites of layer II-III neurons was significantly increased from 1.997 ± 0.053 spines μm^{-1} in heterozygous control animals to 2.267 ± 0.050 spines μm^{-1} in NOMA-GAP-deficient mice (Figure 19B). Classification into mushroom/thin, stubby, atypical spines and filopodia showed no alteration in the distribution of protrusion types in NOMA-GAP-deficient animals along basal dendrites (Figure 19C). As seen *in vitro*, dendritic spines of NOMA-GAP-deficient neurons showed a significant increase in spine neck length *in vivo* (0.799 ± 0.019 µm) compared to heterozygous control animals (0.712 ± 0.017 µm) (Figure 19D).

Cumulative frequency plot of basal dendritic spine neck length illustrates a shift towards longer spine necks in NOMA-GAP-deficient animals compared to control animals (Figure 19C). I observed no change in dendritic spine head width in basal dendrites in the absence of NOMA-GAP compared to heterozygous control (Figures 19F and 19G).

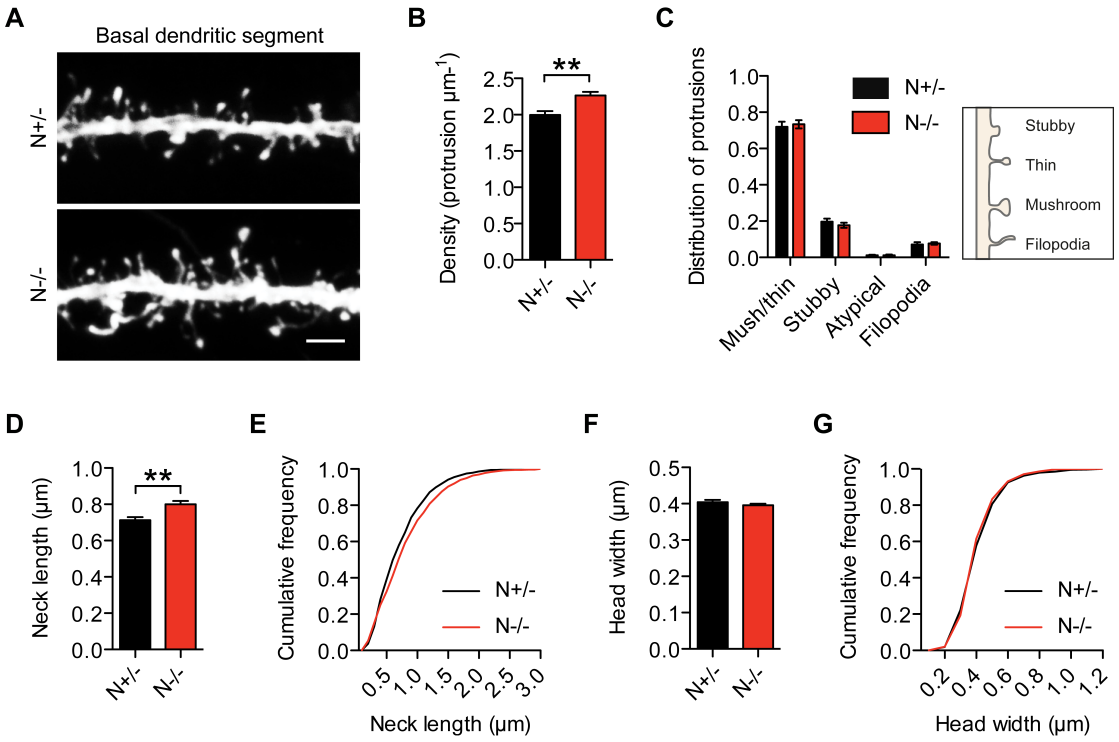

Figure 19: Basal spine neck length and spine density is increased in NOMA-GAP-deficient layer II-III neurons of the neocortex. (A) Representative basal dendritic segments of NOMA-GAP-deficient and heterozygous control layer II-III pyramidal neurons expressing eGFP, visualized at P23 following *in utero* electroporation at E15.5. Scale bar = 2 µm. (B) Mean spine density of basal dendrites. n = 13 N+/- and 14 N-/- dendritic segments of approximate length of 40 µm. Student´s t test, $^{**}p = 0.0011$. (C) Distribution of dendritic protrusion from basal dendrites between mushroom/thin, stubby, atypical spines and filopodia. Student´s t test, $p = 0.680$ mush/thin; $p = 0.372$ for stubby. Mann-Whitney U test, $p = 0.316$ for atypical and $p = 0.254$ for filopodia. (D) Mean spine neck length of basal dendrites. n = 615 N+/- and 765 N-/-. Mann-Whitney U test, $^{**}p = 0.0050$. (E) Cumulative frequency plot of dendritic spine neck length in basal dendrites. (F) Mean spine head width of basal dendrites. n = 615 N+/- and 765 N-/-. Mann-Whitney U test, $p = 0.6725$. (G) Cumulative frequency plot of dendritic spine head width in basal dendrites. Three animals per genotype were used. Modified after Schuster et al., 2015.

Basal and apical dendrites of layer II-III pyramidal neurons receive synaptic inputs from different areas of the brain (Spruston, 2008). I analyzed whether density and morphology of dendritic spines might be differentially regulated by NOMA-GAP in apical and basal dendrites of layer II-III pyramidal neurons. Dendritic spines along apical dendrites of GFP expressing layer II-III neurons in the somatosensory cortex

were imaged at P23 (Figure 20A). Interestingly no significant difference in spine density (Figure 20B), distribution of mushroom/thin, stubby, atypical spines and filopodia was observed along apical dendrites of NOMA-GAP-deficient animals (Figure 20C), spine neck length (Figures 20D and 20E) and spine head width (Figures 20F and 20G) along apical dendrites of NOMA-GAP-deficient animals compared to heterozygous controls. This result reveals that NOMA-GAP differentially regulates dendritic spine density and morphology in layer II-III neurons. While NOMA-GAP plays an important role in the appearance and morphology of dendritic spines along basal dendrites, it seems to be dispensable for dendritic spine formation and morphology along apical dendrites.

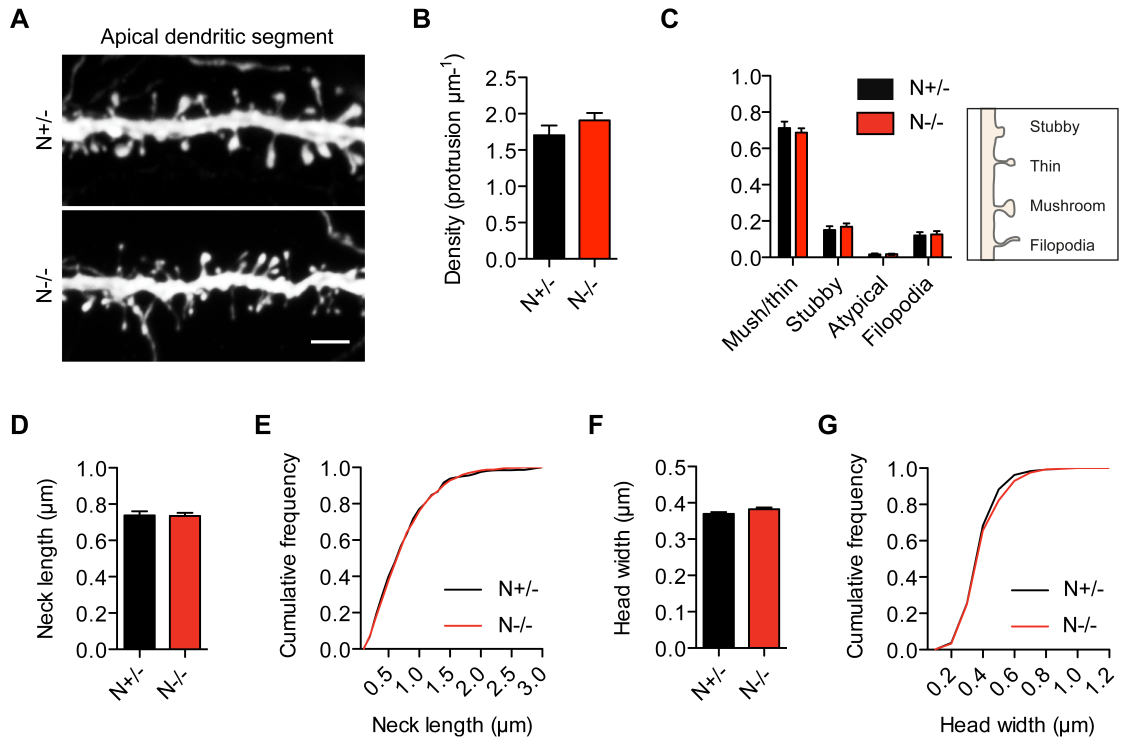

Figure 20: Apical dendritic spine density and morphology are not affected in NOMA-GAP-deficient layer II-III pyramidal neurons. (A) Representative apical dendritic segments of control heterozygous and NOMA-GAP-deficient layer II-III pyramidal neurons expressing eGFP, visualized at P23 following *in utero* electroporation at E15.5. Scale bar = 2 µm. (B) Mean spine density. n = 10 N+/- and 13 N-/- apical dendritic segments of approximate length of 40 µm. Student´s t test, p = 0.5102. (C) Distribution of dendritic protrusion from apical dendrites between mushroom/thin, stubby, atypical spines and filopodia. Student´s t test, p = 0.540 for mush/thin; p = 0.511 for stubby. Mann-Whitney U test, p = 0.888 for atypical; p = 0.877 for filopodia. (D) Mean apical spine neck length. n = 532 N+/- and 761 N-/-. Mann-Whitney U test, p = 0.6984. (E) Cumulative frequency plot of apical spine neck length. (F) Mean spine head width of apical dendrites. n = 532 N+/- and 761 N-/-. Mann-Whitney U test, p = 0.1709. (G) Cumulative frequency of apical dendritic spine head width. Three animals per genotype were used.

3.3 NOMA-GAP regulates the composition of the postsynaptic density

3.3.1 NOMA-GAP regulates synapse density

Dendritic spines are postsynaptic structures of excitatory synapses (Yuste, 2011). Since NOMA-GAP regulates spine morphology, loss of NOMA-GAP might affect excitatory synapse formation. First, I quantified the number of excitatory synapses by the opposing expression of the presynaptic marker synaptophysin and the postsynaptic marker PSD-95 in mature cortical neurons. I transfected cultured cortical neurons at DIV14 with eGFP and stained for GFP, synaptophysin and PSD-95 at DIV20 (Figure 21A). Loss of NOMA-GAP in cultured cortical neurons results in a significant reduction of excitatory synapses containing synaptophysin and PSD-95 compared to heterozygous controls (Figure 21B).

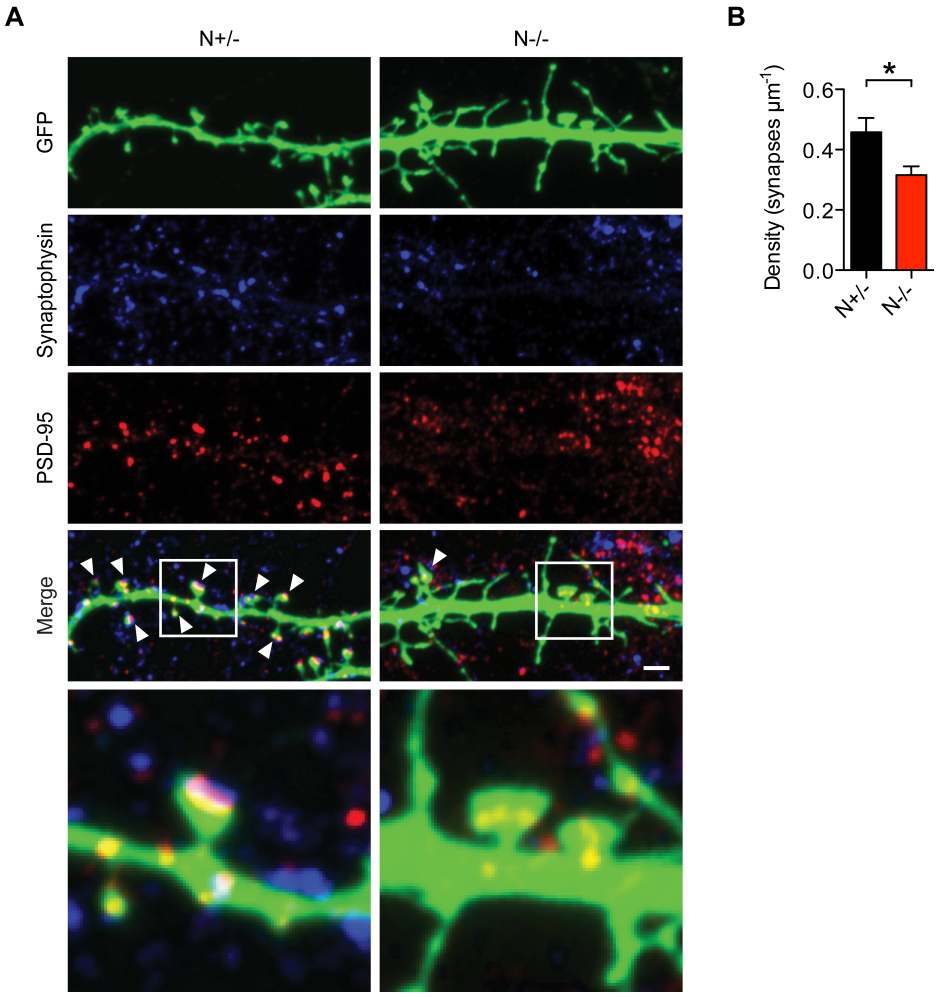

Figure 21: Cultured NOMA-GAP-deficient neurons show a decrease in the number of synapses. (A) Dendritic segments from cultured cortical neurons at DIV20 expressing GFP and stained for

endogenous synaptophysin (presynpatic) and endogenous PSD-95 (postsynaptic). Arrowheads indicate the opposing expression of synaptophysin and PSD-95. Scale bar = 2 µm. (B) Mean density of synaptophsyin and PSD-95 positive synapses. n = 15 N+/- and 12 N-/- dendritic segments with approximate length of 60 µm. Students t test, $*p = 0.0244$. Modified after Schuster et al., 2015.

Since NOMA-GAP accumulates in dendritic spine heads of mature cortical neurons, I investigated whether NOMA-GAP co-localizes with the postsynaptic scaffold protein PSD-95. Cultured cortical neurons were infected with a lentiviral GFP-tagged NOMA-GAP expression vector at DIV10 and stained for endogenous PSD-95 and GFP at DIV20 (Figure 22). Indeed, GFP-tagged NOMA-GAP co-localizes with endogenous PSD-95 at dendritic spine heads of mature cortical neurons (Figure 22, arrowhead magnified panel). Interestingly, GFP-tagged NOMA-GAP does not seem to co-localize with extrasynaptic PSD-95 in the dendritic shaft (Figure 22, open arrowhead in magnified panel).

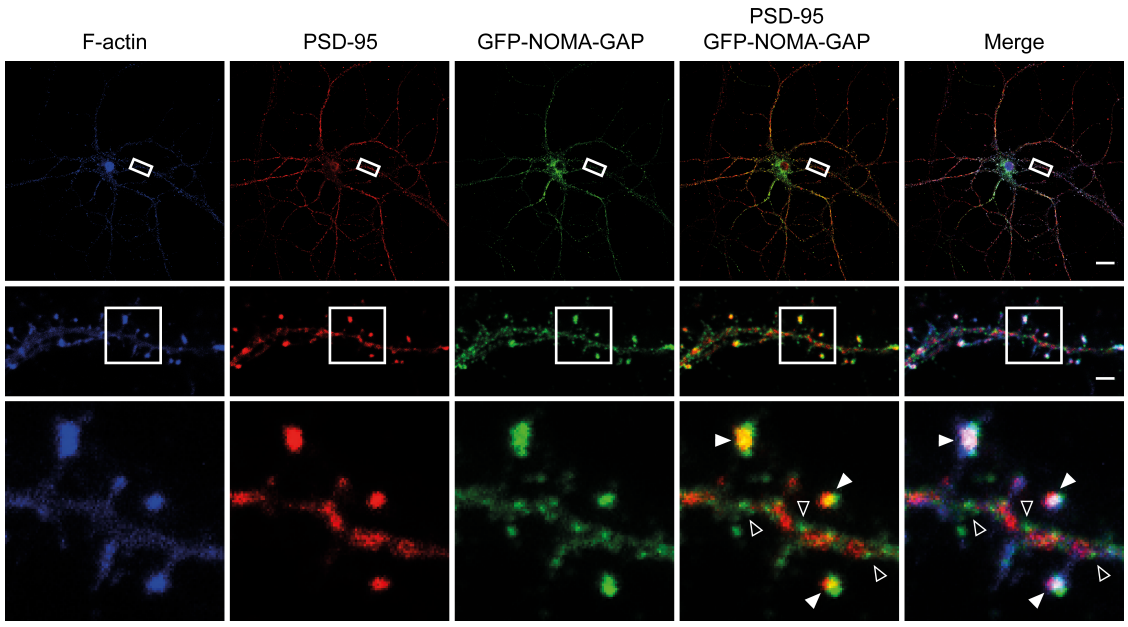

Figure 22: NOMA-GAP co-localize with PSD-95 in dendritic spine heads but not in the dendritic shaft. Primary cortical neurons where infected with lentiviral vector expressing GFP-tagged NOMA-GAP at DIV10 and stained for F-actin (blue), endogenous PSD-95 (red) and GFP (green) at DIV20. Scale bars = 20 µm (upper panel) and 2 µm (middle panel). Modified after Schuster et al., 2015.

3.3.2 NOMA-GAP interacts with TrkB receptor and MAGUK family proteins

Previously, Rosário and colleagues showed that NOMA-GAP directly interacts with TrkA (Rosário et al., 2007). Since BDNF binding to TrkB has emerged as a key signaling during neural circuit development and function, I examined whether NOMA-GAP might interact with TrkB (Park and Poo, 2013). In addition, PSD-95 and TrkB have been found in the same complex *in vivo*, although they do not interact directly (Ji et al., 2005; Kato et al., 2004).

Immunoprecipitations of endogenous NOMA-GAP were performed using an antibody against N-terminal or C-terminal sequences, and cortical lysates of adult wild type mice. Interestingly, Trks and endogenous PSD-95 co-immunoprecipitated together with NOMA-GAP from cortical lysates, showing that NOMA-GAP exists in a complex with both, Trk-receptors and PSD-95 *in vivo* (Figure 23A). Subsequently, I tested if NOMA-GAP might interact directly with PSD-95 and the most prominent Trk-receptor family member in the brain, TrkB. To examine this, I overexpressed tagged proteins of PSD-95, TrkB and NOMA-GAP in HEK 293 cells, since this cell line does not express NOMA-GAP or any other synaptic proteins and tested if PSD-95 and TrkB could co-immunoprecipitate with NOMA-GAP (Figure 23B). PSD-95 and TrkB can be co-immunprecipitated with NOMA-GAP, suggesting that NOMA-GAP interacts directly with PSD-95 and TrkB (Figure 23B). However, other proteins expressed in HEK cells may bridge the interaction. Thus, the interaction of NOMA-GAP with TrkB seems to be increased when PSD-95 is co-expressed.

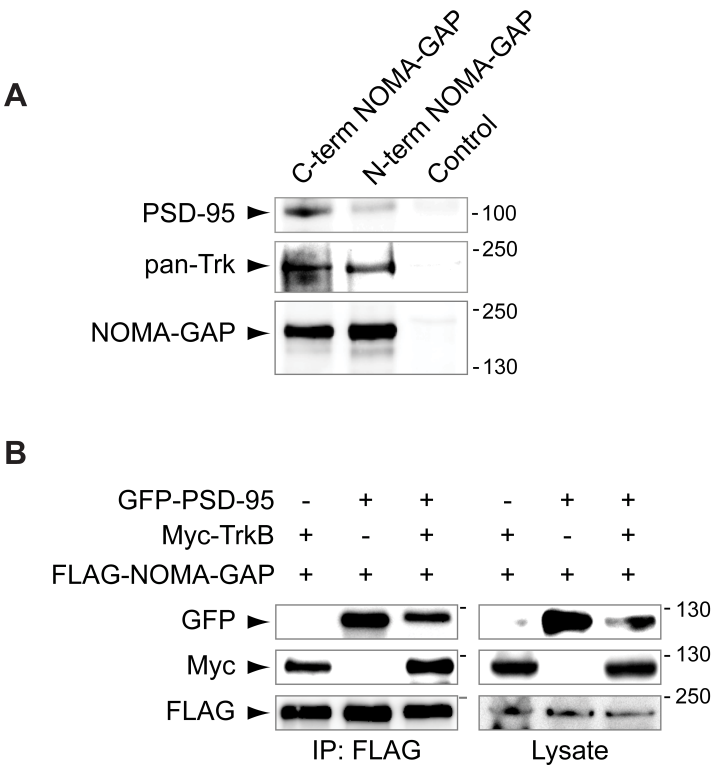

Figure 23: NOMA-GAP interacts with PSD-95 and TrkB receptor. (A) NOMA-GAP exists in a complex *in vivo* with PSD-95 and Trk-receptors. Endogenous NOMA-GAP was immunoprecipitated from adult mouse cortical lysates using antibodies against a C-terminal or N-terminal sequence. NOMA-GAP immunoprecipitates were probed for the presence of endogenous PSD-95 and Trk-receptors. Modified after Schuster et al., 2015. (B) GFP-tagged PSD-95 and Myc-tagged TrkB were co-expressed together with FLAG-tagged NOMA-GAP in HEK 293 cells. The presence of GFP-tagged PSD-95 and Myc-tagged TrkB in anti-FLAG immunoprecipitates was detected by western blotting as indicated.

PSD-95 belongs to the MAGUK protein family. Given that MAGUKs are highly conserved proteins, I tested whether NOMA-GAP interacts with other MAGUK family members. FLAG-tagged proteins of SAP97, PSD-93, SAP102 and PSD-95 were co-expressed together with Myc-tagged NOMA-GAP in HEK 293 cells and the presence of MAGUKs analyzed in anti-Myc immmunoprecipitates. In addition to PSD-95, I found that PSD-93 and SAP102 could interact with NOMA-GAP, but not SAP97 (Figure 24). This demonstrates that NOMA-GAP can directly interact with multiple MAGUK proteins.

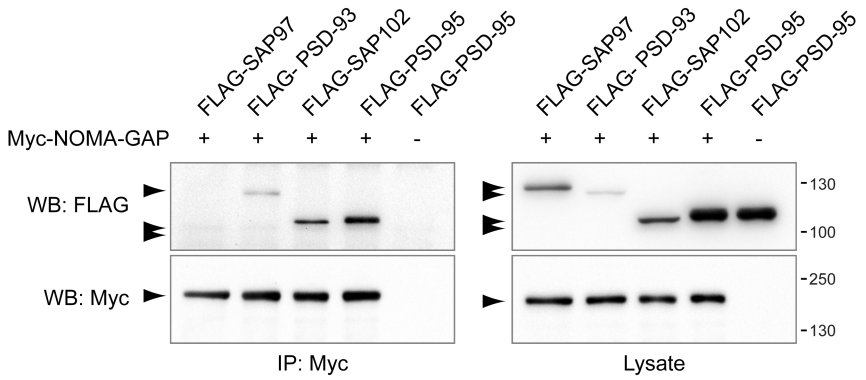

Figure 24: NOMA-GAP can interact with multiple MAGUK family proteins. FLAG-tagged MAGUK family proteins SAP97, PSD-93, SAP102 and PSD-95 were co-expressed with Myc-tagged NOMA-GAP in HEK 293 cells. The presence of FLAG-tagged MAGUK proteins in anti-Myc immunoprecipitates was detected by western blotting as indicated. Modified after Schuster et al., 2015.

3.3.3 NOMA-GAP regulates subcellular localization and phosphorylation of PSD-95

To shed light on the role of NOMA-GAP during excitatory synaptic development, I analyzed the enrichment of various proteins at excitatory synapses in the presence or absence of NOMA-GAP. I prepared crude synaptosomes from cortices of adult NOMA-GAP-deficient and wild type littermate animals. Synaptosomes are isolated synapses produced by subcellular fractionation of brain tissue and contain both the presynaptic terminal and the PSD. Preliminary results from western blot analyses demonstrated the enrichment of synaptic proteins in crude synaptosomal fractions (P2) compared to homogenates (H), including receptors (NMDAR1, NMDAR2B and Trk-receptors), cell adhesion proteins (EphA4 and ephrinB1/2/3), scaffold protein PSD-95, signaling protein Cdc42 and the presynaptic vesicle protein synaptophysin (Figure 25). In contrast, I detected decreased levels of phosphorylated Erk1/2 in synaptosomal fractions. By comparing NOMA-GAP-deficient with wild type crude synaptosomes, I observed decreased PSD-95 levels at synaptic structures in the absence of NOMA-GAP.

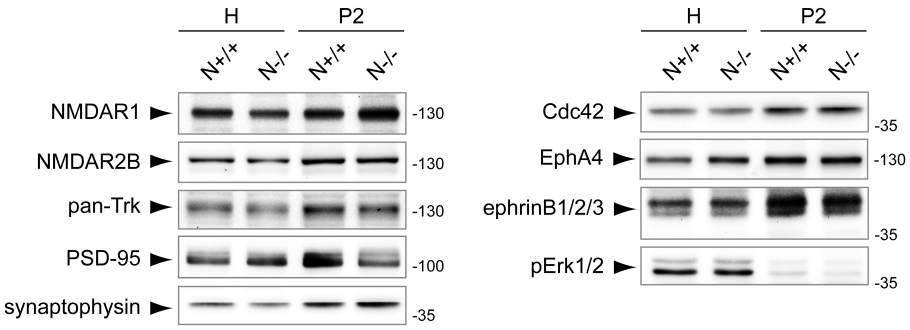

Figure 25: Decreased PSD-95 levels in NOMA-GAP-deficient cortical crude synaptosomes. Western blot analyses show enrichment of various synaptic proteins in cortical synaptosomes (P2) compared to total protein lysates (H), including NMDAR1, NMDAR2B, pan-Trk, synaptophysin, EphA4, ephrinB1/2/3 and Cdc42. Levels of phospho-Erk1/2 levels were decreased in P2 compared to H. Crude synaptosomes from NOMA-GAP-deficient compared to wild type cortices showed decreased PSD-95 levels.

Given that PSD-95 levels were decreased in NOMA-GAP-deficient cortical crude synaptosomes, I explored the role of NOMA-GAP in regulating the subcellular localization of PSD-95 more closely. NOMA-GAP-deficient and heterozygous cortical neurons, transfected with eGFP at DIV14, were stained for endogenous PSD-95 at DIV20 (Figure 26A). In heterozygous control neurons, PSD-95 clusters are mostly concentrated at the spine head and absent from the neck of dendritic spines. In contrast, NOMA-GAP-deficient neurons showed PSD-95 clusters in the spine head, but in addition a significant increase in PSD-95 clusters in the neck of dendritic spines (Figure 26B). These results suggest that NOMA-GAP modulates synaptic clustering of PSD-95 in cortical neurons.

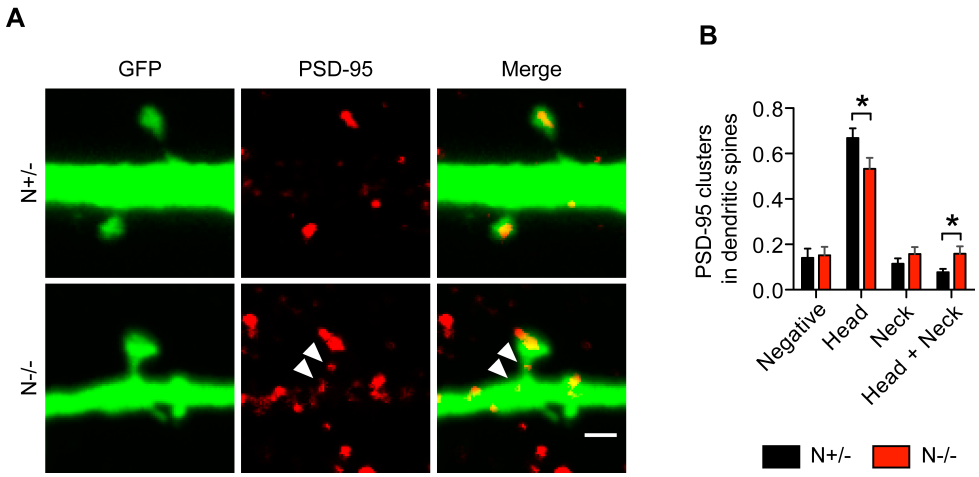

Figure 26: NOMA-GAP regulates PSD-95 clustering and the subcellular localization of PSD-95 in cortical neurons. (A) Representative dendritic segments of eGFP expressing NOMA-GAP-deficient and heterozygous control cortical neurons (DIV20), stained for endogenous PSD-95 (shown in red). Scale bar = 1 µm. (B) Quantification of the number of PSD-95 clusters in dendritic spine head and/or spine

neck. n = 13 N+/+ and 12 N-/- dendritic segments of a mean length of 60 µm. Student´s t tests, $p = 0.9348$ for PSD-95 negative, $*p = 0.0475$ for PSD-95 only in spine head; $p = 0.2803$ for PSD-95 only in spine neck, $*p = 0.0286$ for PSD-95 in spine head and neck. Modified after Schuster et al., 2015.

Synaptic localization of PSD-95 is thought to be regulated by posttranslational modifications including palmitoylation, ubiquitination and phosphorylation (Colledge et al., 2003; Kim et al., 2007; Perez de Arce et al., 2010; Yoshii et al., 2011). Both, phosphorylation of serine and tyrosine residues of PSD-95 have been reported to regulate synaptic localization and excitatory synapse formation (Kim et al., 2007; Perez de Arce et al., 2010). To characterize the interaction between NOMA-GAP with PSD-95 more closely, we analyzed the phosphorylation state of PSD-95 in the neocortex of adult NOMA-GAP-deficient compared to wild type littermate animals (Figure 27). Endogenous PSD-95 was immunoprecipitated from NOMA-GAP-deficient and wild type cortical lysates and probed for tyrosine phosphorylation (Figure 27A). Quantification of the level of specific tyrosine phosphorylated PSD-95 in immunoprecipitates of adult cortices revealed no difference between NOMA-GAP-deficient and wild type cortices (Figure 27B). However, quantification of the phosphorylation levels of PSD-95 in endogenous immunoprecipitates and in whole cell lysates of adult mouse cortices showed a two fold increase in serine 295 phosphorylation of PSD-95 in NOMA-GAP-deficient animals (Figures 27C and 27D). This result indicates that NOMA-GAP is an important regulator of PSD-95 phosphorylation in the mouse neocortex.

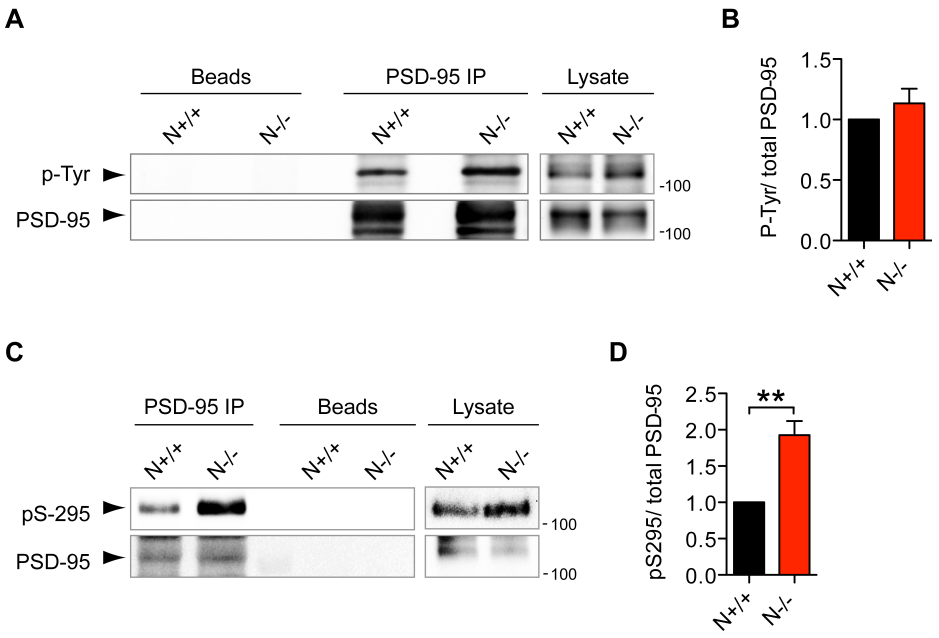

Figure 27: NOMA-GAP regulates the phosphorylation state of PSD-95 *in vivo*. (A) The levels of tyrosine phosphorylation of PSD-95 were analyzed in immunoprecipitates of endogenous PSD-95 and in

whole cell lysates of adult NOMA-GAP-deficient and wild type mouse cortices. (B) Quantification of the level of tyrosine phosphorylated PSD-95 per total PSD-95 in immunoprecipitates of adult mouse cortices. Four independent experiments were performed. Student´s t test, $p = 0.3453$. (C) The levels of serine 295 phosphorylation of PSD-95 were analyzed in immunoprecipitates and whole cell lysates of adult NOMA-GAP-deficient and wild type mouse cortices. (D) Quantification of the level of serine 295 phosphorylated PSD-95 per total PSD-95 in whole cell lysates of adult mouse cortices. Five independent experiments were performed. Student´s t test, $^{**}p = 0.0091$. Modified after Schuster et al., 2015.

Phosphorylation of PSD-95 at serine 295 has been described to localize PSD-95 specifically to postsynaptic sites (Kim et al., 2007). I stained mature cultured cortical neurons from NOMA-GAP-deficient and wild type littermate animals for PSD-95 phosphorylated at serine 295 and the dendritic marker MAP2 to analyze total fluorescence intensity and subcellular localization (Figure 28A). Analysis of phospho-serine 295 fluorescence intensity measurements showed a significant increase in NOMA-GAP-deficient neurons compared to control (Figure 28B). As reported previously for wild type neurons, pS295 PSD-95 was mostly localized to dendritic spine heads. However, in NOMA-GAP-deficient neurons PSD-95 phosphorylated at serine 295 was mostly localized to the dendritic shaft (Figure 28C). These results revealed, that NOMA-GAP is an important regulator of PSD-95 phosphorylation and subcellular localization.

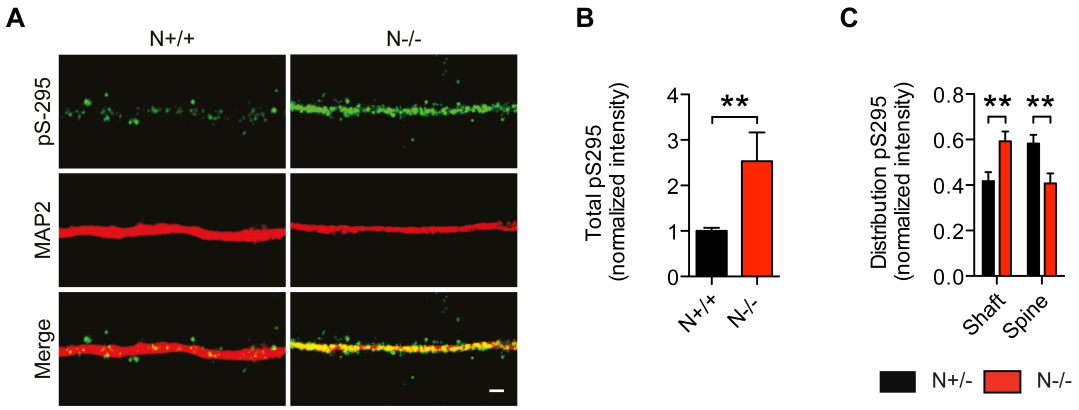

Figure 28: Serine 295 phosphorylated PSD-95 is mislocalized in NOMA-GAP-deficient cultured cortical neurons. (A) Dendritic segments of NOMA-GAP-deficient and wild type mature cortical neurons at DIV 22 stained for pS295 PSD-95 (shown in green) and for the dendritic marker MAP2 (shown in red). Scale bar = 2 µm. (B) Quantification of total fluorescence intensity of serine 295 phosphorylated PSD-95 in dendritic segments of NOMA-GAP-deficient and wild type neurons. n = 10 N+/+ and 10 N-/- dendritic segments of a mean length of 60 µm. Mann-Whitney U test, $^{**}p = 0.0052$. (C) Localization of pS295 PSD-95 in the dendritic shaft (MAP2+) and dendritic spines (MAP2-) of NOMA-GAP-deficient and wild type littermate neurons. n = 10 N+/+ and 10 N-/- dendritic segments of a mean length of 60 µm. Student´s t test, $^{**}p_{\text{Shaft}} = 0.0078$, $^{**}p_{\text{Spines}} = 0.0078$. Modified after Schuster et al., 2015.

3.3.4 PSD-95 regulates Cdc42-GAP activity of NOMA-GAP

Our group identified that the binding site of PSD-95 lies in close proximity to the RhoGAP domain of NOMA-GAP. This raised the possibility that interaction with PSD-95 could regulate the RhoGAP activity of NOMA-GAP towards Cdc42. To test this, we expressed NOMA-GAP in the absence or presence of PSD-95 in HEK 293 cells and analyzed Cdc42 mediated downstream signaling by western blot (Figure 29). Activation of Cdc42 and thus downstream phosphorylation of PAK1/2 was induced by epidermal growth factor (EGF) stimulation. As expected, expression of NOMA-GAP reduced phosphorylation of PAK1/2 implying inhibition of Cdc42 signaling. Supporting our hypothesis, co-expression of increasing levels of PSD-95 counteracted NOMA-GAP-mediated inhibition of PAK1/2 phosphorylation. In contrast, EGF-induced ERK1/2 MAP kinase phosphorylation was not affected by expression of NOMA-GAP or PSD-95. This result suggests that interaction with PSD-95 inhibits the Cdc42-GAP activity of NOMA-GAP.

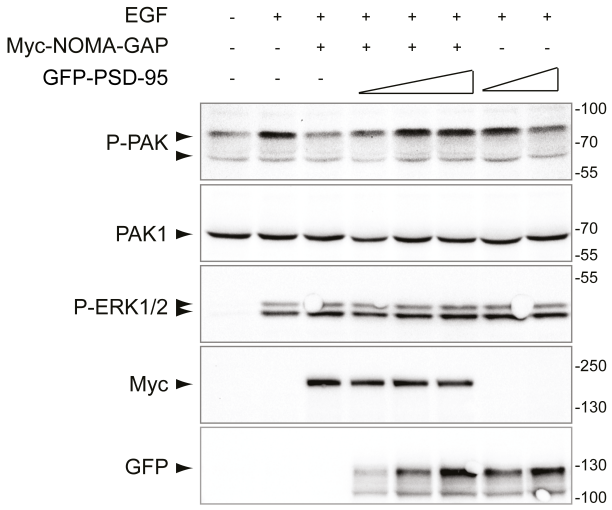

Figure 29: PSD-95 interaction inhibits the RhoGAP activity of NOMA-GAP towards Cdc42. Representative western blots of HEK 293 cell lysates, which expressed Myc-tagged NOMA-GAP in the absence or presence of increasing levels of GFP-tagged PSD-95. Activation of Cdc42 signaling and thus phosphorylation of endogenous PAK1/2 was achieved by a 10min stimulation with 100 µg/ml EGF. Modified after Schuster et al., 2015.

3.3.5 NOMA-GAP regulates surface expression of GluR1

Various studies suggest a key role for PSD-95 in regulating synaptic AMPAR trafficking and clustering (Béïque et al., 2006; El-Husseini et al., 2000; Huganir and Nicoll, 2013; Schnell et al., 2002; Stein et al., 2003). We hypothesized that loss of NOMA-GAP and thus aberrant localization of PSD-95 may cause reduced surface AMPARs. To test this,

I performed immunostainings for either total or only surface expressed AMPAR subunit GluR1 in NOMA-GAP-deficient and wild type cortical neurons at DIV22 (Figures 30A and 30C). Quantification of immunostainings for total GluR1 showed no difference in the fluorescence level in dendrites of NOMA-GAP-deficient neurons (Figure 30B). However, quantification of immunostainings for surface expressed GluR1 in dendrites showed a significant reduction in NOMA-GAP-deficient neurons compared to wild type controls (Figure 30D). To verify these results, I labeled surface proteins on NOMA-GAP-deficient and wild type cultured cortical neurons by biotinylation and performed protein pulldown of biotinylated proteins (Figure 30E). Quantification of GluR1 levels in biotinylated protein pulldown showed a significant reduction of GluR1 from the surface of NOMA-GAP-deficient neurons compared to wild type (Figure 30F). These results suggest, that NOMA-GAP plays a critical role in determining the number of AMPARs in synaptic membranes.

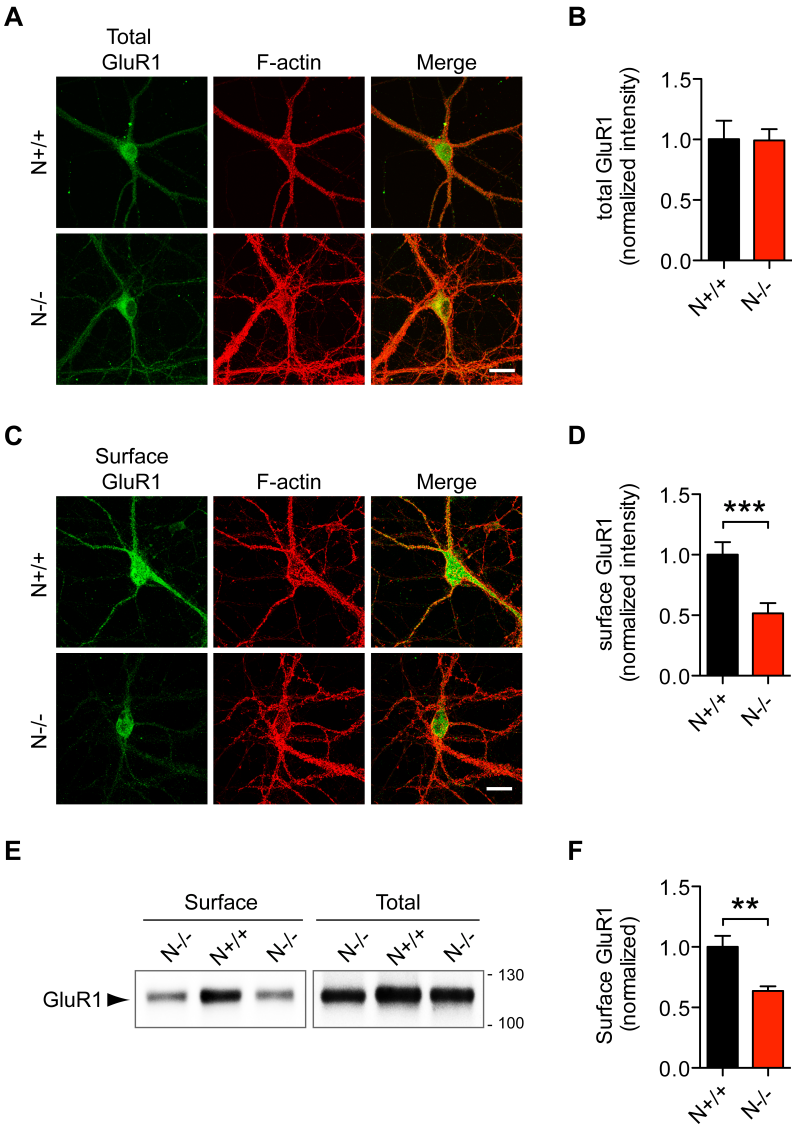

Figure 30: NOMA-GAP regulates surface expression of GluR1. (A) Permeabilized NOMA-GAP-deficient and wild type cortical neurons were stained at DIV22 for total expression of endogenous GluR1 (shown in green) and F-actin (shown in red). Scale bar = 20 µm. (B) Quantification of normalized fluorescence intensity of total GluR1 expression in permeabilized NOMA-GAP-deficient and wild type cortical neurons. n = 12 N+/+ and 12 N-/-. Student´s t test, p = 0.2727. (C) Non-permeabilized NOMA-GAP-deficient and wild type cortical neurons were stained at DIV22 for surface expression of endogenous GluR1 (shown in green) and after permeabilization for F-actin (shown in red). Scale bar = 20 µm. (D) Quantification of normalized fluorescence intensity of surface GluR1 expression in non-permeabilized NOMA-GAP-deficient and wild type cortical neurons. n = 10 N+/+ and 10 N-/-. Student´s t test, ***p < 0.0001. (E) Surface expressed proteins of NOMA-GAP-deficient and wild type cultured cortical neurons (DIV20-22) were labeled with biotin. Biotinylated proteins were precipitated and the levels of labeled and total GluR1 were analyzed by western blotting. (F) Quantification of surface biotinylated GluR1 in NOMA-GAP-deficient and wild type neurons. n = 9 N+/+ and 10 N-/-. Student´s t test, **p = 0.0015. Modified after Schuster et al., 2015.

3.4 Inhibition of Cdc42 signaling by NOMA-GAP is critical for dendritic branching but not for dendritic spine morphology

3.4.1 NOMA-GAP promotes dendritic complexity by inhibition of Cdc42 signaling

Previously, our group showed that the RhoGAP domain of NOMA-GAP specifically inactivates the RhoGTPase Cdc42 and that loss of NOMA-GAP leads to elevated levels of active Cdc42 in the neocortex (Rosário et al., 2007, 2012). To test whether elevated levels of Cdc42 impairs proper dendritic branching of layer II-III pyramidal neurons, a constitutively active mutant of Cdc42, V12 Cdc42, was expressed *in vivo* together with a membrane-targeted GFP construct by *in utero* electroporation in wild type NMRI mice at E15.5. Expression of V12 Cdc42 was under control of the neuron-specific postmitotic promoter NeuroD1. I imaged GFP fluorescence of layer II-III pyramidal neurons in the primary somatosensory cortex at P23 (Figure 31A). Post-mitotic expression of V12 Cdc42 does not affect the number of primary dendrites per neuron (Figure 31B). However, Sholl analysis revealed that overexpression of V12 Cdc42 in wild type layer II-III neurons lead to a downward shift of the dendritic intersection curve and a significant reduction in total number of dendritic intersections with concentric circles per neuron compared to GFP control (Figures 31C and 31D). Thus, increased Cdc42 activity in layer II-III pyramidal neurons leads to a reduction in dendritic complexity.

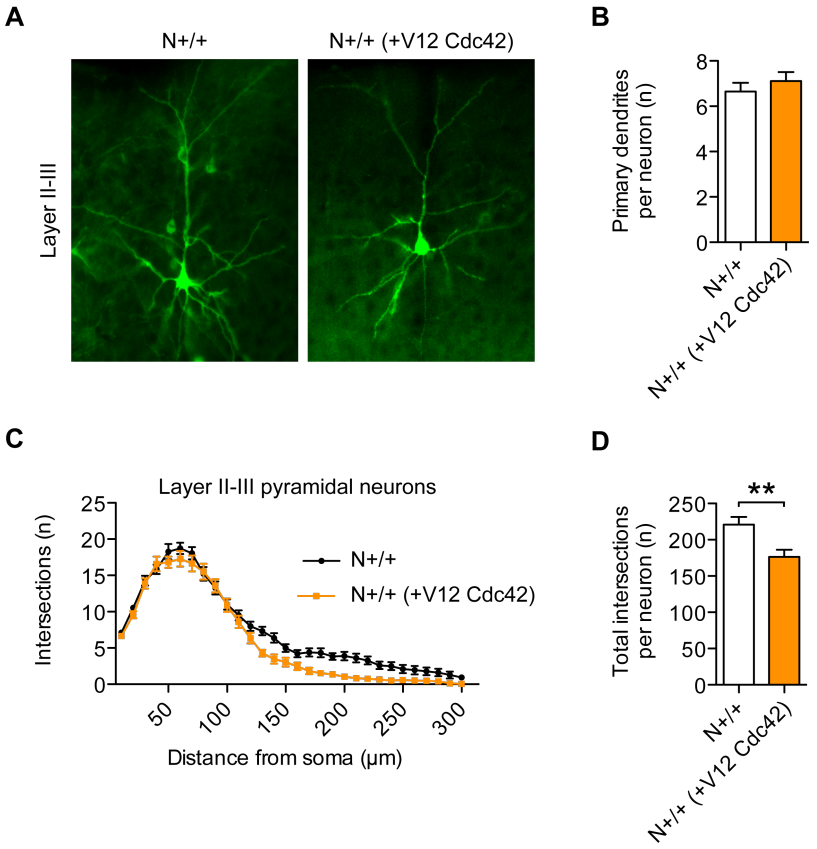

Figure 31: Post-mitotic expression of constitutively active Cdc42 (NeuroD1 - V12 Cdc42) impairs dendritic complexity of layer II-III pyramidal neurons. (A) Representative z-stack projections of layer II-III pyramidal neurons in cortical slices of P23 animals expressing membrane targeted GFP alone or V12 Cdc42 and membrane targeted GFP. V12 Cdc42 was expressed under the control of the NeuroD1 promoter in post-mitotic pyramidal neurons by *in utero* electroporation of wild type NMRI strain at E15.5. Membrane targeted GFP was co-electroporated to visualize neuronal morphology. (B) Quantification of the number of primary dendrites per neuron. Student´s t test, p = 0.4059. (C) Sholl profile of wild type layer II-III neurons expressing GFP alone as a control or GFP together with V12 Cdc42. (D) The average number of total dendritic intersections with concentric circles per layer II-III neuron. Student´s t test, $^{**}p$ = 0.0048. n = 18 N+/+ and 17 N+/+ (+V12 Cdc42) layer II-III pyramidal neurons from three and two animals, respectively. Modified after Rosario et al., 2012.

To test if elevated levels of active Cdc42 downstream of NOMA-GAP inhibit dendritic branching in NOMA-GAP-deficient animals, I used a mouse line where NOMA-GAP-deficient animals had been crossed to floxed Cdc42 and Nex1-Cre animals (Figure 32A). This line enables the reduction of Cdc42 expression by conditional deletion using the cre/loxP system. Since it was shown that Cdc42 activity is necessary for neural precursor function (Cappello et al., 2006), it was important to express Cre recombinase only in post-mitotic pyramidal neurons. For this reason, a Nex1-Cre mouse line was used, in which the Nex1 promoter driven Cre recombinase is expressed only in post-mitotic pyramidal neurons, but is absent from proliferating progenitors, interneurons, oligodendrocytes and astrocytes (Goebbels et al., 2006).

Western blot analysis showed that Nex1-cre-mediated post-mitotic deletion of Cdc42 was able to reduce protein levels in the neocortex of E17.5 animals (Figures 32B and 32C).

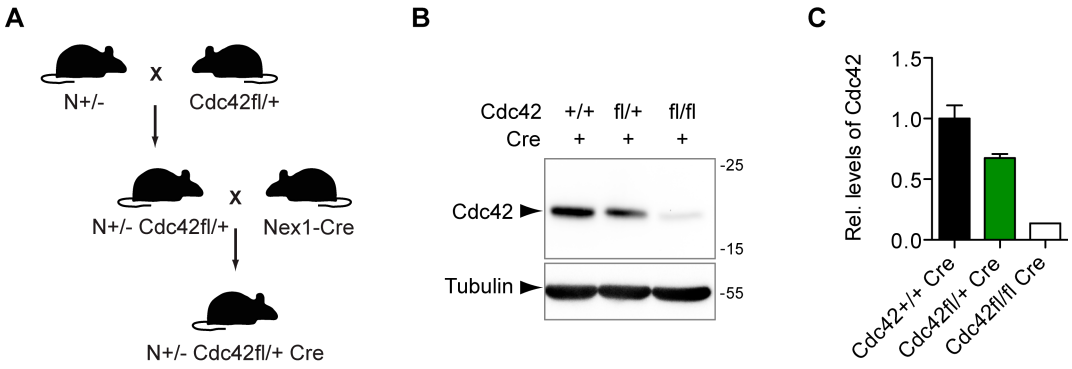

Figure 32: Protein-levels of Cdc42 can be decreased *in vivo* by Cre/loxP recombination. (A) Generation of floxed Cdc42 mice with post-mitotic Nex1-Cre recombinase expression. (B) Western blot analysis shows, that expression of Cre recombinase under the control of the Nex1 promoter deleted floxed Cdc42 alleles, which leads to decreased protein levels of Cdc42 in the neocortex of E17.5 mice. (C) Quantification of normalized Cdc42 protein expression in the neocortex of E17.5 animals, expressing Nex1-Cre recombinase and containing no, one or two floxed Cdc42 alleles. n = two, three and one animal, respectively. Modified after Rosario et al., 2012.

I imaged layer II-III pyramidal neurons in P25-26 adult brain sections that have been previously stained by our group using the Golgi-method and analyzed their dendritic complexity by Sholl analysis (Figure 33A). Nex1-Cre driven heterozygous deletion of Cdc42 in post-mitotic neurons did not affect the number of primary dendrites (Figure 33B). However, heterozygous deletion of Cdc42 in NOMA-GAP-deficient animals partially restored dendritic complexity, as seen by an increase of dendritic intersections with concentric circles and in the average number of total dendritic intersections with concentric circles per neuron (Figures 33C and 33D). These results reveal that post-mitotic inhibition of Cdc42 signaling by NOMA-GAP is necessary for dendritic branching and thus complexity of layer II-III pyramidal neurons in the neocortex.

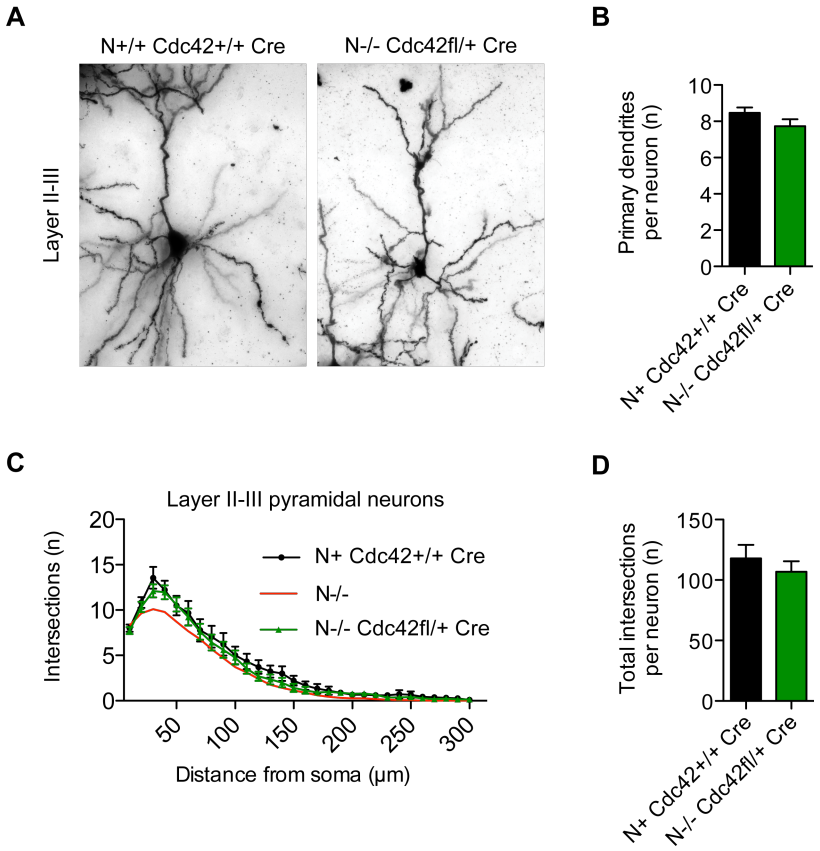

Figure 33: Postmitotic heterozygous deletion of Cdc42 in NOMA-GAP-deficient mice partially rescues dendritic branching of layer II-III neurons. (A) Representative z-stack projections of Golgi-stained layer II-III pyramidal neurons in cortical slices of P25-26 animals. (B) The average number of primary dendrites of N+ Cdc+/+ and N-/- Cdcfl/+ Cre layer II-III pyramidal neurons. Mann-Whitney U test, p = 0.1228. (C) Sholl profile of NOMA-GAP-deficient layer II-III pyramidal neurons show an improvement in dendritic complexity following deletion of one Cdc42 allele (N-/- Cdcfl/+ Cre), compared to N+ Cdc42+/+ Cre and N-/-. (D) Quantification of the average number of total intersections with concentric circles per neuron in N-/- Cdc42fl/+ Cre compared to N+ Cdc+/+ Cre control neurons. n = 18 N+ Cdc42+/+ Cre and 26 N-/- Cdc42fl/+ Cre layer II-III pyramidal neurons from two NMRI wild type animals each. Mann-Whitney U test, p = 0.3396. Modified after Rosario et al., 2012.

3.4.2 NOMA-GAP activates cofilin downstream of Cdc42 to promote dendritic branching

Our group showed that loss of NOMA-GAP leads to increased phosphorylation of PAK1/2 downstream of Cdc42 in the neocortex (Rosário et al., 2012). Our group performed phospho-immunoprecipitations from embryonic NOMA-GAP-deficient and wild type littermate cortices and analyzed these by mass spectrophotometry. In this screen, they detected elevated phosphorylation levels of the actin binding protein cofilin in NOMA-GAP-deficient mouse cortices. They were however unable to identify the phosphorylation site. The major phosphorylation site on cofilin is serine 3, which has been shown to inhibit the actin depolymerization activity of cofilin (Moriyama et al.,

1996). We therefore analyzed the level of phosphorylated cofilin at serine 3 in NOMA-GAP-deficient compared to heterozygous littermate animals by western blotting of E17.5 cortical lysates using a phospho-specific antibody (Figure 34A). I observed a two-fold increase in serine 3 phosphorylation of cofilin in cortical lysates derived from NOMA-GAP-deficient animals compared to heterozygous control (Figure 34B). This suggests that expression of NOMA-GAP regulates the activation of cofilin in the developing neocortex.

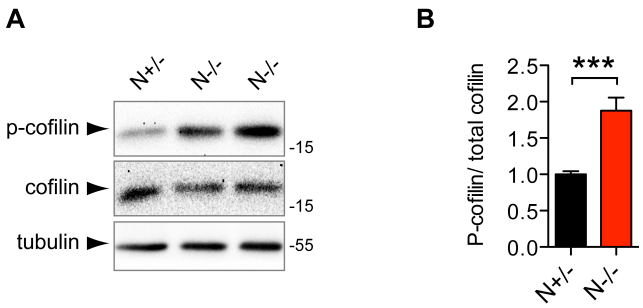

Figure 34: Loss off NOMA-GAP leads to increased phosphorylation of cofilin at serine 3 in the neocortex of E17.5 mice. (A) Total and phospho-Ser3 cofilin were detected by western blot of cortical lysates from E17.5 littermate embryos. (B) Quantification of phospho-Ser3 cofilin levels from western blot analysis, normalized to total cofilin. n = 14 N+/- and 16 N-/- E17.5 animals. Student´s t test, ****p* = 0.0001. Modified after Rosario et al., 2012.

Phosphorylation of cofilin at serine 3 and thus inactivation was shown to be mediated by LIMK (Arber et al., 1998; Yang et al., 1998). Furthermore it was reported that the Cdc42 effector PAK phosphorylates LIMK (Edwards et al., 1999) (Figure 35A). Since NOMA-GAP prevents phosphorylation of PAK and cofilin at serine 3, we hypothesized that we could restore increased PAK and cofilin phosphorylation by decreasing post-mitotic Cdc42 levels *in vivo*. My western blot analysis showed that phosphorylation of PAK (Figure 35B), LIMK (Figure 35C) and Ser3 cofilin (Figure 35D) are increased in the neocortex of NOMA-GAP-deficient animals compared to heterozygous controls at E17.5, containing either one floxed Cdc42 allele or expressing Cre under the NEX1 promoter. Importantly, Cre-mediated post-mitotic deletion of one Cdc42 allele was able to restore phosphorylation levels of PAK, LIMK and cofilin in NOMA-GAP-deficient cortices (Figures 35B, 35C and 35D). This suggests that NOMA-GAP regulates activation of cofilin activation through inhibition of Cdc42 signaling.

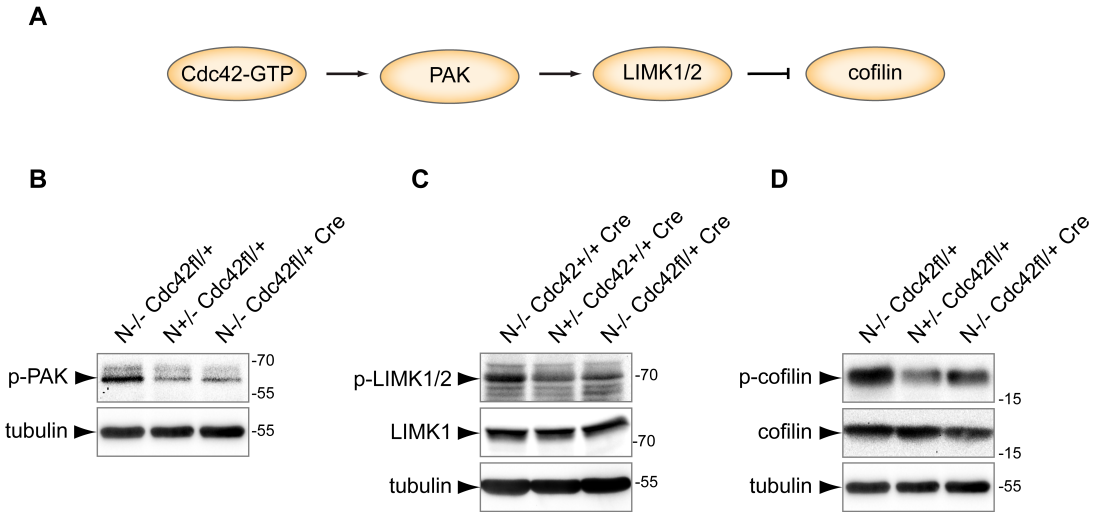

Figure 35: Phosphorylation of PAK, LIMK and cofilin are regulated by Cdc42 downstream of NOMA-GAP. (A) Cdc42-PAK-LIMK-cofilin signaling cascade (B-D) Representative western blots of cortical lysates from E17.5 littermate animals. Western blot analysis was carried out on membranes with phospho-specific antibodies and tubulin as a loading control. (B) Phosphorylation of PAK is increased in N-/- Cdc42fl/+ animals compared to N+/- Cdc42fl/+ control animals. Heterozygous deletion of Cdc42 in the neocortex decreased phosphorylation of PAK in NOMA-GAP-deficient animals (N-/- Cdc42fl/+ Cre). (C) Phosphorylation of LIMK is increased in N-/- Cdc+/+ Cre animals compared to N+/- Cdc42+/+ Cre control animals. Deletion of one Cdc42 allele restored increased phosphorylation in NOMA-GAP-deficient animals (N-/- Cdc42fl/+ Cre). (D) Phospho-Ser3-cofilin levels were also restored after heterozygous deletion of Cdc42 in NOMA-GAP-deficient animals (N-/- Cdc42fl/+ Cre) compared to N-/- Cdc42fl/+ control animals. Modified after Rosario et al., 2012.

From these results we hypothesized that reduced dendritic complexity of layer II-III pyramidal neurons of the neocortex in NOMA-GAP-deficient mice is caused by reduced activation of the actin binding protein cofilin. To test this hypothesis directly, a phosphorylation-resistant and thus constitutively active cofilin mutant, S3A cofilin, was expressed in the neocortex of NOMA-GAP-deficient and littermate controls by *in utero* electroporation at E15.5 to target layer II-III pyramidal neurons. To visualize neuronal morphology and as a control, a plasma membrane targeted GFP was co-electroporated. I collected the brains at P23 and imaged GFP fluorescence of layer II-III pyramidal neurons in the somatosensory cortex (Figure 36A). Subsequently, I analyzed the complexity of the dendritic tree of GFP expressing neurons by Sholl analysis. As seen before, loss of NOMA-GAP resulted in reduced dendritic complexity of layer II-III pyramidal neurons *in vivo* (Figures 36B and 36C). Independent analysis of apical and basal dendritic complexity showed that dendritic complexity is significantly reduced in basal dendrites upon loss of NOMA-GAP, but not in apical dendrites (Figures 36D-36G). Expression of S3A cofilin in NOMA-GAP heterozygous layer II-III pyramidal neurons did not show a significant effect on overall dendritic complexity compared to heterozygous control (Figures 36B and 36C), even though apical dendritic

branching was slightly increased (Figures 36D and 36E). Supporting our hypothesis, my results showed that *in vivo* expression of S3A cofilin in NOMA-GAP-deficient neurons significantly stimulates dendritic branching and was able to restore overall dendritic complexity (Figures 36B and 36C). Particularly, complexity of basal dendrites was restored by expression of S3A cofilin in NOMA-GAP-deficient neurons (Figures 36F and 36G). These results demonstrated that activation of cofilin downstream of NOMA-GAP is necessary for dendritic complexity of layer II-III pyramidal neurons in the murine neocortex. Thereby NOMA-GAP is a major regulator of cofilin activity during the formation of highly branched dendrites in the neocortex.

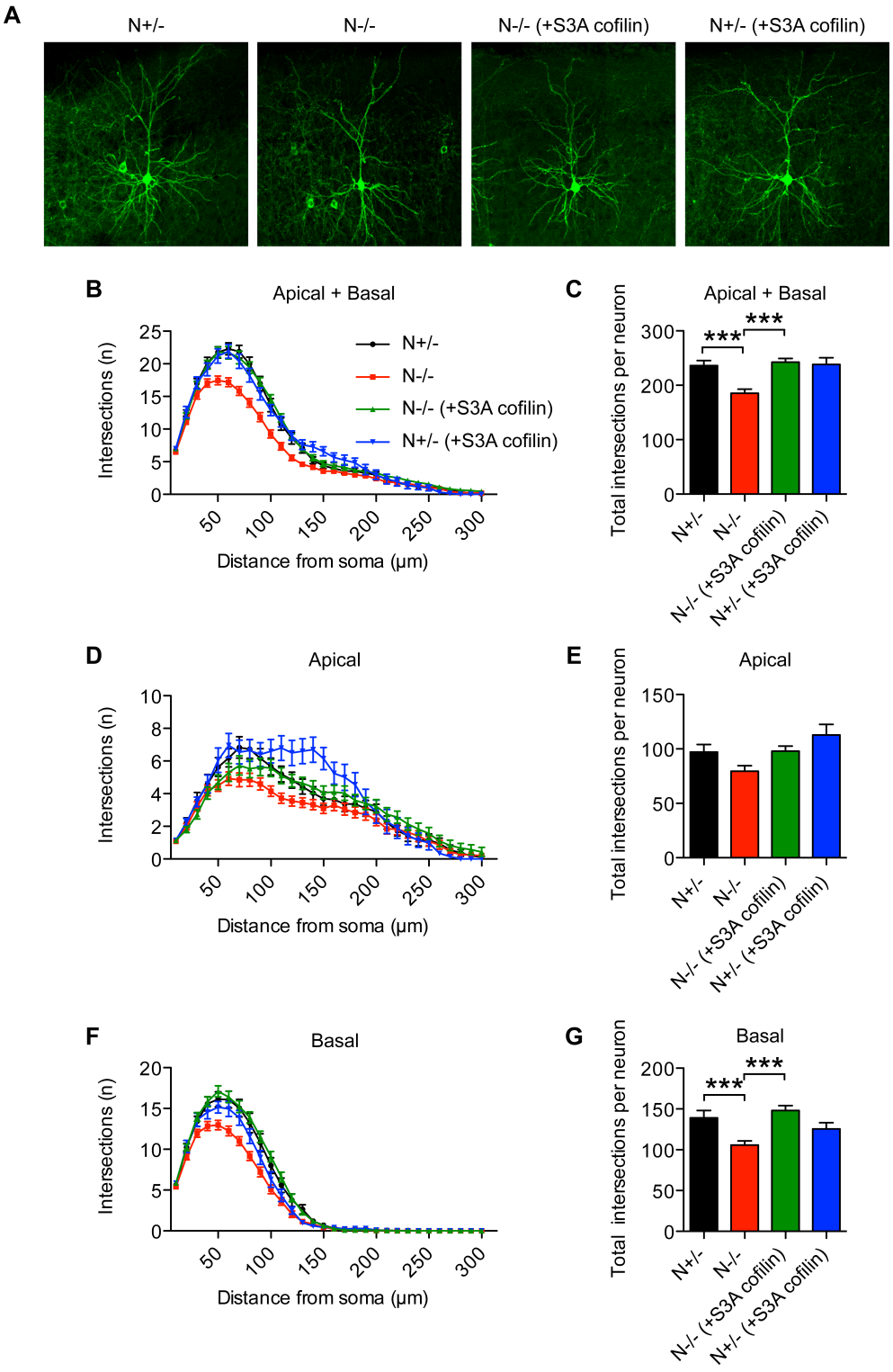

Figure 36: Activation of cofilin downstream of NOMA-GAP promotes dendritic branching *in vivo*. The constitutively active S3A cofilin mutant was expressed in layer II-III pyramidal neurons by *in utero* electroporation in NOMA-GAP-deficient and heterozygous controls at E15.5. For visualization and as a control membrane targeted GFP was co-electroporated. Dendritic morphology of layer II-III pyramidal neurons expressing GFP were analyzed in sections of P23 brains. (A) Representative z-stack projections of GFP fluorescence in layer II-III pyramidal neurons. (B) Sholl profile of N+/- and N-/- layer II-III pyramidal neurons expressing GFP alone as a control or GFP with S3A cofilin. (C) The average number of total dendritic intersections with concentric circles per neuron. 1way ANOVA, ***$p < 0.001$ for N+/- vs. N-/-;

***p < 0.001 for N-/- vs. N-/- (+S3A); p = 0.50 for N+/- vs. N+/- (+S3A). (D) Sholl profile of apical dendrites. (E) Quantification of the average number of total intersections of apical dendrites per neuron. 1way ANOVA, p = 0.06 for N+/- vs. N-/-; p = 0.93 for N-/-vs. N-/-(+S3A); p = 0.02 for N-/- vs. N-/- (+S3A); p = 0.18 for N+/- vs. N+/- (+S3A). (F) Sholl profile of basal dendrites. (G) The average number of total intersections of basal dendrites per neuron. 1way ANOVA, ***p < 0.001 for N+/-vs. N-/-; p = 0.59 for N+/- vs. N-/- (+S3A) ; ***p < 0.001 for N-/- vs. N-/- (+S3A); p = 0.29 N+/- vs. N+/- (+S3A). n = 30 N+/-, 40 N-/-, 30 N-/- (+S3A) and 20 N+/- (+S3A) layer II-III pyramidal neurons from three, four, three and two animals, respectively. Modified after Rosario et al., 2012.

3.4.3 Inhibition of Cdc42 signaling by NOMA-GAP is not sufficient to restore spine morphology

Loss of NOMA-GAP leads to a reduction in dendritic complexity of layer II-III pyramidal neurons of the neocortex (Figures 13 and 36), through a Cdc42-dependent pathway (Figure 33). In addition, I showed that loss of NOMA-GAP in layer II-III pyramidal neurons specifically affects the morphology of dendritic spines in basal dendrites (Figure 17).

To investigate whether dendritic spine development is also dependent on Cdc42 signaling downstream of NOMA-GAP, I tested whether the dendritic spine morphology of basal dendrites could be restored in NOMA-GAP-deficient mice by heterozygous post-mitotic deletion of Cdc42. Dendritic spines of floxed Cdc42 mice were visualized by *in utero* electroporation of eGFP at E15.5. I imaged GFP fluorescence of basal dendritic segments of layer II-III neurons in brain section of P23 mice (Figure 37A). As I observed earlier, the length of spine necks in basal dendrites was significantly increased from 0.711 ± 0.015 µm in N+/- Cdc42fl/+ mice to 0.772 ± 0.014 µm in N-/- Cdc42fl/+ mice, without a change in the distribution of dendritic protrusion types and spine head width (Figures 37C - 37E). The previously detected increase in spine density was not observed in this mouse line upon loss of NOMA-GAP (Figure 37B). However, restoration of Cdc42 signaling in N-/- Cdc42fl/+ Cre animals was not able to restore increased spine neck length (0.770 ± 0.018 µm) (Figures 35B and 36D). On the other hand, heterozygous post-mitotic deletion of Cdc42 in NOMA-GAP-deficient mice significantly increased the spine head width from 0.413 ± 0.005 µm in N+/- Cdc42fl/+ control animals to 0.440 ± 0.006 µm in N-/- Cdc42fl/+ Cre animals. These results indicate, that restoration of Cdc42 signaling in NOMA-GAP-deficient mice by heterozygous deletion of Cdc42, although sufficient for the restoration of dendritic complexity, is not able to restore the neck length of dendritic spines in layer II-III pyramidal cortical neurons.

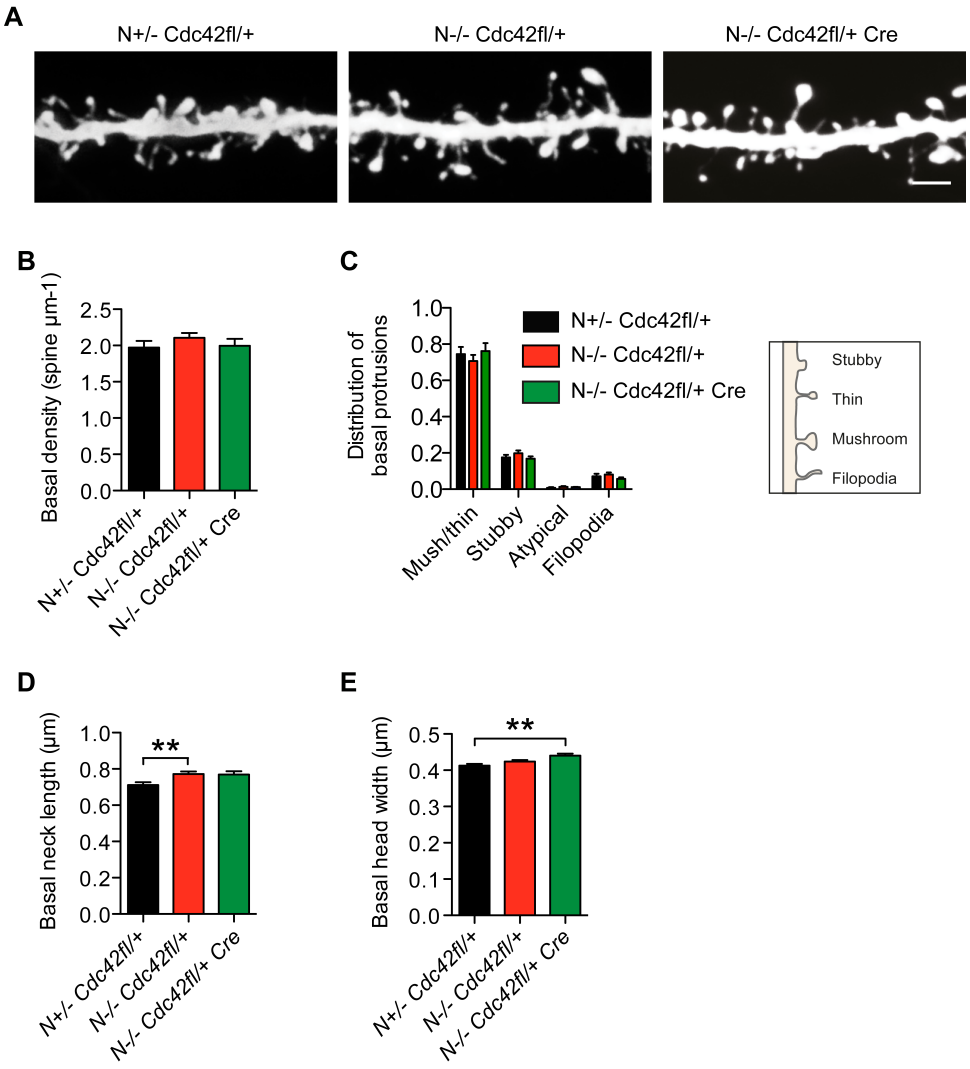

Figure 37: Heterozygous deletion of Cdc42 does not restore dendritic spine morphology in NOMA-GAP-deficient layer 2-3 cortical neurons. (A) Representative basal dendritic segments of layer II-III pyramidal neurons expressing eGFP following *in utero* electroporation at E15.5 of N+/- Cdc42fl/+, N-/- Cdc42fl/+ and N-/- Cdc42fl/+ Cre animals were visualized at P23. Scale bar = 2 µm. (B) Mean spine density. n = 14 N+/- Cdc42fl/+, 18 N-/- Cdc42fl/+ and 13 N-/- Cdc42fl/+ Cre dendritic segments of approximate length of 40 µm. Student´s t test, $p = 0.226$ for N+/- Cdc42fl/+ vs. N-/- Cdc42fl/+; $p = 0.340$ for N-/- Cdc42fl/+ vs. N-/- Cdc42fl/+ Cre; $p = 0.847$ for N+/- Cdc42fl/+ vs. N-/- Cdc42fl/+ Cre. (C) Distribution of dendritic protrusion in basal dendrites between mushroom/thin, stubby, atypical spines and filopodia. (D) Mean spine neck length. n = 763 N+/- Cdc42 fl/+, 1004 N-/- Cdc42fl/+ and 746 N-/- Cdc42fl/+ Cre. Mann-Whitney U test, $^{**}p = 0.005$ for N+/- Cdc42fl/+ vs. N-/- Cdc42fl/+; $p = 0.329$ for N-/- Cdc42fl/+ vs. N-/- Cdc42fl/+ Cre; $p = 0.113$ for N+/- Cdc42 fl/+ vs. N-/- Cdc42 fl/+ Cre. (E) Mean spine head width. n = 763 N+/- Cdc42 fl/+, 1004 N-/- Cdc42fl/+ and 746 N-/- Cdc42fl/+ Cre. Mann-Whitney U test, $p = 0.056$ for N+/-Cdc42fl/+ vs. N-/-Cdc42fl/+; $p = 0.216$ for N-/- Cdc42fl/+ vs. N-/- Cdc42 l/+ Cre; $^{**}p = 0.004$ for N+/- Cdc42fl/+ vs. N-/- Cdc42fl/+ Cre. Three animals per genotype were used. Modified after Schuster et al., 2015.

To confirm that increased neck length in NOMA-GAP-deficient layer II-III pyramidal neurons is independent of NOMA-GAP-mediated inhibition of Cdc42 signaling,

wild type NOMA-GAP (wtNOMA-GAP) or a deletion mutant of NOMA-GAP that lacks the RhoGAP domain (delRhoGAP) was expressed in NOMA-GAP-deficient mice by *in utero* electroporation at E15.5 and analyzed at P23 in brain slices (Figure 38). For visualization of dendritic morphology an eGFP construct was co-electroporated (Figure 38A). I observed that expression of wtNOMA-GAP restored dendritic spine density and spine neck length in layer II-III neurons of NOMA-GAP-deficient mice (Figures 38B and 38C). This indicates a cell autonomous role of NOMA-GAP in the regulation of dendritic spine development. Expression of delRhoGAP in NOMA-GAP-deficient neurons in the mouse neocortex was also able to restore dendritic spine density and spine neck length (Figures 38B and 38C). This is in line with my previous observation that dendritic spine morphology is independent of NOMA-GAP mediated inhibition of Cdc42 signaling. Overexpression of wtNOMA-GAP and delRhoGAP in NOMA-GAP-deficient neurons also significantly increased spine head width (Figure 38D). This result further demonstrates that regulation of Cdc42 signaling by NOMA-GAP is not required for proper dendritic spine development of layer II-III pyramidal neurons of the neocortex.

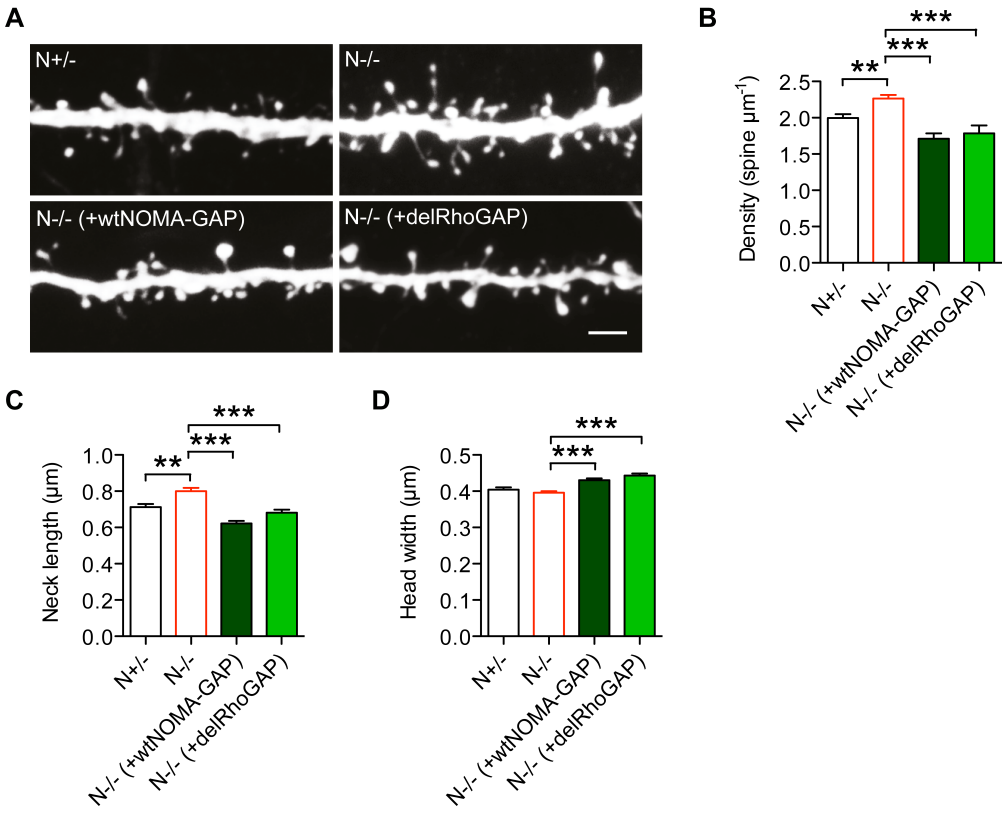

Figure 38: Expression of a RhoGAP deletion mutant of NOMA-GAP (delRhoGAP) in NOMA-GAP-deficient neurons restores increased dendritic spine neck length. (A) Segments of basal dendrites of NOMA-GAP-deficient layer II-III neurons expressing wild type NOMA-GAP (wtNOMA-GAP) or a RhoGAP deletion mutant of NOMA-GAP (delRhoGAP) together with eGFP following *in utero* electroporation at

E15.5 were visualized at P23. As controls heterozygous and NOMA-GAP-deficient neurons were electroporated with eGFP only. Scale bar = 2 µm. (B) Mean spine density. n = 13 N+/-, 14 N-/-, 13 N-/- (+wtNOMA-GAP) and 13 N-/- (+delRhoGAP) dendritic segments of approximate length of 40 µm. Student´s t test, $^{**}p$ = 0.0044 for N+/- vs. N-/- (+wtNOMA-GAP); $^{***}p$ < 0.0001 for N-/- vs. N-/- (+wtNOMA-GAP); p = 0.0979 for N+/- vs. N-/- (+delRhoGAP); $^{***}p$ = 0.0005 for N-/- vs. N-/- (+delRhoGAP); p = 0.5897 for N-/- (+wtNOMA-GAP) vs. N-/- (+delRhoGAP). (C) Mean spine neck length. n = 615 N+/-, 765 N-/-, 824 N-/- (+wtNOMA-GAP) and 782 N-/- (+delRhoGAP). Mann-Whitney U test, $^{***}p$ < 0.0001 for N+/- vs. N-/- (+wtNOMA-GAP); $^{***}p$ < 0.0001 for N-/- vs. N-/- (+wtNOMA-GAP); $^{*}p$ = 0.0482 for N+/- vs. N-/- (+delRhoGAP); $^{***}p$ < 0.0001 for N-/- vs. N-/- (+delRhoGAP); p = 0.0377 for N-/- (+wtNOMA-GAP) vs. N-/- (+delRhoGAP). (D) Mean spine head width. n = 615 N+/-, 765 N-/-, 824 N-/- (+wtNOMA-GAP) and 782 N-/- (+delRhoGAP). Mann-Whitney U test, $^{***}p$ < 0.0001 for N+/- vs. N-/- (+wtNOMA-GAP); $^{***}p$ < 0.0001 N-/- vs. N-/- (+wtNOMA-GAP); $^{***}p$ < 0.0001 for N+/- vs. N-/- (+delRhoGAP); $^{***}p$ < 0.0001 for N-/- vs. N-/- (+delRhoGAP); p = 0.1627 for N-/- (+wtNOMA-GAP) vs. N-/- (+delRhoGAP). Three animals per condition were used. Modified after Schuster et al., 2015.

4 Discussion

The Cdc42-specific GAP, NOMA-GAP, regulates fundamental steps of neuronal differentiation in the developing neocortex: namely the initiation of dendritic complexity, spine maturation and excitatory synapse development. Interestingly, my work indicates that NOMA-GAP differentially controls dendritic complexity and spine maturation by independent mechanisms (Figure 39). NOMA-GAP initiates dendritic branching of layer II-III pyramidal neurons by inhibition of Cdc42 signaling that enables the activation of the actin binding protein cofilin. In contrast, NOMA-GAP regulates spine maturation in basal dendrites of layer II-III pyramidal neurons through a mechanism that is not dependent on the inhibition of Cdc42 signaling. Moreover, NOMA-GAP interacts with several MAGUK family proteins and regulates the surface expression of the AMPAR subunit GluR1. Importantly, we have evidence for a cross-regulation between NOMA-GAP and PSD-95. NOMA-GAP regulates the phosphorylation and synaptic localization of PSD-95, whereas binding of PSD-95 to NOMA-GAP inhibits the Cdc42-GAP activity. Thus, NOMA-GAP specifies cortical connectivity and is likely involved in the establishment of cognitive circuits.

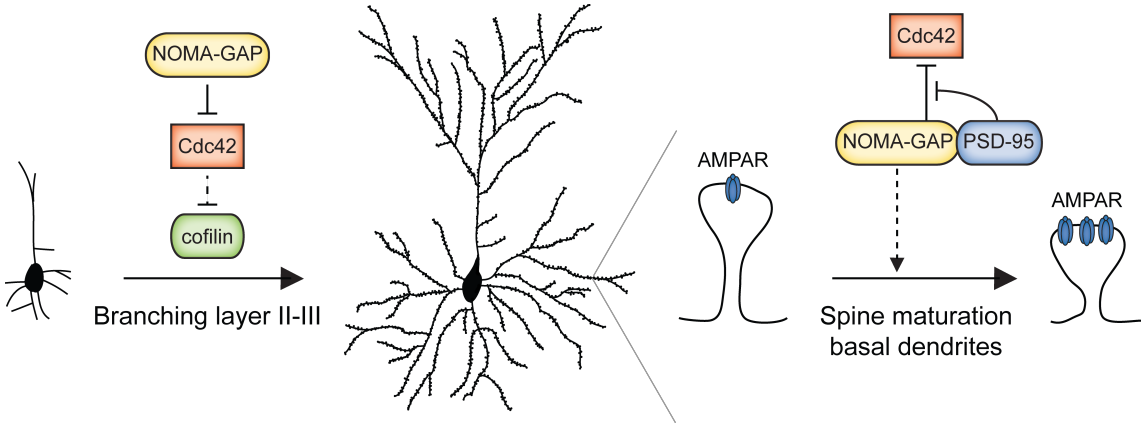

Figure 39: NOMA-GAP initiates layer-specific dendritic complexity and compartment-specific spine maturation by independent mechanisms: NOMA-GAP induces dendritic branching of layer II-III cortical neurons by inhibition of Cdc42 signaling that enables the activation of cofilin. Later in development, NOMA-GAP regulates spine maturation along basal dendrites of layer II-III cortical neurons. In addition, NOMA-GAP regulates synaptic localization of PSD-95 and surface expression of the AMPAR subunit GluR1. In turn, binding of PSD-95 to NOMA-GAP inhibits the Cdc42-GAP activity of NOMA-GAP at synaptic sites.

4.1 Inactivation of Cdc42 by NOMA-GAP initiates dendritic branching

Pyramidal neurons generate complex dendritic trees with thousands of synaptic connections per cell. The development of highly branched dendrites occurs after most projection neurons have been generated, migrated to their final positions and extended their axons (Polleux and Snider, 2010; Simó and Cooper, 2012). It is still poorly understood how dendritic branching is inhibited during migration and subsequently initiated immediately after the neuron has reached the predetermined position in the neocortex.

Initial work of our group showed that genetic deletion of NOMA-GAP is associated with hyperactivation of Cdc42 signaling and a dramatic reduction of cortical thickness of around 20% without increased cell death (Rosário et al., 2012). Several studies indicate that Cdc42 activity is necessary for early stages of cortical development, namely progenitor fate, neuronal polarity, neurite initiation and axonal connectivity (Cappello et al., 2006; Garvalov et al., 2007; Hall and Lalli, 2010; Threadgill et al., 1997; Yokota et al., 2010). Here I show that loss of NOMA-GAP has no significant effect on cell number, neuronal fate and radial migration (Figure 6). Moreover, NOMA-GAP has only little effect on axonal connectivity in the developing brain (Figures 7-11). Genetic deletion of NOMA-GAP did not affect cortico-cortico, cortico-thalamic and thalamo-cortical connections (Figures 7 and 9). In addition, NOMA-GAP is dispensable for the precise arrangement of thalamo-cortical afferents in layer IV, as seen by correct barrel cortex pattern in NOMA-GAP-deficient mice (Figure 11). However, I observed a mild delay in the formation of subcerebral layer V projections through the cerebral peduncle in NOMA-GAP-deficient animals at E18.5, which is overcome at P6 (Figures 8 and 10). This indicates that elevated Cdc42 signaling does not impair the early stages of neuronal differentiation and axon growth.

Once cortical projections neurons have reached the predetermined position in the neocortex, primary basal dendrites are formed *de novo* and extend. Postmitotic expression of CA-Cdc42 was reported to promote primary dendrite initiation and outgrowth in *Drosophila* peripheral nervous system neurons (Gao et al., 1999). In agreement with this, expression of DN-Cdc42 in rat cortical neurons has been shown to reduce the number of primary dendrites, indicating that Cdc42 is required for the formation of primary dendrites (Threadgill et al., 1997). I found that loss of NOMA-GAP did not affect the initiation and outgrowth of primary dendrites *in vivo* (Figures 15B, 16B, 17B). This indicates that NOMA-GAP does not inhibit Cdc42 activity during the initiation of primary dendrites. Indeed, specific expression of the reporter gene *lacZ*

under the control of the NOMA-GAP promoter showed that NOMA-GAP is expressed first at E14.5 specifically in the cortical plate but not in migrating neurons (Rosário et al., 2012). Thus, NOMA-GAP is likely not required for the initiation of primary dendrites.

However, my findings reveal that sustained Cdc42 activity in post-mitotic pyramidal neurons of the neocortex impairs later stages of cortical development, namely dendritic branching and thus complexity. I show that elevated Cdc42 signaling in post-mitotic cortical neurons impairs dendritic complexity in wild type animals (Figure 31). Thus, a switch from Cdc42 activation to inactivation is necessary during neuronal development and/or at specific subcellular locations to initiate dendritic branching. Here, I present evidence that this switch is mediated by post-mitotic expression of NOMA-GAP. Genetic inactivation of NOMA-GAP that result in hyperactivation of Cdc42 is associated with a significant reduction in dendritic complexity of cortical neurons *in vivo* (Figures 15C and 15D). Heterozygous post-mitotic reduction of Cdc42 expression was able to partially restore dendritic complexity in NOMA-GAP-deficient mice (Figure 33). In agreement with our results, Gao and colleagues have shown that overexpression of CA-Cdc42 inhibits dendritic branching in *Drosophila* peripheral nervous system neurons (Gao et al., 1999). In contrast, overexpression of CA-Cdc42 was observed to increase the amount of dendritic branches in *Xenopus* optic tectal neurons (Li et al., 2000), while others reported that expression of both DN-Cdc42 and CA-Cdc42 reduce dendritic complexity in *Xenopus* retinal ganglion cells (Ruchhoeft et al., 1999). Loss of Cdc42 in *Drosophila* vertical system neurons has been shown to affect the branching pattern but not the number of branch points (Scott et al., 2003). These different effects of Cdc42 on dendritic branching may be due to the diversity of species, neuron types, age of neurons or targeting already progenitor cells or the use of non-specific DN-mutants and CA-mutants that do not mimic wild type activation cycling. Furthermore, the work of Ruchhoeft and colleagues suggests that the function of Cdc42 may be depending on the cycling rate between active GTP-bound and inactive GDP-bound states at different subcellular localizations and specific steps of dendrite development.

It is widely accepted that activity-dependent mechanisms can regulate dendritic complexity (Parrish et al., 2007; Wong and Ghosh, 2002). However, our group has observed dendritic defects, as shown by reduced dendritic branching of NOMA-GAP-deficient cultured cortical neurons at DIV5, disturbed MAP2 staining in brain slices at P5 and reduced cortical thickness in NOMA-GAP-deficient mice already at P5 (Rosário et al., 2012). Thus, dendritic defects and cortical thinning in NOMA-GAP mutant mice precede synaptogenesis in the neocortex (Desai et al., 2002; Katz and Shatz, 1996; Stern et al., 2001). This suggests that regulation of dendritic branching by NOMA-GAP

is independent of synaptic activity. Nevertheless, NOMA-GAP is expressed in the adult brain and it is conceivable that activity-dependent processes regulate NOMA-GAP during dendrite development and/or maintenance.

4.2 Cofilin-induced actin dynamics enable dendritic branching

Cofilin is an actin-depolymerizing protein which plays a key role in actin-filament dynamics in eukaryotic cells (Bernstein and Bamburg, 2010). Whether cofilin mediates actin-filament assembly or disassembly depends on the concentration of cofilin relative to actin and the relative concentrations of other actin-binding proteins. Cofilin is necessary for multiple steps during development of the cerebral cortex, including regulation of cell cycle exit, radial migration, Reelin-mediated detachment from radial glia processes, axon guidance and maturation of dendritic spines (Aizawa et al., 2001; Bellenchi et al., 2007; Chai et al., 2009; Shi et al., 2009).

I showed for the first time, that cofilin is essential for complex dendritic branching of pyramidal neurons in the mammalian neocortex. Loss of NOMA-GAP *in vivo* results in increased phosphorylation of cofilin at serine 3 (Figure 34). Previously, phosphorylation of cofilin at serine 3 has been shown to inhibit the actin depolymerization activity of cofilin (Moriyama et al., 1996). Postmitotic expression of NOMA-GAP mediates inhibition of Cdc42 signaling, which in turn leads to the activation of downstream cofilin (Figure 36). Expression of the active cofilin mutant restores dendritic branching in NOMA-GAP-deficient layer II-III pyramidal neurons (Figure 36). Previous studies have indicated that Cdc42 mediates inhibition of cofilin through activation of LIMK by PAK (Edwards et al., 1999). Our group had previously shown that PAK1 activity was elevated in brains of NOMA-GAP-deficient mice at late embryonal stages (Rosário et al., 2012). PAK1 activates the protein kinase LIMK, which is known to phosphorylate and inhibit the depolymerizing protein cofilin (Arber et al., 1998). Indeed, heterozygous postmitotic deletion of Cdc42 in the neocortex of NOMA-GAP-deficient embryos restored activity of the Cdc42 downstream effectors PAK, LIMK and cofilin (Figure 35).

Cofilin is a member of the ADF/coflin family that acts as an actin-severing protein. It depolymerizes actin filaments and thereby regenerates a pool of actin subunits, which is thought to be essential for the reorganization of actin superstructures. A previous study showed that deletion of cofilin suppresses neurite formation *in vivo* and *in vitro* (Bellenchi et al., 2007). Furthermore, it was shown that cofilin mediates actin turnover that is required for the initiation of neurite outgrowth (Flynn et al., 2012). This suggests

that inactivation of cofilin by the Cdc42 signaling cascade may stabilize existing actin filaments and inhibit the formation of new ones during dendritic branching. The restoration of dendritic complexity in NOMA-GAP mutants by overexpressing active cofilin confirms the importance of actin dynamics during dendritic branching. Given that NOMA-GAP accumulates at dendritic branch points, it may be involved in locally reorganizing the actin cytoskeleton (Figure 13). Therefore, NOMA-GAP might initiate local filopodia dynamics along dendrites which is thought to precede dendritic branch formation (Niell et al., 2004; Wu et al., 1999). However, the stabilization of newly formed branches would require stabilization of F-actin and inhibition of NOMA-GAP. One possible inhibitor of the Cdc42-GAP activity of NOMA-GAP is PSD-95. PSD-95 has been reported to inhibit local dendritic branching (Charych et al., 2006; Sweet et al., 2011). I showed that the interaction of PSD-95 with NOMA-GAP inhibits the RhoGAP activity of NOMA-GAP towards Cdc42 (Figure 29) (see chapter 4.6 for further discussion).

Mosaic expression of the active cofllin mutant in individual layer II-III pyramidal neurons of NOMA-GAP-deficient animals was sufficient to rescue dendritic complexity (Figure 36). The restoration of dendritic complexity by expressing active cofilin in a subset of neurons indicates a cell-autonomous mechanism of dendritic branching. This is supported by the observation of our group that dendritic branching could be rescued in NOMA-GAP-deficient cultured cortical neurons by re-expressing NOMA-GAP (Rosário et al., 2012).

4.3 Cdc42-independent regulation of spine morphology by NOMA-GAP

The morphology and density of dendritic spines determines the number, strength and stability of synaptic contacts (Tada and Sheng, 2006). My data show that NOMA-GAP regulates the morphology of dendritic spines along basal dendrites of layer II-III neurons by a Cdc42-independent mechanism. Loss of NOMA-GAP results in longer dendritic spine necks without a change in the spine head width in cultured cortical neurons and in layer II-III neurons (Figures 18, 19 and 37). The spine neck length is thought to inversely correlate with spine maturity and to be critical for compartmentalized signaling at the postsynaptic site (Araya et al., 2014; Tønnesen et al., 2014; Yuste, 2011). This indicates that dendritic spines of NOMA-GAP-deficient neurons are more immature compared to control neurons and that NOMA-GAP is crucial for postsynaptic signaling. Importantly, my data shows that inactivation of Cdc42 by NOMA-GAP is not required for dendritic spine maturation (Figures 37 and 38).

Abnormal spine morphology upon loss of NOMA-GAP is consistent *in vivo* and *in vitro*. In contrast, increased spine density in basal dendrites of NOMA-GAP-deficient mice was not observed in cultured cortical neurons or in NOMA-GAP-deficient mice with a floxed Cdc42 allele (Figures 18, 19 and 37). This suggests that extracellular conditions may influence the formation of dendritic spines and that the impact of NOMA-GAP on the formation of spines is dependent on the mouse background. Contradictory results have been reported concerning the role of Cdc42 in regulating spine formation and maintenance. Tashiro and colleagues reported that expression of CA-Cdc42 or DN-Cdc42 does not have a significant effect on spine density or length in cortical pyramidal neurons (Tashiro et al., 2000). In contrast, others reported that expression of DN-Cdc42 in hippocampal neurons inhibits dendritic spine formation *in vitro* and *in vivo* (Irie and Yamaguchi, 2002; Vadodaria et al., 2013). A recent report suggests that Cdc42 regulates spine density dependent on the brain region. Conditional deletion of the Cdc42 gene using a CaMKII-Cre strain results in a mild reduction of spine density in pyramidal neurons of the hippocampus, but not in pyramidal neurons of the medial prefrontal cortex and anterior cingulate cortex (Kim et al., 2014). During my studies two groups reported a role of NOMA-GAP during spine formation with contradictory results (Kim et al., 2013; Shen et al., 2011). Both groups used RNAi to knockdown NOMA-GAP and analyzed the density of spines. Shen and colleagues reported that knockdown of NOMA-GAP results in reduced number of spines in basal dendrites of layer II-III pyramidal neurons. In contrast, Kim and colleagues reported that knockdown of NOMA-GAP results in increased number of spines in cultured hippocampal neurons. My work is the first to analyze the role of NOMA-GAP on spine morphology. It is important to note that the morphology of dendritic spines is distinct from the their formation. I found that loss of NOMA-GAP does not change the distribution of dendritic spine types or the conversion of filopodia into dendritic spines *in vitro* and *in vivo* (Figures 18C, 19C and 20C). Even though some early studies classify spines into morphological categories, spines have a high natural variability of morphologies leading researchers to argue against the use of this strict classification method and in favor of quantitative measurements to use a qualitative analysis of spine geometry (Arellano et al., 2007).

4.4 Layer- and compartment-specific regulation of dendritic structures by NOMA-GAP

Several molecules have been identified that influence the morphology of dendritic trees and dendritic spines (Hotulainen and Hoogenraad, 2010; Jan and Jan, 2010).

However, little is known about mechanisms that preferentially modulate dendritic structures in restricted neuronal subpopulations and different dendritic domains. My results indicate that NOMA-GAP preferentially regulates dendritic complexity and dendritic spine morphology in basal dendrites of layer II-III pyramidal neurons in the mouse neocortex. Loss of NOMA-GAP specifically reduced dendritic complexity of layer II-III neurons, but not layer V neurons (Figures 15 and 16). Moreover, the complexity of basal dendrites is significantly reduced in NOMA-GAP-deficient layer II-III neurons, while apical dendrites show only a tendency towards lower complexity (Figures 36E and 36G). Postmitotic heterozygous deletion of Cdc42 results in a partial rescue of dendritic complexity in NOMA-GAP-deficient mice, which appears to be more complete proximal to the soma (Figure 33). Proximal dendritic complexity derives mostly from the branching of basal dendrites. This indicates that the specific temporal and spatial regulation of Cdc42 during neuronal differentiation differentially regulates dendritic complexity in apical and basal dendrites. Furthermore, NOMA-GAP specifically regulates dendritic spine morphology in basal dendrites but not in distal apical dendrites of layer II-III neurons (Figures 19 and 20). Apical and basal dendrites are functionally specialized structures that distinctly influence input integration and excitability of a neuron (Branco and Häusser, 2011; Jia et al., 2010). Usually basal and proximal apical dendrites of layer II-III cortical neurons receive excitatory inputs from layer IV cells and also local areas whereas the distal apical tuft receives inputs from more distant cortical and thalamic locations (Spruston, 2008). Thus, NOMA-GAP enables specialized layer II-III neuron differentiation that may contribute to the precise organization of intracortical circuits and potentially higher associative functions. Importantly, post-mortem ASD and schizophrenia human brain tissue revealed layer- and compartment specific alterations in dendritic complexity and dendritic spines (see chapter 4.8). Recent studies reported ASD susceptibility genes that specifically regulate the development of apical or basal dendrites in the neocortex, namely *Epac2*, *TAOK2*, *Ube3a* (de Anda et al., 2012; Miao et al., 2013; Srivastava et al., 2012). This indicates the importance of mechanisms that differentially regulate dendritic maturation in distinct dendritic compartments.

NOMA-GAP expression appears to be uniformly distributed in all cortical layers and dendritic compartments. It is possible that we could not detect a differential distribution of NOMA-GAP between cortical layers and dendritic compartments. Layer-specific regulation of dendritic development might be a consequence of differences in intrinsic and extrinsic factors among cortical layers, Indeed, deep sequencing studies revealed that thousands of genes are differentially expressed across cortical layers (Belgard et al., 2011). Differential development of apical and basal dendrites could be achieved by

subcellular compartmentalization of molecules that act upstream and/or downstream of NOMA-GAP. In particular, the Golgi apparatus is preferentially localized towards the apical dendrite and may thereby enable polarized trafficking of cargo into dendrites (Horton and Ehlers, 2003; Horton et al., 2005; Ori-McKenney et al., 2012).

Differential expression of other Cdc42 regulators could explain the layer- and compartment specific branching phenotype in NOMA-GAP-deficient animals. Potentially, other RhoGAPs or RhoGDIs in layer V neurons or in the apical dendrite of layer II-III neurons may compensate for the loss of NOMA-GAP. It is also conceivable that an upper layer-specific expression of RhoGEFs leads to an increase in Cdc42 activation and therefore requires active inhibition. RICS (also known as GRIT/GC-GAP/p200RhoGAP) is highly similar to NOMA-GAP in structure and function and encoded by the *ARHGAP32* gene (Chiang et al., 2003; Hayashi et al., 2007; Liu et al., 2006; Nakamura et al., 2002; Rosário et al., 2007). Both proteins contain an N-terminal phosphoinositide-binding PX domain, followed by a SH3 domain, a RhoGAP domain and finally a long C-terminal tail with several proline-rich sequences. The C-terminal tail of RICS contains a β-catenin binding site which does not exist in NOMA-GAP (Okabe et al., 2003). TrkA binds to the C-terminal tail of both NOMA-GAP and RICS (Nakamura et al., 2002; Rosário et al., 2007). RICS-deficient mice develop normally and are barely indistinguishable from littermate animals (Nasu-Nishimura et al., 2006). However, Simó and Cooper considered the possibility that the dendritic phenotype was overlooked in RICS-deficient mice, since RNAi knockdown of RICS in the developing rat cortex reduced dendritic complexity of layer II-III pyramidal neurons at P3 (Long et al., 2012; Simó and Cooper, 2012). This would suggest that NOMA-GAP and RICS have different upstream regulators and/or downstream effectors. Indeed, while NOMA-GAP specifically inactivates Cdc42, RICS was demonstrated to inactivate Cdc42 and Rac1 (Hayashi et al., 2007; Rosário et al., 2007). NOMA-GAP becomes tyrosine phosphorylated at the RhoGAP domain by Src family kinase Fyn and at the C-terminal tail by TrkA. (Liu et al., 2006; Rosário et al., 2007). Similarly, RICS becomes tyrosine phosphorylated by Src family kinases and TrkA, but in addition by CaMKII (Moon et al., 2003; Nakamura et al., 2002; Okabe et al., 2003). The temporal and spatial expression of NOMA-GAP and RICS is different in the murine brain. NOMA-GAP expression gradually decreases from embryonal stages to adult stages, while RICS shows an opposing trend (Hayashi et al., 2007; Liu et al., 2006; Long et al., 2012; Nasu-Nishimura et al., 2006; Rosário et al., 2007, 2012). At adult stages both proteins are expressed in the cerebral cortex, hippocampus, thalamus and striatum, but NOMA-GAP specific expression was observed in the olfactory bulb, nucleus accumbens and Purkinje cells of the cerebellum and RICS specific expression was

detected in the amygdala 1(Liu et al., 2006; Nasu-Nishimura et al., 2006; Rosário et al., 2012).

Differential expression could be achieved by layer-specific transcription factors. For example *Fezf2* is specifically expressed in layer V subcortical projection neurons and was reported to be required for complex dendritic branching of subcortical projection neurons (Chen et al., 2008, 2005). Compared to this, *Cux1* and *Cux2* are specifically expressed in the layer II-III projection neurons (Cubelos et al., 2010). Interestingly, analysis of *Cux1/Cux2*-deficient mice showed reduced dendritic complexity and immature dendritic spines specifically in layer II-III pyramidal neurons of the neocortex, similar to NOMA-GAP-deficient mice. Moreover, it was shown that *Cux1* primarily regulates the development of basal dendrites whereas *Cux2* mainly regulates apical dendrites (Cubelos et al., 2014).

Other regulators of dendritic complexity are secreted molecules like Reelin, semaphorins and neurotrophins. They have been shown to have distinct effects on different cortical layers and dendritic compartments. The extracellular matrix glycoprotein Reelin is secreted by Cajal-Retzius cells located in the marginal zone and diffuses down through the cortical plate (D'Arcangelo et al., 1995; Frotscher, 1998). Despite the pivotal role in neuronal migration, Reelin was shown to induce dendritic complexity and dendritic spine formation mainly in apical dendrites of hippocampal and cortical pyramidal neurons (D'Arcangelo, 2014; Niu et al., 2004; Olson et al., 2006). Furthermore, Reelin signaling was shown to be required for the extension of the Golgi apparatus into the apical dendrites of pyramidal neurons and thus cell polarization (Matsuki et al., 2010). Given that Reelin stimulates the Src family tyrosine kinases Src and Fyn and these tyrosine kinases stimulate many RhoGEFs, it is conceivable that the Reelin concentration gradient from upper to deeper cortical layers could lead to increased Cdc42 activation in layer II-III neurons (Arnaud et al., 2003; Schiller, 2006). Moreover, a recent study reported that Reelin specifically activates Cdc42 signaling in an apolipoprotein E receptor 2-, Disabled-1-, and phosphatidylinositol-3-kinase-dependent manner (Leemhuis et al., 2010). Thereby layer II-III neurons would be more dependent on NOMA-GAP activity to compensate increased Cdc42 activity.

Similar to Reelin, Semaphorin-3A forms a concentration gradient from upper to deeper cortical layers (Polleux et al., 2000). In addition to regulating the growth direction of apical dendrites, it has been reported that Semaphorin-3A promotes neurite formation and dendritic branching of cultured cortical neurons, in part through a cascade mediated by Fyn (Morita et al., 2006). Moreover, binding of Semaphorin-3A to neuropilin-1 receptor was reported to induce dendritic complexity in basal dendrites of layer V cortical pyramidal neurons but does not influence spine formation and

morphology (de Anda et al., 2012; Fenstermaker et al., 2004; Gu et al., 2003). In contrast, binding of Semaphorin-3F, another semaphorin family member, to its receptor neuropilin-2 specifically regulates the number and morphology of spines along apical dendrites of layer V cortical neurons but does not influence dendritic complexity (Tran et al., 2009). These distinct functions of semaphorin signaling are thought to derive from the restricted localization of neuropilin-2 to apical dendrites and of neuropilin-1 to all dendrites (Tran et al., 2009). Hence, spatially segregated signaling orchestrates layer- and compartment-specific development of dendritic structures.

Other regulators of dendritic complexity are neurotrophins, which have been shown to differentially influence dendritic length and complexity of cortical neurons (McAllister et al., 1995, 1997). Pyramidal neurons in each cortical layer respond to a subset of neurotrophins with distinct effects on apical and basal dendrites (McAllister et al., 1995). The neurotrophic factors BDNF and NT-3 increased the length and complexity specifically in basal dendrites of layer II-III pyramidal neurons in the rat neocortex, but not apical dendrites (Baker et al., 1998; Niblock et al., 2000). Moreover, NT-3 antagonizes BDNF-induced dendritic complexity in layer IV, while BDNF inhibits NT-3-induced dendritic complexity in layer VI (McAllister et al., 1997). Our group has shown that NOMA-GAP interacts with the neurotrophin receptor TrkA and becomes phosphorylated upon binding of NGF to TrkA (Rosário et al., 2007). Furthermore, NOMA-GAP and Trk-receptors exists in a complex in the neocortex of mice and can co-immunoprecipitate when overexpressed in cell lines (Figures 23A and 23B). Thus, NOMA-GAP activity may be differentially regulated in specific cortical layers and dendritic compartment by extracellular signals such as Reelin, semaphorins and neurotrophins.

4.5 NOMA-GAP interacts with multiple MAGUK family proteins

MAGUKs family proteins play an important role in synapse development and function (Oliva et al., 2012). I found that NOMA-GAP directly interacts with the MAGUK family proteins PSD-95, PSD-93 and SAP102, but not with SAP97 (Figure 24).

During neuronal development MAGUK family proteins are expressed in a regulated manner. PSD-95 and PSD-93 expression level increases from early postnatal stages to adult stages, while SAP97 and SAP102 expression show the opposite pattern (Oliva et al., 2012). Similar to SAP97 and SAP102, NOMA-GAP expression decreases from early postnatal stages to adult stages (Liu et al., 2006; Rosário et al., 2007). This

suggests that the interaction of NOMA-GAP with SAP102 may be important during early developmental stages whereas the interaction of NOMA-GAP to PSD-95 and PSD-93 becomes more important at adult stages. PSD-95, PSD-93 and SAP102 are mainly postsynaptic proteins, while SAP97 is found at the presynaptic and postsynaptic site (Aoki et al., 2001). Electron micrographs show that PSD-95 and PSD-93 are distributed evenly throughout the PSD, while SAP97 is distributed near the edges next to the cleft and away from the cleft (DeGiorgis et al., 2006). Our data suggests that NOMA-GAP is mainly a postsynaptic protein (Figure 12). However, we cannot exclude the presence of NOMA-GAP at presynaptic sites. Given that the interaction of NOMA-GAP mainly with MAGUKs that localize specifically at the postsynaptic site, strengthens the hypothesis that NOMA-GAP is mainly a postsynaptic protein.

The formation and maturation of the postsynaptic site is a highly regulated process that involves the trafficking of glutamate receptors to synaptic sites (Hanse et al., 2013; Sheng and Kim, 2011). It is assumed that MAGUKs are not essential for the initial steps of synapse formation (Oliva et al., 2012). Nevertheless, MAGUKs are necessary for the clustering and anchoring of glutamate receptors once synapses are formed (Waites et al., 2005). All four MAGUKs can directly bind the cytoplasmatic domain of NMDAR subunits (Zheng et al., 2011). SAP97 is the only MAGUK that directly binds to the C-terminus of the AMPAR subunit GluR1 (Leonard et al., 1998). Because MAGUKs directly interact with the cytoplasmatic domains of NMDAR subunits, it has long been assumed that MAGUKs mainly control synaptic targeting and clustering of NMDARs (Huganir and Nicoll, 2013). More recent studies suggesting a primary role of MAGUKs in targeting and anchoring AMPARs to synaptic sites (Xu, 2011; Zheng et al., 2011). The indirect interaction of MAGUKs with AMPARs is mediated by transmembrane AMPAR regulatory proteins (TARPs), including stargazing (Ziff, 2007). It was reported that overexpression and knockdown of PSD-93 and PSD-95 increase or decrease synaptic AMPARs, respectively (Béïque and Andrade, 2003; Ehrlich and Malinow, 2004; El-Husseini et al., 2000; Elias et al., 2006; Schlüter et al., 2006; Schnell et al., 2002). Similar results were obtained for SAP97 and SAP102, even though the effects were less dramatic (Elias et al., 2006; Howard et al., 2010; Waites et al., 2009). Recently published studies indicate that SAP97 and SAP102 mediates synaptic targeting of AMPARs during early stages of synaptic differentiation, while PSD-95 and PSD-93 determine synaptic targeting of AMPARs in more mature synapses (Elias et al., 2006; Howard et al., 2010). While overexpression and knockdown experiments uncovered the function of MAGUKs in synaptic development, loss of function experiments have shown inconsistent results. Knockout mutant mice for PSD-93 and SAP102 are viable and do not display defects in synaptic development (Cuthbert et al.,

2007; McGee et al., 2001). SAP97-deficient mice die at perinatal stages due to major defects in cell-cell contact formation during embryonic development (Caruana and Bernstein, 2001). However, neuronal cultures from SAP97-deficient embryos develop normally and show normal levels of synaptic AMPAR (Klöcker et al., 2002). While some studies in PSD-95-deficient mice showed normal synaptic development, others reported a reduction in basal AMPAR-mediated synaptic transmission (Béïque et al., 2006; Carlisle et al., 2008; Elias et al., 2006; Migaud et al., 1998). The discrepancy could be explained by the usage of different knockout mice. The PSD-95-deficient mice without synaptic defects during development still express at low levels a functionally truncated form of PSD-95 (Ehrlich and Malinow, 2004; Schnell et al., 2002). In summary, different MAGUK proteins seem to compensate the loss of SAP97, PSD-93 and SAP102 during synaptic development. In contrast, loss of PSD-95 lead to defective formation and maturation of postsynaptic sites, similar to loss of NOMA-GAP (see chapter 4.7 for further discussion).

Synaptic plasticity describes any process that lead to changes in the strength of synaptic transmission between neurons (Mayford et al., 2012). Prolonged strengthening of synaptic transmission, called long-term potentiation (LTP), is thought to accompanied by an increase in synaptic AMPAR and enlargement of the spine head (Hotulainen and Hoogenraad, 2010). Prolonged depression of synaptic transmission, called long-term depression (LTD), results in less synaptic AMPAR and spine head shrinkage. The size of the spine head is supposed to be proportional to the area of the postsynaptic density (Holtmaat and Svoboda, 2009). I showed that loss of NOMA-GAP does not alter spine head size of cortical pyramidal neurons, suggesting that NOMA-GAP does not regulate structural plasticity (Figures 18F, 19F and 20F). However, a recent study presented evidence that LTD-inducing stimuli increased the expression levels of NOMA-GAP, whereas LTP-inducing stimuli reduced it (Kim et al., 2013). Supporting a role of NOMA-GAP during synaptic plasticity, I found that NOMA-GAP interacts with several MAGUK family proteins (Figure 24). The role of MAGUKs during structural and functional plasticity has been extensively studied during the last decade. The overexpression of PSD-95 was shown to increase spine density and spine head size, while LTP was blocked and LTD enhanced (El-Husseini et al., 2000). Consistent with this, acute knockdown of PSD-95 resulted in reduced spine density and number of mushroom shaped spines, while the induction of LTP was not affected (Ehrlich et al., 2007; Steiner et al., 2008). In contrast, PSD-95-deficent mice showed no change in spine head size but longer spine necks (Béïque et al., 2006). Nevertheless, loss of PSD-95 in mice results in greatly enhanced LTP, whereas LTD was absent (Béïque et al., 2006; Carlisle et al., 2008; Migaud et al., 1998). These results indicate that PSD-95

is a negative regulator of LTP and indispensable for the induction of LTD. Furthermore, PSD-95 seems to have a different effect on functional and structural plasticity. In contrast to PSD-95-deficient mice, PSD-93-deficent mice showed deficits in LTP and normal LTD (Carlisle et al., 2008). So far it is still unclear what causes the opposite effect of PSD-95 and PSD-93 during synaptic plasticity. It is presumable that PSD-95 and PSD-93 form different protein complexes that result in a different signaling (Xu, 2011). In addition, there is evidence that PSD-95 and PSD-93 may be localized on non-overlapping subsets of synapses with different properties (Béïque et al., 2006; Elias et al., 2006). The overexpression of SAP97 was shown to increase the size of dendritic spines without changing spine density (Poglia et al., 2011; Rumbaugh et al., 2003). Conditional knockout mice for SAP97 showed no defect in synaptic plasticity, whereas acute knockdown of SAP97 occluded LTP (Howard et al., 2010; Nakagawa et al., 2004). Overexpression of SAP102 in hippocampal neurons was shown to result in increased spine neck length without changing spine head width and density (Chen et al., 2011). Similar to PSD-95, SAP102-deficient mice showed enhanced LTP, although the underlying signaling pathway seems to be different (Cuthbert et al., 2007). In summary, MAGUKs are functionally diverse during structural and functional plasticity. My finding that NOMA-GAP interacts with a subset of MAGUKs may help to gain insight on how the diversity of MAGUKs during structural and functional plasticity could be achieved.

4.6 Cross-regulation of NOMA-GAP and PSD-95

In this work I present evidence for a cross-regulation between NOMA-GAP and PSD-95 in the mouse cortex. My results indicate that NOMA-GAP is an important regulator of PSD-95 function. Both phosphorylation and synaptic localization of PSD-95 are dependent on NOMA-GAP. Phosphorylation of PSD-95 at serine 295 has previously been shown to induce postsynaptic accumulation of PSD-95 and consequently the maturations and strengthening of excitatory synapses by synaptic targeting of AMPARs (Kim et al., 2007). In contrast, dephoshorylation of PSD-95 at serine 295 induces a rapid loss of PSD-95 from synaptic sites and subsequent loss of synaptic AMPAR. I found that loss of NOMA-GAP results in a two-fold increase in serine 295 phosphorylated PSD-95 in primary cortical neurons and in the neocortex of adult mice (Figures 27 and 28). In addition, serine 295 phosphorylated PSD-95 is strongly mislocalized in NOMA-GAP mutant neurons from the dendritic spine head towards the dendritic shaft (Figure 28). This indicates that the correct subcellular localization of PSD-95 to postsynaptic sites requires not only serine 295

phosphorylation but also NOMA-GAP function. NOMA-GAP could regulate synaptic localization of PSD-95 through direct interaction or complex signaling events. Interestingly, it has been shown that BDNF-TrkB signaling induces the vesicular transport of PSD-95 to synaptic sites in cultured mouse cortical neurons and in mouse visual cortical layer II-III neurons (Yoshii and Constantine-Paton, 2007; Yoshii et al., 2011). In accordance, TrkB-deficient mice show decreased number of hippocampal excitatory synapses (Luikart et al., 2005). Given that NOMA-GAP interacts with the TrkB receptor, it is conceivable that NOMA-GAP may induce synaptic accumulation of PSD-95 by regulating TrkB signaling (Figure 23). Further studies will clarify if NOMA-GAP regulates specifically the subcellular localization of PSD-95 or also of other MAGUKs.

In addition, our data indicates that the interaction with PSD-95 inhibits the Cdc42-GAP activity of NOMA-GAP (Figure 29). This suggests that the expression of PSD-95 act as a developmental switch for NOMA-GAP signaling and functions. Initially, NOMA-GAP increases dendritic branching by inhibition of Cdc42 signaling. Postnatal expression of PSD-95, around postnatal day 10, is expected to abolish NOMA-GAP-mediated inhibition of Cdc42 signaling and restrain excessive dendritic branching. Indeed, PSD-95 has been shown to negatively regulate dendritic branching (Charych et al., 2006; Sweet et al., 2011). In addition, NOMA-GAP may exist in two pools with different signaling functions. My results show that NOMA-GAP co-localizes with PSD-95 at the dendritic spine head but not in the dendritic shaft in mature cultured cortical neurons (Figure 22). Thus, presumably at the tip dendritic spines, PSD-95 inhibits the RhoGAP activity of NOMA-GAP and would therefore enable high Cdc42 activity. In line with this, induction of structural plasticity at single dendritic spines by glutamate uncaging experiments revealed that Cdc42 becomes rapidly activated in the stimulated spine head (Murakoshi et al., 2011). Unlike other RhoGTPases, Cdc42 activation is sharply restricted to the stimulated dendritic spine head, despite similar protein mobility. Therefore, inhibition of Cdc42 by NOMA-GAP seems to be actively suppressed by the interaction with PSD-95, which enables high Cdc42 activity in spine heads. Importantly, inhibition of Cdc42-PAK-signaling blocked the maintenance of sustained structural plasticity (Murakoshi et al., 2011). On the other hand, unbound NOMA-GAP may prevent expansion of Cdc42 activity into the spine neck and dendritic shaft. Future studies may shed light into the distinct interaction dynamics of NOMA-GAP and PSD-95 during development.

4.7 NOMA-GAP regulates surface expression of AMPAR

Synapses are constantly generated during postnatal development. Newly generated glutamatergic synapses are AMPA-silent synapses, which lack AMPAR-mediated transmission (Hanse et al., 2013). Most of these silent synapses are eliminated during development or converted into functional AMPAR-containing synapses by correlated pre- and postsynaptic activity. Premature or delayed activation of AMPA-silent synapses are associated with neurodevelopmental disorders (Aoto et al., 2013; Banko et al., 2005; Clement et al., 2013; Harlow et al., 2010). MAGUK family proteins play a primary role in targeting and anchoring AMPARs to postsynaptic sites (see chapter 4.5). Béïque and colleagues could show that PSD-95-deficient mice revealed a greater proportion of AMPAR-silent synapses (Béïque et al., 2006). Interestingly, it has been reported that the distribution of functional AMPAR is correlated with spine geometry. In detail, dendritic spines with a small heads and long necks express less AMPARs on their surface than spines with large heads and short necks (Matsuzaki et al., 2001). According to that, PSD-95-deficient mice revealed that AMPA-silent synapses are distributed on longer dendritic spines (Béïque et al., 2006). My work shows that surface expression of AMPAR is dramatically reduced and dendritic spine necks are longer in NOMA-GAP-deficient neurons (Figures 18 and 30). These results further indicate that spine morphology correlate with the conversion of AMPAR-silent synapses to functional synapses.

NOMA-GAP-mediated synaptic accumulation of PSD-95 could indirectly promote the recruitment of AMPARs to the postsynaptic membrane. It is also conceivable that NOMA-GAP directly binds to AMPAR subunits and thereby promoting exocytosis or inhibiting endocytosis at the plasma membrane. Furthermore, actin dynamics have been shown to play a critical role in controlling surface expression of AMPARs (Hanley, 2014). In particular, the study of Gu and colleagues indicates that cofilin-mediated actin dynamics enhance the surface expression of AMPARs (Gu et al., 2010). Thus, inhibition of Cdc42 by NOMA-GAP enables the activation of cofilin that would promote surface expression of AMPARs. It is important to note that this scenario is potentially only possible at extrasynaptic sites, since PSD-95 inhibits the Cdc42-GAP activity of NOMA-GAP and thus activation of cofilin at dendritic spine heads (Figure 29). Nonetheless, exocytosis of AMPARs occur mostly at extrasynaptic sites and AMPARs travel into dendritic spines by lateral diffusion (Krugers et al., 2010; Lin et al., 2009).

Our collaborators Luminita Stoenica and Ulf Strauss tested if immature spine morphology and reduced surface expression of AMPAR in NOMA-GAP mutant mice may result in aberrant basal synaptic transmission. They recorded spontaneous

postsynaptic currents and miniature excitatory postsynaptic currents of layer II-III cortical pyramidal neurons in brain slices from adult littermate animals. In contrast to wild type neurons, NOMA-GAP-deficient neurons showed a dramatic reduction in spontaneous postsynaptic current frequency without an alteration in amplitude (Schuster et al., 2015). They and others suggested that most if not all spontaneous events in layer II-III neurons in cortical slices around resting potential are AMPAR-mediated postsynaptic currents and not inhibitory or presynaptic events (Simkus and Stricker, 2002). Similar to PSD-95-deficent mice, reduced miniature excitatory postsynaptic current frequency in NOMA-GAP-deficient mice may arise mainly from a decrease in AMPAR-containing synapses that may reflect the defective conversion of AMPA-silent synapses to functional synapses (Béïque et al., 2006). It is important to note that dendritic complexity has been shown to modulate the electrophysiological properties of a neuron (London and Häusser, 2005; Peng et al., 2009; Petrinovic et al., 2013; Spruston, 2008). However, reduction of Cdc42 activity in NOMA-GAP-deficient neurons that partially restored dendritic complexity had no significant effect on the reduced frequency or on the amplitude of spontaneous postsynaptic currents (Schuster et al., 2015). These results suggest that surface expression of AMPAR is not dependent on inhibition of Cdc42 by NOMA-GAP. Future experiments will help to uncover the mechanism of NOMA-GAP-mediated surface expression of AMPARs.

4.8 NOMA-GAP and neuropsychiatric developmental disorders

The development of dendritic trees and dendritic spines are fundamental for neuronal connectivity and information processing. Abnormalities in dendritic structures are commonly associated with several neuropsychiatric developmental disorders, including autism spectrum disorder (ASD) and schizophrenia (Kulkarni and Firestein, 2012; Penzes et al., 2011). Emerging evidence indicate that ASD and schizophrenia result from a developmental disconnection of brain areas that are involved in higher-order association (Geschwind and Levitt, 2007; Yizhar et al., 2011; Zoghbi and Bear, 2012)

ASD is a highly heterogeneous neurodevelopmental spectrum disorder, characterized by impaired social interaction and deficits in communication and repetitive stereotyped behaviors (Abrahams and Geschwind, 2008). ASD comprises of idiopathic autism, Asperger´s syndrome, Rett´s syndrome and pervasive developmental disorder not otherwise specified. ASD affects approximately 1% of the population and most of the features of ASD develop before two or three years of age, with a strong male bias (Penzes et al., 2011; Ronemus et al., 2014). The majority of identified ASD

susceptibility genes identified so far encode for proteins at the postsynaptic site of glutamatergic synapses. This fact leads to the hypothesis that synaptic dysfunction could be a common process associated with ASD, probably due to imbalance of excitation and inhibition in the developing brain (Ebert and Greenberg, 2013; Toro et al., 2010). Post-mortem ASD human brain tissue revealed an increase in dendritic spine density on apical dendrites of layer II pyramidal neurons in frontal, temporal and parietal lobes and layer V only in the temporal lobe of the neocortex (Hutsler and Zhang, 2010; Tang et al., 2014). Interestingly, increased spine density inversely correlated with cognitive function (Hutsler and Zhang, 2010). Shank proteins are one of the most characterized PSD scaffold proteins that have been linked to ASD (Jiang and Ehlers, 2013). Deletion of Shank3 in mice leads to deficits in social interaction and repetitive grooming, reduced protein levels of scaffolding proteins and glutamate receptor subunits in striatal PSD fractions, increased dendritic complexity, fewer dendritic spines and decreased miniature excitatory postsynaptic currents frequency of striatal medium spiny neurons (Peça et al., 2011). Shank2-deficient mice also show autistic-like behavior, including impaired social interaction, defective vocalization as well as repetitive grooming behavior. Moreover, deletion of Shank2 in mice results in altered expression of AMPAR and NMDAR subunits, decreased dendritic spine density and reduced miniature excitatory postsynaptic currents frequency (Schmeisser et al., 2012). Rare mutations in the genes encoding for synaptic cell adhesion proteins NLGN3 and NLGN4 and their presynaptic ligand NRXN1 have been frequently found in ASD patients (Zoghbi and Bear, 2012). Knock-in mice that express the missense mutation in NLGN3 (R451C), display impaired social interactions accompanied with enhanced inhibitory neurotransmission (Tabuchi et al., 2007). In contrast, deletion of NLGN3 in mice did not cause such phenotypes, indicating that the R451C missense mutation causes a gain-of-function (Tabuchi et al., 2007). Another missense mutation in NLGN3 (R704C) caused a decrease in AMPAR-mediated synaptic transmission in the hippocampus, but not in GABA-receptor-mediated synaptic transmission (Etherton et al., 2011). A deletion of NLGN4 ortholog in mice causes impaired social behavior and decreased ultrasonic vocalization (Jamain et al., 2008). In summary, proteins with genetic association with ASD regulate dendritic spine morphogenesis and synaptic transmission. Interestingly, a large number of them are directly or indirectly associated with and regulated by MAGUK family proteins.

Schizophrenia is a s psychiatric disorder affecting approximately 1% of the population, with onset typically occurring during adolescence and early adulthood (Penzes et al., 2011). Individuals suffer from delusions, disorganized thinking, lack of emotions and motivation, thereby resulting in social impairments. Schizophrenia is a highly heritable

disorder with genetic factors accounting for approximately 80% of the liability for developing the disease (Pocklington et al., 2014). One of the defining neuropathological features of schizophrenia is a brain-region specific loss of gray matter mostly in the prefrontal cortex (Cannon et al., 2002; Gogtay, 2008). Several postmortem studies indicate that regional loss of gray matter in the brain of schizophrenic patients is accompanied by an increase in cell density, decrease dendrite complexity specifically in basal dendrites and loss of dendritic spines particularly in layer III pyramidal neurons (Broadbelt et al., 2002; Garey et al., 1998; Glantz and Lewis, 2000; Selemon et al., 1995). Individuals diagnosed for schizophrenia show reduced activity in the prefrontal cortex during cognitive tasks (Tan et al., 2007). Collectively, these studies reveal that individuals with schizophrenia are characterized by hypoconnectivity between specific brain regions. Neurobiological studies on transgenic mouse lines underline that schizophrenia-associated molecules are important regulator for the development of dendritic structures and maturation of excitatory synapses. Hundreds of gene variants have been associated with schizophrenia, including disrupted in schizophrenia (DISC) 1, the RacGEF Kalirin-7, ERBB4 and the RacGEF Kalirin-7 (Penzes et al., 2011). DISC1 was identified in a Scottish pedigree with balance translocation of chromosome 1, leading to a disruption of the DISC1 gene. Altered expression of DISC1 predispose individuals to the development of schizophrenia, bipolar disorder and depression (Brandon and Sawa, 2011). DISC1 has a manifold impact on neuronal development. It encodes an intracellular scaffold protein that has been shown to regulate dendritic branching, spine formation, surface levels of the AMPAR subunit GluR1 and the frequency of miniature excitatory postsynaptic currents (Hayashi-Takagi et al., 2010; Kamiya et al., 2005; Kang et al., 2011). DISC1 exists at the postsynaptic site in a trimolecular complex with PSD-95 and Kalirin-7. At the baseline condition, DISC1 enhances binding of Kalirin-7 and PSD-95 and thereby limiting access of Kalirin-7 to Rac1. The activation of NMDARs lead to disruption of the trimolecular complex, leading to the activation of Rac1 by Kalirin-7 (Hayashi-Takagi et al., 2010). Another rare CNV that predispose individuals for the development of schizophrenia was identified for ERBB4, leading to the expression of a truncated protein lacking the intracellular domain (Walsh et al., 2008). ERBB4 is a postsynaptic receptor tyrosine kinase that interacts with PSD-95 and gets activated upon neuregulin binding (Huang et al., 2000). ERBB4 activation was shown to regulate glutamatergic synapse maturation and function by stabilizing synaptic AMPAR (Li et al., 2007). Thus, similar to ASD, proteins with genetic association with schizophrenia regulate dendritic spine morphogenesis and synaptic

transmission, and are directly or indirectly associated with and regulated by MAGUK family proteins.

So far only a few common genetic risk factors for ASD and schizophrenia have been identified. Recent findings support the hypothesis that the occurrence of *de novo* mutations could explain the high prevalence of ASD and schizophrenia since they are associated with a marked reduction in fecundity (Ku et al., 2013; Lee et al., 2013). Genome-wide association studies identified rare *de novo* mutations in hundreds of genes that are linked to ASD and schizophrenia. Non-synonymous mutations in *DLG1*/SAP97 and *DLG4*/PSD-95 have been found to be associated with risk for ASD and non-synonymous mutations in all genes encoding MAGUK family proteins are associated with risk for schizophrenia (Fromer et al., 2014; Li et al., 2014; Purcell et al., 2014; Stone et al., 2008; Walsh et al., 2008; Xu et al., 2008). Indeed, PSD-95 and PSD-93-deficient mice partly mimic mechanisms that are associated with the clinical condition. PSD-95-deficient mice display increased repetitive behavior, abnormal communication and social behavior (Béïque et al., 2006; Feyder et al., 2010). The cognitive defects observed in PSD-93-deficient mice show high similarity compared to those observed in patients with schizophrenia, such as deficits in attention, visual-discrimination and cognitive flexibility (Nithianantharajah et al., 2013). Interestingly, recent whole-exome-sequencing studies from schizophrenic patients identified a rare *de novo* mutation at the NOMA-GAP gene loci that is enriched in patients with schizophrenia, although it was reported to be a synonymous mutation (Fromer et al., 2014; Purcell et al., 2014). Future work might reveal the importance of NOMA-GAP in patients with neuropsychiatric developmental disorders.

The dendritic and synaptic defects in NOMA-GAP-deficient mice prompted us to uncover the role of NOMA-GAP in animal behavior. Our collaboration with Marion Rivalan and York Winter revealed that NOMA-GAP-deficient mice show no alteration in general behavior, animal health, motoric and sensory function (Schuster et al., 2015). However, NOMA-GAP mutant animals showed increased hindlimb clasping, a phenotype observed in neurological disorders including ASD and related disorders (Guy et al., 2001; Schmeisser et al., 2012). Importantly, we observed that NOMA-GAP-deficient males show impaired social interaction. Mutant male mice showed both lack of interest in an unfamiliar mouse and an inability to discriminate between a familiar and a novel mouse (Schuster et al., 2015). Similar to spine morphology and synaptic transmission, social behavior could not be restored by heterozygous deletion of Cdc42 in postmitotic neurons using a Nex1 promoter-driven Cre recombinase. The observed behavioral phenotype in NOMA-GAP-deficient male mice might reflect the deficits in social communication and social interaction in individuals with ASD or schizophrenia

(Crawley, 2007; Sachs et al., 2004; Sigman et al., 2006). Interestingly, NOMA-GAP-deficient mice show a gender-associated phenotype that is also observed in humans with ASD or schizophrenia (Baron-Cohen et al., 2011; Häfner, 2005; Hennah et al., 2003). While social interaction deficits are restricted to male NOMA-GAP-deficient mice, female NOMA-GAP-deficient mice show evidence of increased anxiety. Female mice had an increased latency to enter the center of an open field, build more complex nests and display increased burrowing behavior. Elevated anxiety symptoms commonly co-occur in patients with ASD and schizophrenia and have been shown to be more prevalent in females (Achim et al., 2011; Gotham et al., 2013).

However, the neocortex is not the only area of the brain that is thought to be involved in social behavior. Subcortical structures such as the amygdala, striatum, nucleus accumbens and the ventral tegmental area are also important modulators of social behavior (Adolphs, 2009; Gunaydin et al., 2014; Lukas et al., 2011; Peça et al., 2011). Recently, the group of Karl Deisseroth optically recorded neural activity in genetically and connectivity defined projections to uncover the role of specified pathways in social behavior (Gunaydin et al., 2014). They found that activation of the projections from the ventral tegmental area to the nucleus accumbens, but not of the ventral tegmental area to the medial prefrontal cortex, favor social interaction in mice. NOMA-GAP is strongly expressed in the nucleus accumbens (Rosário et al., 2012). Further studies will help to understand which specific neural projections underlie social impairments in NOMA-GAP-deficient mice. In summary, NOMA-GAP is a promising candidate molecule for neuropsychiatric pathophysiology.

4.9 Conclusion

The molecular mechanisms for disturbances in dendritic structures that are observed in neuropsychiatric developmental disorders such as ASD and schizophrenia are mostly unknown. This work identified NOMA-GAP as a key regulator of dendritic structures and function in pyramidal neurons of the mammalian neocortex. NOMA-GAP specifically initiates dendritic complexity of layer II-III neurons by a Cdc42-dependent mechanism, and promotes dendritic spine maturation along basal dendrites of layer II-III neurons through a Cdc42-independent mechanism. Moreover, NOMA-GAP interacts with MAGUK family proteins and regulates the surface expression of AMPARs. Interestingly, NOMA-GAP and PSD-95 may spatially and temporally cross-regulate each other. Our collaborations revealed that NOMA-GAP-deficient mice show impaired synaptic transmission and gender-associated social abnormalities that are not dependent on inhibition of Cdc42 signaling downstream of NOMA-GAP (Schuster et

al., 2015). These novel molecular mechanisms shed light on the development of dendritic structures that are fundamental for the precise developmental organization of cortical networks. This new mouse model may help to discover the etiologies of neuropsychiatric disorders and may help to generate novel, mechanism-based treatments.

References

Abrahams, B.S., and Geschwind, D.H. (2008). Advances in autism genetics: on the threshold of a new neurobiology. Nat. Rev. Genet. *9*, 341–355.

Achim, A.M., Maziade, M., Raymond, É., Olivier, D., Mérette, C., and Roy, M.A. (2011). How prevalent are anxiety disorders in schizophrenia? a meta-analysis and critical review on a significant association. Schizophr. Bull. *37*, 811–821.

Adolphs, R. (2009). The social brain: neural basis of social knowledge. Annu. Rev. Psychol. *60*, 693–716.

Aizawa, H., Wakatsuki, S., Ishii, A., Moriyama, K., Sasaki, Y., Ohashi, K., Sekine-Aizawa, Y., Sehara-Fujisawa, A., Mizuno, K., Goshima, Y., et al. (2001). Phosphorylation of cofilin by LIM-kinase is necessary for semaphorin 3A-induced growth cone collapse. Nat. Neurosci. *4*, 367–373.

Aizawa, H., Hu, S.-C., Bobb, K., Balakrishnan, K., Ince, G., Gurevich, I., Cowan, M., and Ghosh, A. (2004). Dendrite development regulated by CREST, a calcium-regulated transcriptional activator. Science *303*, 197–202.

de Anda, F.C., Rosario, A.L., Durak, O., Tran, T., Gräff, J., Meletis, K., Rei, D., Soda, T., Madabhushi, R., Ginty, D.D., et al. (2012). Autism spectrum disorder susceptibility gene TAOK2 affects basal dendrite formation in the neocortex. Nat. Neurosci. *15*, 1022–1031.

Anggono, V., and Huganir, R.L. (2012). Regulation of AMPA receptor trafficking and synaptic plasticity. Curr. Opin. Neurobiol. *22*, 461–469.

Aoki, C., Miko, I., Oviedo, H., Mikeladze-Dvali, T., Alexandre, L., Sweeney, N., and Bredt, D.S. (2001). Electron microscopic immunocytochemical detection of PSD-95, PSD-93, SAP-102, and SAP-97 at postsynaptic, presynaptic, and nonsynaptic sites of adult and neonatal rat visual cortex. Synapse *40*, 239–257.

Aoto, J., Martinelli, D.C., Malenka, R.C., Tabuchi, K., and Südhof, T.C. (2013). Presynaptic neurexin-3 alternative splicing trans-synaptically controls postsynaptic AMPA receptor trafficking. Cell *154*, 75–88.

Araya, R., Vogels, T.P., and Yuste, R. (2014). Activity-dependent dendritic spine neck changes are correlated with synaptic strength. Proc. Natl. Acad. Sci. U. S. A. *111*, 2895–2904.

Arber, S., Barbayannis, F. a, Hanser, H., Schneider, C., Stanyon, C. a, Bernard, O., and Caroni, P. (1998). Regulation of actin dynamics through phosphorylation of cofilin by LIM-kinase. Nature *393*, 805–809.

Arellano, J.I., Benavides-Piccione, R., Defelipe, J., and Yuste, R. (2007). Ultrastructure of dendritic spines: correlation between synaptic and spine morphologies. Front. Neurosci. *1*, 131–143.

Arnaud, L., Ballif, B. a., Förster, E., and Cooper, J. a. (2003). Fyn tyrosine kinase is a critical regulator of Disabled-1 during brain development. Curr. Biol. *13*, 9–17.

Artavanis-Tsakonas, S., Rand, M.D., and Lake, R.J. (1999). Notch signaling: cell fate control and signal integration in development. Science *284*, 770–776.

Baas, P.W., and Lin, S. (2011). Hooks and comets: The story of microtubule polarity orientation in the neuron. Dev. Neurobiol. *71*, 403–418.

Bagri, A., Marín, O., Plump, A.S., Mak, J., Pleasure, S.J., Rubenstein, J.L.R., and Tessier-Lavigne, M. (2002). Slit proteins prevent midline crossing and determine the dorsoventral position of major axonal pathways in the mammalian forebrain. Neuron *33*, 233–248.

Baker, R.E., Dijkhuizen, P. a., Van Pelt, J., and Verhaagen, J. (1998). Growth of pyramidal, but not non-pyramidal, dendrites in long-term organotypic explants of neonatal rat neocortex chronically exposed to neurotrophin-3. Eur. J. Neurosci. *10*, 1037–1044.

Banko, J.L., Poulin, F., Hou, L., DeMaria, C.T., Sonenberg, N., and Klann, E. (2005). The translation repressor 4E-BP2 is critical for eIF4F complex formation, synaptic plasticity, and memory in the hippocampus. J. Neurosci. *25*, 9581–9590.

Baron-Cohen, S., Lombardo, M. V., Auyeung, B., Ashwin, E., Chakrabarti, B., and Knickmeyer, R. (2011). Why are Autism Spectrum conditions more prevalent in Males? PLoS Biol. *9*.

Béïque, J.-C., and Andrade, R. (2003). PSD-95 regulates synaptic transmission and plasticity in rat cerebral cortex. J. Physiol. *546*, 859–867.

Béïque, J.-C., Lin, D.-T., Kang, M.-G., Aizawa, H., Takamiya, K., and Huganir, R.L. (2006). Synapse-specific regulation of AMPA receptor function by PSD-95. Proc. Natl. Acad. Sci. U. S. A. *103*, 19535–19540.

Belgard, T.G., Marques, A.C., Oliver, P.L., Abaan, H.O., Sirey, T.M., Hoerder-Suabedissen, A., García-Moreno, F., Molnár, Z., Margulies, E.H., and Ponting, C.P. (2011). A transcriptomic atlas of mouse neocortical layers. Neuron *71*, 605–616.

Bellenchi, G.C., Gurniak, C.B., Perlas, E., Middei, S., Ammassari-Teule, M., and Witke, W. (2007). N-cofilin is associated with neuronal migration disorders and cell cycle control in the cerebral cortex. Genes Dev. *21*, 2347–2357.

Bernstein, B.W., and Bamburg, J.R. (2010). ADF/cofilin: a functional node in cell biology. Trends Cell Biol. *20*, 187–195.

Bliss, T. V, and Collingridge, G.L. (1993). A synaptic model of memory: long-term potentiation in the hippocampus. Nature *361*, 31–39.

Branco, T., and Häusser, M. (2011). Synaptic Integration Gradients in Single Cortical Pyramidal Cell Dendrites. Neuron *69*, 885–892.

Brandon, N.J., and Sawa, A. (2011). Linking neurodevelopmental and synaptic theories of mental illness through DISC1. Nat. Rev. Neurosci. *12*, 707–722.

Broadbelt, K., Byne, W., and Jones, L.B. (2002). Evidence for a decrease in basilar dendrites of pyramidal cells in schizophrenic medial prefrontal cortex. Schizophr. Res. *58*, 75–81.

Brose, K., Bland, K.S., Wang, K.H., Arnott, D., Henzel, W., Goodman, C.S., Tessier-Lavigne, M., and Kidd, T. (1999). Slit proteins bind Robo receptors and have an evolutionarily conserved role in repulsive axon guidance. Cell *96*, 795–806.

Brown, M.D., Cornejo, B.J., Kuhn, T.B., and Bamburg, J.R. (2000). Cdc42 stimulates neurite outgrowth and formation of growth cone filopodia and lamellipodia. J. Neurobiol. *43*, 352–364.

Cannon, T.D., Thompson, P.M., van Erp, T.G.M., Toga, A.W., Poutanen, V.-P., Huttunen, M., Lonnqvist, J., Standerskjold-Nordenstam, C.-G., Narr, K.L., Khaledy, M., et al. (2002). Cortex mapping reveals regionally specific patterns of genetic and disease-specific gray-matter deficits in twins discordant for schizophrenia. Proc. Natl. Acad. Sci. U. S. A. *99*, 3228–3233.

Cappello, S., Attardo, A., Wu, X., Iwasato, T., Itohara, S., Wilsch-Bräuninger, M., Eilken, H.M., Rieger, M. a, Schroeder, T.T., Huttner, W.B., et al. (2006). The Rho-GTPase cdc42 regulates neural progenitor fate at the apical surface. Nat. Neurosci. *9*, 1099–1107.

Carlisle, H.J., Fink, A.E., Grant, S.G.N., and O'Dell, T.J. (2008). Opposing effects of PSD-93 and PSD-95 on long-term potentiation and spike timing-dependent plasticity. J. Physiol. *586*, 5885–5900.

Caruana, G., and Bernstein, A. (2001). Craniofacial dysmorphogenesis including cleft palate in mice with an insertional mutation in the discs large gene. Mol. Cell. Biol. *21*, 1475–1483.

Chai, X., Förster, E., Zhao, S., Bock, H.H., and Frotscher, M. (2009). Reelin stabilizes the actin cytoskeleton of neuronal processes by inducing n-cofilin phosphorylation at serine3. J. Neurosci. *29*, 288–299.

Chan, C.B., Liu, X., Pradoldej, S., Hao, C., An, J., Yepes, M., Luo, H.R., and Ye, K. (2011). Phosphoinositide 3-kinase enhancer regulates neuronal dendritogenesis and survival in neocortex. J. Neurosci. *31*, 8083–8092.

Charych, E.I., Akum, B.F., Goldberg, J.S., Jörnsten, R.J., Rongo, C., Zheng, J.Q., and Firestein, B.L. (2006). Activity-independent regulation of dendrite patterning by postsynaptic density protein PSD-95. J. Neurosci. *26*, 10164–10176.

Chen, B., Wang, S.S., Hattox, A.M., Rayburn, H., Nelson, S.B., and McConnell, S.K. (2008). The Fezf2-Ctip2 genetic pathway regulates the fate choice of subcortical projection neurons in the developing cerebral cortex. Proc. Natl. Acad. Sci. U. S. A. *105*, 11382–11387.

Chen, B.-S., Thomas, E. V, Sanz-Clemente, A., and Roche, K.W. (2011). NMDA receptor-dependent regulation of dendritic spine morphology by SAP102 splice variants. J. Neurosci. *31*, 89–96.

Chen, J.-G., Rasin, M.-R., Kwan, K.Y., and Sestan, N. (2005). Zfp312 is required for subcortical axonal projections and dendritic morphology of deep-layer pyramidal neurons of the cerebral cortex. Proc. Natl. Acad. Sci. U. S. A. *102*, 17792–17797.

Chiang, S.-H., Hwang, J., Legendre, M., Zhang, M., Kimura, A., and Saltiel, A.R. (2003). TCGAP, a multidomain Rho GTPase-activating protein involved in insulin-stimulated glucose transport. EMBO J. *22*, 2679–2691.

Cingolani, L. a, and Goda, Y. (2008). Actin in action: the interplay between the actin cytoskeleton and synaptic efficacy. Nat. Rev. Neurosci. *9*, 344–356.

Clement, J.P., Ozkan, E.D., Aceti, M., Miller, C. a, and Rumbaugh, G. (2013). SYNGAP1 links the maturation rate of excitatory synapses to the duration of critical-period synaptic plasticity. J. Neurosci. *33*, 10447–10452.

Colledge, M., Snyder, E.M., Crozier, R. a., Soderling, J. a., Jin, Y., Langeberg, L.K., Lu, H., Bear, M.F., and Scott, J.D. (2003). Ubiquitination Regulates PSD-95 Degradation and AMPA Receptor Surface Expression. Neuron *40*, 595–607.

Collingridge, G.L., Isaac, J.T.R., and Wang, Y.T. (2004). Receptor trafficking and synaptic plasticity. Nat. Rev. Neurosci. *5*, 952–962.

Conde, C., and Cáceres, A. (2009). Microtubule assembly, organization and dynamics in axons and dendrites. Nat. Rev. Neurosci. *10*, 319–332.

Crawley, J.N. (2007). Mouse behavioral assays relevant to the symptoms of autism. In Brain Pathology, pp. 448–459.

Cubelos, B., Sebastián-Serrano, A., Beccari, L., Calcagnotto, M.E., Cisneros, E., Kim, S., Dopazo, A., Alvarez-Dolado, M., Redondo, J.M., Bovolenta, P., et al. (2010). Cux1 and Cux2 regulate dendritic branching, spine morphology, and synapses of the upper layer neurons of the cortex. Neuron *66*, 523–535.

Cubelos, B., Briz, C.G., Esteban-Ortega, G.M., and Nieto, M. (2014). Cux1 and Cux2 selectively target basal and apical dendritic compartments of layer II-III cortical neurons. Dev. Neurobiol. *5*, 163–172.

Cui-Wang, T., Hanus, C., Cui, T., Helton, T., Bourne, J., Watson, D., Harris, K.M., and Ehlers, M.D. (2012). Local zones of endoplasmic reticulum complexity confine cargo in neuronal dendrites. Cell *148*, 309–321.

Cuthbert, P.C., Stanford, L.E., Coba, M.P., Ainge, J.A., Fink, A.E., Opazo, P., Delgado, J.Y., Komiyama, N.H., O'Dell, T.J., and Grant, S.G.N. (2007). Synapse-associated protein 102/dlgh3 couples the NMDA receptor to specific plasticity pathways and learning strategies. J. Neurosci. *27*, 2673–2682.

D'Arcangelo, G. (2014). Reelin in the Years: Controlling Neuronal Migration and Maturation in the Mammalian Brain. Adv. Neurosci. *2014*, 1–19.

D'Arcangelo, G., Miao, G.G., Chen, S.C., Soares, H.D., Morgan, J.I., and Curran, T. (1995). A protein related to extracellular matrix proteins deleted in the mouse mutant reeler. Nature *374*, 719–723.

Dailey, M.E., and Smith, S.J. (1996). The dynamics of dendritic structure in developing hippocampal slices. J. Neurosci. *16*, 2983–2994.

Dalva, M.B., McClelland, A.C., and Kayser, M.S. (2007). Cell adhesion molecules: signalling functions at the synapse. Nat. Rev. Neurosci. *8*, 206–220.

DeGiorgis, J.A., Galbraith, J.A., Dosemeci, A., Chen, X., and Reese, T.S. (2006). Distribution of the scaffolding proteins PSD-95, PSD-93, and SAP97 in isolated PSDs. Brain Cell Biol. *35*, 239–250.

Dent, E.W., Kwiatkowski, A. V, Mebane, L.M., Philippar, U., Barzik, M., Rubinson, D. a, Gupton, S., Van Veen, J.E., Furman, C., Zhang, J., et al. (2007). Filopodia are required for cortical neurite initiation. Nat. Cell Biol. *9*, 1347–1359.

Desai, N.S., Cudmore, R.H., Nelson, S.B., and Turrigiano, G.G. (2002). Critical periods for experience-dependent synaptic scaling in visual cortex. Nat. Neurosci. *5*, 783–789.

Dong, X., Shen, K., and Bülow, H.E. (2014). Intrinsic and Extrinsic Mechanisms of Dendritic Morphogenesis. Annu. Rev. Physiol. *77*, 271–300.

Ebert, D.H., and Greenberg, M.E. (2013). Activity-dependent neuronal signalling and autism spectrum disorder. Nature *493*, 327–337.

Edwards, D.C., Sanders, L.C., Bokoch, G.M., and Gill, G.N. (1999). Activation of LIM-kinase by Pak1 couples Rac/Cdc42 GTPase signalling to actin cytoskeletal dynamics. Nat. Cell Biol. *1*, 253–259.

Ehrlich, I., and Malinow, R. (2004). Postsynaptic density 95 controls AMPA receptor incorporation during long-term potentiation and experience-driven synaptic plasticity. J. Neurosci. *24*, 916–927.

Ehrlich, I., Klein, M., Rumpel, S., and Malinow, R. (2007). PSD-95 is required for activity-driven synapse stabilization. Proc. Natl. Acad. Sci. U. S. A. *104*, 4176–4181.

El-Husseini, A.E., Schnell, E., Chetkovich, D.M., Nicoll, R.A., and Bredt, D.S. (2000). PSD-95 involvement in maturation of excitatory synapses. Science *290*, 1364–1368.

Elias, G.M., Funke, L., Stein, V., Grant, S.G., Bredt, D.S., and Nicoll, R. a. (2006). Synapse-Specific and Developmentally Regulated Targeting of AMPA Receptors by a Family of MAGUK Scaffolding Proteins. Neuron *52*, 307–320.

Etherton, M.R., Tabuchi, K., Sharma, M., Ko, J., and Südhof, T.C. (2011). An autism-associated point mutation in the neuroligin cytoplasmic tail selectively impairs AMPA receptor-mediated synaptic transmission in hippocampus. EMBO J. *30*, 2908–2919.

Etienne-Manneville, S., and Hall, A. (2002). Rho GTPases in cell biology. Nature *420*, 629–635.

Feldman, D.E., and Brecht, M. (2005). Map plasticity in somatosensory cortex. Science *310*, 810–815.

Fenstermaker, V., Chen, Y., Ghosh, A., and Yuste, R. (2004). Regulation of Dendritic Length and Branching by Semaphorin 3A. J. Neurobiol. *58*, 403–412.

Feyder, M., Karlsson, R.M., Mathur, P., Lyman, M., Bock, R., Momenan, R., Munasinghe, J., Scattoni, M.L., Ihne, J., Camp, M., et al. (2010). Association of mouse Dlg4 (PSD-95) gene deletion and human DLG4 gene variation with phenotypes relevant to autism spectrum disorders and Williams' syndrome. Am. J. Psychiatry *167*, 1508–1517.

Flynn, K.C., Hellal, F., Neukirchen, D., Jacob, S., Tahirovic, S., Dupraz, S., Stern, S., Garvalov, B.K., Gurniak, C., Shaw, A.E., et al. (2012). ADF/cofilin-mediated actin retrograde flow directs neurite formation in the developing brain. Neuron *76*, 1091–1107.

Franco, S.J., and Müller, U. (2013). Shaping our minds: stem and progenitor cell diversity in the mammalian neocortex. Neuron *77*, 19–34.

Fromer, M., Pocklington, A.J., Kavanagh, D.H., Williams, H.J., Dwyer, S., Gormley, P., Georgieva, L., Rees, E., Palta, P., Ruderfer, D.M., et al. (2014). De novo mutations in schizophrenia implicate synaptic networks. Nature *506*, 179–184.

Frotscher, M. (1998). Cajal-Retzius cells, Reelin, and the formation of layers. Curr. Opin. Neurobiol. *8*, 570–575.

Gao, F.B., Brenman, J.E., Jan, L.Y., and Jan, Y.N. (1999). Genes regulating dendritic outgrowth, branching, and routing in Drosophila. Genes Dev. *13*, 2549–2561.

Gao, Z., Ure, K., Ables, J.L., Lagace, D.C., Nave, K.-A., Goebbels, S., Eisch, A.J., and Hsieh, J. (2009). Neurod1 is essential for the survival and maturation of adult-born neurons. Nat. Neurosci. *12*, 1090–1092.

Garey, L.J., Ong, W.Y., Patel, T.S., Kanani, M., Davis, a, Mortimer, a M., Barnes, T.R., and Hirsch, S.R. (1998). Reduced dendritic spine density on cerebral cortical pyramidal neurons in schizophrenia. J. Neurol. Neurosurg. Psychiatry *65*, 446–453.

Garvalov, B.K., Flynn, K.C., Neukirchen, D., Meyn, L., Teusch, N., Wu, X., Brakebusch, C., Bamburg, J.R., and Bradke, F. (2007). Cdc42 regulates cofilin during the establishment of neuronal polarity. J. Neurosci. *27*, 13117–13129.

Gaudillière, B., Konishi, Y., De La Iglesia, N., Yao, G.L., and Bonni, A. (2004). A CaMKII-NeuroD Signaling Pathway Specifies Dendritic Morphogenesis. Neuron *41*, 229–241.

Geiger, J.C., Lipka, J., Segura, I., Hoyer, S., Schlager, M.A., Wulf, P.S., Weinges, S., Demmers, J., Hoogenraad, C.C., and Acker-Palmer, A. (2014). The GRIP1/14-3-3 pathway coordinates cargo trafficking and dendrite development. Dev. Cell *28*, 381–393.

Geschwind, D.H., and Levitt, P. (2007). Autism spectrum disorders: developmental disconnection syndromes. Curr. Opin. Neurobiol. *17*, 103–111.

Glantz, L.A., and Lewis, D.A. (2000). Decreased dendritic spine density on prefrontal cortical pyramidal neurons in schizophrenia. Arch. Gen. Psychiatry *57*, 65–73.

Goebbels, S., Bormuth, I., Bode, U., Hermanson, O., Schwab, M.H., and Nave, K.A. (2006). Genetic targeting of principal neurons in neocortex and hippocampus of NEX-Cre mice. Genesis *44*, 611–621.

Gogtay, N. (2008). Cortical brain development in schizophrenia: Insights from neuroimaging studies in childhood-onset schizophrenia. Schizophr. Bull. *34*, 30–36.

Gotham, K., Bishop, S.L., Hus, V., Huerta, M., Lund, S., Buja, A., Krieger, A., and Lord, C. (2013). Exploring the relationship between anxiety and insistence on sameness in

autism spectrum disorders. Autism Res. *6*, 33–41.

Govek, E.-E., Newey, S.E., and Van Aelst, L. (2005). The role of the Rho GTPases in neuronal development. Genes Dev. *19*, 1–49.

Greig, L.C., Woodworth, M.B., Galazo, M.J., Padmanabhan, H., and Macklis, J.D. (2013). Molecular logic of neocortical projection neuron specification, development and diversity. Nat. Rev. Neurosci. *14*, 755–769.

Grueber, W.B., Jan, L.Y., and Jan, Y.N. (2003). Different levels of the homeodomain protein cut regulate distinct dendrite branching patterns of Drosophila multidendritic neurons. Cell *112*, 805–818.

Gu, C., Rodriguez, E.R., Reimert, D. V., Shu, T., Fritzsch, B., Richards, L.J., Kolodkin, A.L., and Ginty, D.D. (2003). Neuropilin-1 conveys semaphorin and VEGF signaling during neural and cardiovascular development. Dev. Cell *5*, 45–57.

Gu, J., Lee, C.W., Fan, Y., Komlos, D., Tang, X., Sun, C., Yu, K., Hartzell, H.C., Chen, G., Bamburg, J.R., et al. (2010). ADF/cofilin-mediated actin dynamics regulate AMPA receptor trafficking during synaptic plasticity. Nat. Neurosci. *13*, 1208–1215.

Gunaydin, L. a., Grosenick, L., Finkelstein, J.C., Kauvar, I. V., Fenno, L.E., Adhikari, A., Lammel, S., Mirzabekov, J.J., Airan, R.D., Zalocusky, K. a., et al. (2014). Natural neural projection dynamics underlying social behavior. Cell *157*, 1535–1551.

Guy, J., Hendrich, B., Holmes, M., Martin, J.E., and Bird, a (2001). A mouse Mecp2-null mutation causes neurological symptoms that mimic Rett syndrome. Nat. Genet. *27*, 322–326.

Häfner, H. (2005). Gender differences in schizophrenia. In Estrogen Effects in Psychiatric Disorders, pp. 53–94.

Hall, A., and Lalli, G. (2010). Rho and Ras GTPases in axon growth, guidance, and branching. Cold Spring Harb. Perspect. Biol. *2*, a001818.

Hanley, J.G. (2014). Actin-dependent mechanisms in AMPA receptor trafficking. Front. Cell. Neurosci. *8*, 1–8.

Hanse, E., Seth, H., and Riebe, I. (2013). AMPA-silent synapses in brain development and pathology. Nat. Rev. Neurosci. *14*, 839–850.

Hanus, C., and Ehlers, M.D. (2008). Secretory outposts for the local processing of membrane cargo in neuronal dendrites. Traffic *9*, 1437–1445.

Harlow, E.G., Till, S.M., Russell, T.A., Wijetunge, L.S., Kind, P., and Contractor, A. (2010). Critical Period Plasticity Is Disrupted in the Barrel Cortex of Fmr1 Knockout Mice. Neuron *65*, 385–398.

Hayashi, K. (2002). Pak1 Is Involved in Dendrite Initiation as a Downstream Effector of Rac1 in Cortical Neurons. Mol. Cell. Neurosci. *20*, 579–594.

Hayashi, T., Okabe, T., Nasu-Nishimura, Y., Sakaue, F., Ohwada, S., Matsuura, K., Akiyama, T., and Nakamura, T. (2007). PX-RICS, a novel splicing variant of RICS, is a main isoform expressed during neural development. Genes Cells *12*, 929–939.

Hayashi-Takagi, A., Takaki, M., Graziane, N., Seshadri, S., Murdoch, H., Dunlop, A.J., Makino, Y., Seshadri, A.J., Ishizuka, K., Srivastava, D.P., et al. (2010). Disrupted-in-Schizophrenia 1 (DISC1) regulates spines of the glutamate synapse via Rac1. Nat. Neurosci. *13*, 327–332.

Hennah, W., Varilo, T., Kestilä, M., Paunio, T., Arajärvi, R., Haukka, J., Parker, A., Martin, R., Levitzky, S., Partonen, T., et al. (2003). Haplotype transmission analysis provides evidence of association for DISC1 to schizophrenia and suggests sex-dependent effects. Hum. Mol. Genet. *12*, 3151–3159.

Hirokawa, N., Niwa, S., and Tanaka, Y. (2010). Molecular motors in neurons: Transport mechanisms and roles in brain function, development, and disease. Neuron *68*, 610–638.

Holtmaat, A., and Svoboda, K. (2009). Experience-dependent structural synaptic plasticity in the mammalian brain. Nat. Rev. Neurosci. *10*, 647–658.

Hoogenraad, C.C., Milstein, A.D., Ethell, I.M., Henkemeyer, M., and Sheng, M. (2005). GRIP1 controls dendrite morphogenesis by regulating EphB receptor trafficking. Nat. Neurosci. *8*, 906–915.

Horton, A.C., and Ehlers, M.D. (2003). Dual modes of endoplasmic reticulum-to-Golgi transport in dendrites revealed by live-cell imaging. J. Neurosci. *23*, 6188–6199.

Horton, A.C., Rácz, B., Monson, E.E., Lin, A.L., Weinberg, R.J., and Ehlers, M.D. (2005). Polarized secretory trafficking directs cargo for asymmetric dendrite growth and morphogenesis. Neuron *48*, 757–771.

Hotulainen, P., and Hoogenraad, C.C. (2010). Actin in dendritic spines: connecting dynamics to function. J. Cell Biol. *189*, 619–629.

Howard, M. a, Elias, G.M., Elias, L. a B., Swat, W., and Nicoll, R. a (2010). The role of SAP97 in synaptic glutamate receptor dynamics. Proc. Natl. Acad. Sci. U. S. A. *107*, 3805–3810.

Huang, Y.Z., Won, S., Ali, D.W., Wang, Q., Tanowitz, M., Du, Q.S., Pelkey, K. a., Yang, D.J., Xiong, W.C., Salter, M.W., et al. (2000). Regulation of Neuregulin Signaling by PSD-95 Interacting with ErbB4 at CNS Synapses. Neuron *26*, 443–455.

Huganir, R.L., and Nicoll, R.A. (2013). Perspective AMPARs and Synaptic Plasticity : The Last 25 Years. Neuron *80*, 704–717.

Hutsler, J.J., and Zhang, H. (2010). Increased dendritic spine densities on cortical projection neurons in autism spectrum disorders. Brain Res. *1309*, 83–94.

Irie, F., and Yamaguchi, Y. (2002). EphB receptors regulate dendritic spine development via intersectin, Cdc42 and N-WASP. Nat. Neurosci. *5*, 1117–1118.

Irie, M., Hata, Y., Takeuchi, M., Ichtchenko, K., Toyoda, A., Hirao, K., Takai, Y., Rosahl, T.W., and Südhof, T.C. (1997). Binding of neuroligins to PSD-95. Science *277*, 1511–1515.

Iwasato, T., Datwani, a, Wolf, a M., Nishiyama, H., Taguchi, Y., Tonegawa, S., Knöpfel, T., Erzurumlu, R.S., and Itohara, S. (2000). Cortex-restricted disruption of

NMDAR1 impairs neuronal patterns in the barrel cortex. Nature *406*, 726–731.

Jamain, S., Radyushkin, K., Hammerschmidt, K., Granon, S., Boretius, S., Varoqueaux, F., Ramanantsoa, N., Gallego, J., Ronnenberg, A., Winter, D., et al. (2008). Reduced social interaction and ultrasonic communication in a mouse model of monogenic heritable autism. Proc. Natl. Acad. Sci. U. S. A. *105*, 1710–1715.

Jan, Y.-N., and Jan, L.Y. (2010). Branching out: mechanisms of dendritic arborization. Nat. Rev. Neurosci. *11*, 316–328.

Ji, Y., Pang, P.T., Feng, L., and Lu, B. (2005). Cyclic AMP controls BDNF-induced TrkB phosphorylation and dendritic spine formation in mature hippocampal neurons. Nat. Neurosci. *8*, 164–172.

Jia, H., Rochefort, N.L., Chen, X., and Konnerth, a. (2010). Dendritic organization of sensory input to cortical neurons in vivo. Neuroforum *16*, 236–237.

Jiang, Y.-H., and Ehlers, M.D. (2013). Modeling autism by SHANK gene mutations in mice. Neuron *78*, 8–27.

Kamiya, A., Kubo, K., Tomoda, T., Takaki, M., Youn, R., Ozeki, Y., Sawamura, N., Park, U., Kudo, C., Okawa, M., et al. (2005). A schizophrenia-associated mutation of DISC1 perturbs cerebral cortex development. Nat. Cell Biol. *7*, 1167–1178.

Kang, E., Burdick, K.E., Kim, J.Y., Duan, X., Guo, J.U., Sailor, K. a, Jung, D.-E., Ganesan, S., Choi, S., Pradhan, D., et al. (2011). Interaction between FEZ1 and DISC1 in regulation of neuronal development and risk for schizophrenia. Neuron *72*, 559–571.

Kato, H., Ohno, K., Hashimoto, K., and Sato, K. (2004). Synectin in the nervous system: expression pattern and potential as a binding partner of neurotrophin receptors. FEBS Lett. *572*, 123–128.

Katz, L.C., and Shatz, C.J. (1996). Synaptic activity and the construction of cortical circuits. Science *274*, 1133–1138.

Kidd, T., Bland, K.S., and Goodman, C.S. (1999). Slit is the midline repellent for the robo receptor in Drosophila. Cell *96*, 785–794.

Kim, I.H., Wang, H., Soderling, S.H., and Yasuda, R. (2014). Loss of Cdc42 leads to defects in synaptic plasticity and remote memory recall. Elife *3*, 1–16.

Kim, M.J., Futai, K., Jo, J., Hayashi, Y., Cho, K., and Sheng, M. (2007). Synaptic accumulation of PSD-95 and synaptic function regulated by phosphorylation of serine-295 of PSD-95. Neuron *56*, 488–502.

Kim, Y., Ha, C.M., and Chang, S. (2013). SNX26, a GTPase-activating protein for Cdc42, interacts with PSD-95 protein and is involved in activity-dependent dendritic spine formation in mature neurons. J. Biol. Chem. *288*, 29453–29466.

Klöcker, N., Bunn, R.C., Schnell, E., Caruana, G., Bernstein, A., Nicoll, R.A., and Bredt, D.S. (2002). Synaptic glutamate receptor clustering in mice lacking the SH3 and GK domains of SAP97. Eur. J. Neurosci. *16*, 1517–1522.

Köhr, G. (2006). NMDA receptor function: Subunit composition versus spatial

distribution. Cell Tissue Res. *326*, 439–446.

Kornau, H.C., Schenker, L.T., Kennedy, M.B., and Seeburg, P.H. (1995). Domain interaction between NMDA receptor subunits and the postsynaptic density protein PSD-95. Science *269*, 1737–1740.

Krugers, H.J., Hoogenraad, C.C., and Groc, L. (2010). Stress hormones and AMPA plasticity and memory. Nat. Publ. Gr. *11*, 675–681.

Ku, C.S., Polychronakos, C., Tan, E.K., Naidoo, N., Pawitan, Y., Roukos, D.H., Mort, M., and Cooper, D.N. (2013). A new paradigm emerges from the study of de novo mutations in the context of neurodevelopmental disease. Mol. Psychiatry *18*, 141–153.

Kulkarni, V. a., and Firestein, B.L. (2012). The dendritic tree and brain disorders. Mol. Cell. Neurosci. *50*, 10–20.

De La Torre-Ubieta, L., Gaudillière, B., Yang, Y., Ikeuchi, Y., Yamada, T., Dibacco, S., Stegmüller, J., Schüller, U., Salih, D. a, Rowitch, D., et al. (2010). A FOXO-Pak1 transcriptional pathway controls neuronal polarity. Genes Dev. *24*, 799–813.

Lau, C.G., and Zukin, R.S. (2007). NMDA receptor trafficking in synaptic plasticity and neuropsychiatric disorders. Nat. Rev. Neurosci. *8*, 413–426.

Lee, S.H., Ripke, S., Neale, B.M., Faraone, S. V, Purcell, S.M., Perlis, R.H., Mowry, B.J., Thapar, A., Goddard, M.E., Witte, J.S., et al. (2013). Genetic relationship between five psychiatric disorders estimated from genome-wide SNPs. Nat. Genet. *45*, 984–994.

Lee, T., Winter, C., Marticke, S.S., Lee, a, and Luo, L. (2000). Essential roles of Drosophila RhoA in the regulation of neuroblast proliferation and dendritic but not axonal morphogenesis. Neuron *25*, 307–316.

Leemhuis, J., Bouché, E., Frotscher, M., Henle, F., Hein, L., Herz, J., Meyer, D.K., Pichler, M., Roth, G., Schwan, C., et al. (2010). Reelin signals through apolipoprotein E receptor 2 and Cdc42 to increase growth cone motility and filopodia formation. J. Neurosci. *30*, 14759–14772.

Leonard, A.S., Davare, M.A., Horne, M.C., Garner, C.C., and Hell, J.W. (1998). SAP97 is associated with the α-amino-3-hydroxy-5-methylisoxazole-4- propionic acid receptor GluR1 subunit. J. Biol. Chem. *273*, 19518–19524.

Li, B., Woo, R.-S., Mei, L., and Malinow, R. (2007). The neuregulin-1 receptor erbB4 controls glutamatergic synapse maturation and plasticity. Neuron *54*, 583–597.

Li, J., Shi, M., Ma, Z., Zhao, S., Euskirchen, G., Ziskin, J., Urban, A., Hallmayer, J., and Snyder, M. (2014). Integrated systems analysis reveals a molecular network underlying autism spectrum disorders. Mol. Syst. Biol. *10*, 774–774.

Li, W., Wang, F., Menut, L., and Gao, F.B. (2004). BTB/POZ-zinc finger protein abrupt suppresses dendritic branching in a neuronal subtype-specific and dosage-dependent manner. Neuron *43*, 823–834.

Li, Z., Van Aelst, L., and Cline, H.T. (2000). Rho GTPases regulate distinct aspects of dendritic arbor growth in Xenopus central neurons in vivo. Nat. Neurosci. *3*, 217–225.

Lin, D.-T., Makino, Y., Sharma, K., Hayashi, T., Neve, R., Takamiya, K., and Huganir, R.L. (2009). Regulation of AMPA receptor extrasynaptic insertion by 4.1N, phosphorylation and palmitoylation. Nat. Neurosci. *12*, 879–887.

Liu, H., Nakazawa, T., Tezuka, T., and Yamamoto, T. (2006). Physical and functional interaction of Fyn tyrosine kinase with a brain-enriched Rho GTPase-activating protein TCGAP. J. Biol. Chem. *281*, 23611–23619.

Liu, X., Murray, K., and Jones, E. (2004). Switching of NMDA receptor 2A and 2B subunits at thalamic and cortical synapses during early postnatal development. J. Neurosci. *24*, 8885–8895.

Lois, C., Hong, E.J., Pease, S., Brown, E.J., and Baltimore, D. (2002). Germline transmission and tissue-specific expression of transgenes delivered by lentiviral vectors. Science *295*, 868–872.

London, M., and Häusser, M. (2005). Dendritic computation. Annu. Rev. Neurosci. *28*, 503–532.

Long, H., Zhu, X., Yang, P., Gao, Q., Chen, Y., and Ma, L. (2012). Myo9b and RICS modulate dendritic morphology of cortical neurons. Cereb. Cortex *23*, 71–79.

Lui, J.H., Hansen, D. V, and Kriegstein, A.R. (2011). Development and evolution of the human neocortex. Cell *146*, 18–36.

Luikart, B.W., Nef, S., Virmani, T., Lush, M.E., Liu, Y., Kavalali, E.T., and Parada, L.F. (2005). TrkB has a cell-autonomous role in the establishment of hippocampal Schaffer collateral synapses. J. Neurosci. *25*, 3774–3786.

Lukas, M., Toth, I., Reber, S.O., Slattery, D. a, Veenema, A.H., and Neumann, I.D. (2011). The neuropeptide oxytocin facilitates pro-social behavior and prevents social avoidance in rats and mice. Neuropsychopharmacology *36*, 2159–2168.

Luo, L., Liao, Y.J., Jan, L.Y., and Jan, Y.N. (1994). Distinct morphogenetic functions of similar small GTPases: Drosophila Drac1 is involved in axonal outgrowth and myoblast fusion. Genes Dev. *8*, 1787–1802.

Luo, L., Hensch, T.K., Ackerman, L., Barbel, S., Jan, L.Y., and Jan, Y.N. (1996). Differential effects of the Rac GTPase on Purkinje cell axons and dendritic trunks and spines. Nature.

Marín, O. (2013). Cellular and molecular mechanisms controlling the migration of neocortical interneurons. Eur. J. Neurosci. *38*, 2019–2029.

Matsui, A., Tran, M., Yoshida, A.C., Kikuchi, S.S., U, M., Ogawa, M., and Shimogori, T. (2013). BTBD3 controls dendrite orientation toward active axons in mammalian neocortex. Science *342*, 1114–1118.

Matsuki, T., Matthews, R.T., Cooper, J.A., Van Der Brug, M.P., Cookson, M.R., Hardy, J.A., Olson, E.C., and Howell, B.W. (2010). Reelin and Stk25 have opposing roles in neuronal polarization and dendritic Golgi deployment. Cell *143*, 826–836.

Matsuzaki, M., Ellis-Davies, G.C., Nemoto, T., Miyashita, Y., Iino, M., and Kasai, H. (2001). Dendritic spine geometry is critical for AMPA receptor expression in

hippocampal CA1 pyramidal neurons. Nat. Neurosci. *4*, 1086–1092.

Mayford, M., Siegelbaum, S. a, and Kandel, E.R. (2012). Synapses and memory storage. Cold Spring Harb. Perspect. Biol. *4*.

McAllister, A.K., Lo, D.C., and Katz, L.C. (1995). Neurotrophins regulate dendritic growth in developing visual cortex. Neuron *15*, 791–803.

McAllister, A.K., Katz, L.C., and Lo, D.C. (1997). Opposing roles for endogenous BDNF and NT-3 in regulating cortical dendritic growth. Neuron *18*, 767–778.

McGee, A.W., Topinka, J.R., Hashimoto, K., Petralia, R.S., Kakizawa, S., Kauer, F.W., Aguilera-Moreno, A., Wenthold, R.J., Kano, M., and Bredt, D.S. (2001). PSD-93 knock-out mice reveal that neuronal MAGUKs are not required for development or function of parallel fiber synapses in cerebellum. J. Neurosci. *21*, 3085–3091.

Miao, S., Chen, R., Ye, J., Tan, G.-H., Li, S., Zhang, J., Jiang, Y., and Xiong, Z.-Q. (2013). The Angelman syndrome protein Ube3a is required for polarized dendrite morphogenesis in pyramidal neurons. J. Neurosci. *33*, 327–333.

Migaud, M., Charlesworth, P., Dempster, M., Webster, L.C., Watabe, A.M., Makhinson, M., He, Y., Ramsay, M.F., Morris, R.G., Morrison, J.H., et al. (1998). Enhanced long-term potentiation and impaired learning in mice with mutant postsynaptic density-95 protein. Nature *396*, 433–439.

Molyneaux, B.J., Arlotta, P., Menezes, J.R.L., and Macklis, J.D. (2007). Neuronal subtype specification in the cerebral cortex. Nat. Rev. Neurosci. *8*, 427–437.

Moon, S.Y., Zang, H., and Zheng, Y. (2003). Characterization of a brain-specific Rho GTPase-activating protein, p200RhoGAP. J. Biol. Chem. *278*, 4151–4159.

Morita, A., Yamashita, N., Sasaki, Y., Uchida, Y., Nakajima, O., Nakamura, F., Yagi, T., Taniguchi, M., Usui, H., Katoh-semba, R., et al. (2006). Regulation of Dendritic Branching and Spine Maturation by Semaphorin3A-Fyn Signaling. *26*, 2971–2980.

Moriyama, K., Iida, K., and Yahara, I. (1996). Phosphorylation of Ser-3 of cofilin regulates its essential function on actin. Genes Cells *1*, 73–86.

Murakoshi, H., Wang, H., and Yasuda, R. (2011). Local, persistent activation of Rho GTPases during plasticity of single dendritic spines. Nature *472*, 100–104.

Nakagawa, T., Futai, K., Lashuel, H.A., Lo, I., Okamoto, K., Walz, T., Hayashi, Y., and Sheng, M. (2004). Quaternary structure, protein dynamics, and synaptic function of SAP97 controlled by L27 domain interactions. Neuron *44*, 453–467.

Nakamura, T., Komiya, M., Sone, K., Hirose, E., Gotoh, N., Morii, H., Ohta, Y., and Mori, N. (2002). Grit, a GTPase-activating protein for the Rho family, regulates neurite extension through association with the TrkA receptor and N-Shc and CrkL/Crk adapter molecules. Mol. Cell. Biol. *22*, 8721–8734.

Nakayama, A.Y., Harms, M.B., and Luo, L. (2000). Small GTPases Rac and Rho in the maintenance of dendritic spines and branches in hippocampal pyramidal neurons. J. Neurosci. *20*, 5329–5338.

Nasu-Nishimura, Y., Hayashi, T., Ohishi, T., Okabe, T., Ohwada, S., Hasegawa, Y., Senda, T., Toyoshima, C., Nakamura, T., and Akiyama, T. (2006). Role of the Rho GTPase-activating protein RICS in neurite outgrowth. Genes Cells *11*, 607–614.

Newey, S.E., Velamoor, V., Govek, E.-E., and Van Aelst, L. (2005). Rho GTPases, dendritic structure, and mental retardation. J. Neurobiol. *64*, 58–74.

Newpher, T.M., and Ehlers, M.D. (2008). Glutamate receptor dynamics in dendritic microdomains. Neuron *58*, 472–497.

Ng, J., Nardine, T., Harms, M., Tzu, J., Goldstein, A., Sun, Y., Dietzl, G., Dickson, B.J., and Luo, L. (2002). Rac GTPases control axon growth, guidance and branching. Nature *416*, 442–447.

Niblock, M.M., Brunso-Bechtold, J.K., and Riddle, D.R. (2000). Insulin-like growth factor I stimulates dendritic growth in primary somatosensory cortex. J. Neurosci. *20*, 4165–4176.

Niell, C.M., Meyer, M.P., and Smith, S.J. (2004). In vivo imaging of synapse formation on a growing dendritic arbor. Nat. Neurosci. *7*, 254–260.

Nithianantharajah, J., Komiyama, N.H., McKechanie, A., Johnstone, M., Blackwood, D.H., St Clair, D., Emes, R.D., van de Lagemaat, L.N., Saksida, L.M., Bussey, T.J., et al. (2013). Synaptic scaffold evolution generated components of vertebrate cognitive complexity. Nat. Neurosci. *16*, 16–24.

Niu, S., Renfro, A., Quattrocchi, C.C., Sheldon, M., and D'Arcangelo, G. (2004). Reelin Promotes Hippocampal Dendrite Development through the VLDLR/ApoER2-Dab1 Pathway. Neuron *41*, 71–84.

Noctor, S.C., Flint, A.C., Weissman, T.A., Dammerman, R.S., and Kriegstein, A.R. (2001). Neurons derived from radial glial cells establish radial units in neocortex. Nature *409*, 714–720.

Okabe, T., Nakamura, T., Nishimura, Y.N., Kohu, K., Ohwada, S., Morishita, Y., and Akiyama, T. (2003). RICS, a novel GTPase-activating protein for Cdc42 and Rac1, is involved in the beta-catenin-N-cadherin and N-methyl-D-aspartate receptor signaling. J. Biol. Chem. *278*, 9920–9927.

Oliva, C., Escobedo, P., Astorga, C., Molina, C., and Sierralta, J. (2012). Role of the MAGUK protein family in synapse formation and function. Dev. Neurobiol. *72*, 57–72.

Olson, E.C., Kim, S., and Walsh, C. a (2006). Impaired neuronal positioning and dendritogenesis in the neocortex after cell-autonomous Dab1 suppression. J. Neurosci. *26*, 1767–1775.

Ori-McKenney, K.M., Jan, L.Y., and Jan, Y.-N. (2012). Golgi outposts shape dendrite morphology by functioning as sites of acentrosomal microtubule nucleation in neurons. Neuron *76*, 921–930.

Park, H., and Poo, M. (2013). Neurotrophin regulation of neural circuit development and function. Nat. Rev. Neurosci. *14*, 7–23.

Parrish, J.Z., Emoto, K., Kim, M.D., and Jan, Y.N. (2007). Mechanisms that regulate

establishment, maintenance, and remodeling of dendritic fields. Annu. Rev. Neurosci. *30*, 399–423.

Peça, J., Feliciano, C., Ting, J.T., Wang, W., Wells, M.F., Venkatraman, T.N., Lascola, C.D., Fu, Z., and Feng, G. (2011). Shank3 mutant mice display autistic-like behaviours and striatal dysfunction. Nature *472*, 437–442.

Peng, Y.R., He, S., Marie, H., Zeng, S.Y., Ma, J., Tan, Z.J., Lee, S.Y., Malenka, R.C., and Yu, X. (2009). Coordinated Changes in Dendritic Arborization and Synaptic Strength during Neural Circuit Development. Neuron *61*, 71–84.

Penzes, P., Cahill, M.E., Jones, K. a, VanLeeuwen, J.-E., and Woolfrey, K.M. (2011). Dendritic spine pathology in neuropsychiatric disorders. Nat. Neurosci. *14*, 285–293.

Perez de Arce, K., de Arce, K.P., Varela-Nallar, L., Farias, O., Cifuentes, A., Bull, P., Couch, B. a, Koleske, A.J., Inestrosa, N.C., and Alvarez, A.R. (2010). Synaptic clustering of PSD-95 is regulated by c-Abl through tyrosine phosphorylation. J. Neurosci. *30*, 3728–3738.

Petersen, C.C.H. (2007). The functional organization of the barrel cortex. Neuron *56*, 339–355.

Petrinovic, M.M., Hourez, R., Aloy, E.M., Dewarrat, G., Gall, D., Weinmann, O., Gaudias, J., Bachmann, L.C., Schiffmann, S.N., Vogt, K.E., et al. (2013). Neuronal Nogo-A negatively regulates dendritic morphology and synaptic transmission in the cerebellum. Proc. Natl. Acad. Sci. U. S. A. *110*, 1083–1088.

Pilpel, Y., and Segal, M. (2004). Activation of PKC induces rapid morphological plasticity in dendrites of hippocampal neurons via Rac and Rho-dependent mechanisms. Eur. J. Neurosci. *19*, 3151–3164.

Plump, A.S., Erskine, L., Sabatier, C., Brose, K., Epstein, C.J., Goodman, C.S., Mason, C. a., and Tessier-Lavigne, M. (2002). Slit1 and Slit2 cooperate to prevent premature midline crossing of retinal axons in the mouse visual system. Neuron *33*, 219–232.

Pocklington, A.J., O'Donovan, M., and Owen, M.J. (2014). The synapse in schizophrenia. Eur. J. Neurosci. *39*, 1059–1067.

Poglia, L., Muller, D., and Nikonenko, I. (2011). Ultrastructural modifications of spine and synapse morphology by SAP97. Hippocampus *21*, 990–998.

Pollard, T.D., and Borisy, G.G. (2003). Cellular motility driven by assembly and disassembly of actin filaments. Cell *112*, 453–465.

Polleux, F., and Snider, W. (2010). Initiating and growing an axon. Cold Spring Harb. Perspect. Biol. *2*, a001925.

Polleux, F., Morrow, T., and Ghosh, a (2000). Semaphorin 3A is a chemoattractant for cortical apical dendrites. Nature *404*, 567–573.

Poulain, F.E., and Sobel, A. (2010). The microtubule network and neuronal morphogenesis: Dynamic and coordinated orchestration through multiple players. Mol. Cell. Neurosci. *43*, 15–32.

Puram, S. V, and Bonni, A. (2013). Cell-intrinsic drivers of dendrite morphogenesis. Development *140*, 4657–4671.

Purcell, S.M., Moran, J.L., Fromer, M., Ruderfer, D., Solovieff, N., Roussos, P., O'Dushlaine, C., Chambert, K., Bergen, S.E., Kähler, A., et al. (2014). A polygenic burden of rare disruptive mutations in schizophrenia. Nature *506*, 185–190.

Rakic, P. (1972). Mode of cell migration to the superficial layers of fetal monkey neocortex. J. Comp. Neurol. *145*, 61–83.

Redmond, L., Oh, S.R., Hicks, C., Weinmaster, G., and Ghosh, a (2000). Nuclear Notch1 signaling and the regulation of dendritic development. Nat. Neurosci. *3*, 30–40.

Redmond, L., Kashani, A.H., and Ghosh, A. (2002). Calcium regulation of dendritic growth via CaM kinase IV and CREB-mediated transcription. Neuron *34*, 999–1010.

Ronemus, M., Iossifov, I., Levy, D., and Wigler, M. (2014). The role of de novo mutations in the genetics of autism spectrum disorders. Nat. Rev. Genet. *15*, 133–141.

Rosário, M., Franke, R., Bednarski, C., and Birchmeier, W. (2007). The neurite outgrowth multiadaptor RhoGAP, NOMA-GAP, regulates neurite extension through SHP2 and Cdc42. J. Cell Biol. *178*, 503–516.

Rosário, M., Schuster, S., Jüttner, R., Parthasarathy, S., Tarabykin, V., and Birchmeier, W. (2012). Neocortical dendritic complexity is controlled during development by NOMA-GAP-dependent inhibition of Cdc42 and activation of cofilin. Genes Dev. *26*, 1743–1757.

Ruchhoeft, M.L., Ohnuma, S., McNeill, L., Holt, C.E., and Harris, W. a (1999). The neuronal architecture of Xenopus retinal ganglion cells is sculpted by rho-family GTPases in vivo. J. Neurosci. *19*, 8454–8463.

Rumbaugh, G., Sia, G.-M., Garner, C.C., and Huganir, R.L. (2003). Synapse-associated protein-97 isoform-specific regulation of surface AMPA receptors and synaptic function in cultured neurons. J. Neurosci. *23*, 4567–4576.

Ryan, T.J., and Grant, S.G.N. (2009). The origin and evolution of synapses. Nat. Rev. Neurosci. *10*, 701–712.

Sachs, G., Steger-Wuchse, D., Kryspin-Exner, I., Gur, R.C., and Katschnig, H. (2004). Facial recognition deficits and cognition in schizophrenia. Schizophr. Res. *68*, 27–35.

Sans, N., Petralia, R.S., Wang, Y.X., Blahos, J., Hell, J.W., and Wenthold, R.J. (2000). A developmental change in NMDA receptor-associated proteins at hippocampal synapses. J. Neurosci. *20*, 1260–1271.

Schiller, M.R. (2006). Coupling receptor tyrosine kinases to Rho GTPases-GEFs what's the link. Cell. Signal. *18*, 1834–1843.

Schlüter, O.M., Xu, W., and Malenka, R.C. (2006). Alternative N-Terminal Domains of PSD-95 and SAP97 Govern Activity-Dependent Regulation of Synaptic AMPA Receptor Function. Neuron *51*, 99–111.

Schmeisser, M.J., Ey, E., Wegener, S., Bockmann, J., Stempel, a V., Kuebler, A.,

Janssen, A., Udvardi, P.T., Shiban, E., Spilker, C., et al. (2012). Autistic-like behaviours and hyperactivity in mice lacking ProSAP1/Shank2. Nature *486*, 256–260.

Schnell, E., Sizemore, M., Karimzadegan, S., Chen, L., Bredt, D.S., and Nicoll, R. a (2002). Direct interactions between PSD-95 and stargazin control synaptic AMPA receptor number. Proc. Natl. Acad. Sci. U. S. A. *99*, 13902–13907.

Schuster, S., Rivalan, M., Strauss, U., Stoenica, L., Trimbuch, T., Rademacher, N., Parthasarathy, S., Lajkó, D., Rosenmund, C., Shoichet, S. a, et al. (2015). NOMA-GAP/ARHGAP33 regulates synapse development and autistic-like behavior in the mouse. Mol. Psychiatry 20**,** 1120-31.

Schwenk, J., Baehrens, D., Haupt, A., Bildl, W., Boudkkazi, S., Roeper, J., Fakler, B., and Schulte, U. (2014). Regional Diversity and Developmental Dynamics of the AMPA-Receptor Proteome in the Mammalian Brain. Neuron *84*, 41–54.

Scott, E.K., Reuter, J.E., and Luo, L. (2003). Small GTPase Cdc42 is required for multiple aspects of dendritic morphogenesis. J. Neurosci. *23*, 3118–3123.

Selemon, L.D., Rajkowska, G., and Goldman-Rakic, P.S. (1995). Abnormally high neuronal density in the schizophrenic cortex. A morphometric analysis of prefrontal area 9 and occipital area 17. Arch. Gen. Psychiatry *52*, 805–818; discussion 819–820.

Sestan, N., Artavanis-Tsakonas, S., and Rakic, P. (1999). Contact-dependent inhibition of cortical neurite growth mediated by notch signaling. Science *286*, 741–746.

Sharp, D.J., Yu, W., Ferhat, L., Kuriyama, R., Rueger, D.C., and Baas, P.W. (1997). Identification of a microtubule-associated motor protein essential for dendritic differentiation. J. Cell Biol. *138*, 833–843.

Shen, P.-C., Xu, D.-F., Liu, J.-W., Li, K., Lin, M., Wang, H.-T., Wang, R., and Zheng, J. (2011). TC10β/CDC42 GTPase activating protein is required for the growth of cortical neuron dendrites. Neuroscience *199*, 589–597.

Sheng, M., and Kim, E. (2011). The postsynaptic organization of synapses. Cold Spring Harb. Perspect. Biol. *3*.

Shi, Y., Pontrello, C.G., DeFea, K. a, Reichardt, L.F., and Ethell, I.M. (2009). Focal adhesion kinase acts downstream of EphB receptors to maintain mature dendritic spines by regulating cofilin activity. J. Neurosci. *29*, 8129–8142.

Shimada, A., Mason, C.A., and Morrison, M.E. (1998). TrkB Signaling Modulates Spine Density and Morphology Purkinje Cells. *18*, 8559–8570.

Sholl, D. a (1953). Dendritic organization in the neurons of the visual and motor cortices of the cat. J. Anat. *87*, 387–406.

Sigman, M., Spence, S.J., and Wang, A.T. (2006). Autism from developmental and neuropsychological perspectives. Annu. Rev. Clin. Psychol. *2*, 327–355.

Simkus, C.R.L., and Stricker, C. (2002). Properties of mEPSCs recorded in layer II neurones of rat barrel cortex. J. Physiol. *545*, 509–520.

Simó, S., and Cooper, J. a (2012). Regulation of dendritic branching by Cdc42 GAPs.

Genes Dev. *26*, 1653–1658.

Spacek, J., and Harris, K.M. (1997). Three-dimensional organization of smooth endoplasmic reticulum in hippocampal CA1 dendrites and dendritic spines of the immature and mature rat. J. Neurosci. *17*, 190–203.

Spruston, N. (2008). Pyramidal neurons: dendritic structure and synaptic integration. Nat. Rev. Neurosci. *9*, 206–221.

Srivastava, D.P., Woolfrey, K.M., Jones, K. a, Anderson, C.T., Smith, K.R., Russell, T. a, Lee, H., Yasvoina, M. V, Wokosin, D.L., Ozdinler, P.H., et al. (2012). An autism-associated variant of epac2 reveals a role for ras/epac2 signaling in controlling basal dendrite maintenance in mice. PLoS Biol. *10*, e1001350.

Stein, V., House, D.R.C., Bredt, D.S., and Nicoll, R. a (2003). Postsynaptic density-95 mimics and occludes hippocampal long-term potentiation and enhances long-term depression. J. Neurosci. *23*, 5503–5506.

Steiner, P., Higley, M.J., Xu, W., Czervionke, B.L., Malenka, R.C., and Sabatini, B.L. (2008). Destabilization of the Postsynaptic Density by PSD-95 Serine 73 Phosphorylation Inhibits Spine Growth and Synaptic Plasticity. Neuron *60*, 788–802.

Stern, E. a, Maravall, M., and Svoboda, K. (2001). Rapid development and plasticity of layer 2/3 maps in rat barrel cortex in vivo. Neuron *31*, 305–315.

Stone, J.L., O'Donovan, M.C., Gurling, H., Kirov, G.K., Blackwood, D.H.R., Corvin, A., Craddock, N.J., Gill, M., Hultman, C.M., Lichtenstein, P., et al. (2008). Rare chromosomal deletions and duplications increase risk of schizophrenia. Nature *455*, 237–241.

Südhof, T.C. (2008). Neuroligins and neurexins link synaptic function to cognitive disease. Nature *455*, 903–911.

Sugimura, K., Satoh, D., Estes, P., Crews, S., and Uemura, T. (2004). Development of morphological diversity of dendrites in Drosophila by the BTB-zinc finger protein abrupt. Neuron *43*, 809–822.

Sweet, E.S., Previtera, M.L., Fernández, J.R., Charych, E.I., Tseng, C.-Y., Kwon, M., Starovoytov, V., Zheng, J.Q., and Firestein, B.L. (2011). PSD-95 alters microtubule dynamics via an association with EB3. J. Neurosci. *31*, 1038–1047.

Tabuchi, K., Blundell, J., Etherton, M.R., Hammer, R.E., Liu, X., Powell, C.M., and Südhof, T.C. (2007). A neuroligin-3 mutation implicated in autism increases inhibitory synaptic transmission in mice. Science *318*, 71–76.

Tada, T., and Sheng, M. (2006). Molecular mechanisms of dendritic spine morphogenesis. Curr. Opin. Neurobiol. *16*, 95–101.

Tahirovic, S., and Bradke, F. (2009). Neuronal polarity. Cold Spring Harb. Perspect. Biol. *1*, 10623–10623.

Tan, H.Y., Callicott, J.H., and Weinberger, D.R. (2007). Dysfunctional and compensatory prefrontal cortical systems, genes and the pathogenesis of schizophrenia. Cereb. Cortex *17*.

Tanaka, J.-I., Horiike, Y., Matsuzaki, M., Miyazaki, T., Ellis-Davies, G.C.R., and Kasai, H. (2008). Protein synthesis and neurotrophin-dependent structural plasticity of single dendritic spines. Science *319*, 1683–1687.

Tang, G., Gudsnuk, K., Kuo, S.H., Cotrina, M.L., Rosoklija, G., Sosunov, A., Sonders, M.S., Kanter, E., Castagna, C., Yamamoto, A., et al. (2014). Loss of mTOR-Dependent Macroautophagy Causes Autistic-like Synaptic Pruning Deficits. Neuron *83*, 1–13.

Tashiro, A., Minden, A., and Yuste, R. (2000). Regulation of dendritic spine morphology by the rho family of small GTPases: antagonistic roles of Rac and Rho. Cereb. Cortex *10*, 927–938.

Threadgill, R., Bobb, K., and Ghosh, a (1997). Regulation of dendritic growth and remodeling by Rho, Rac, and Cdc42. Neuron *19*, 625–634.

Tønnesen, J., Katona, G., Rózsa, B., and Nägerl, U.V. (2014). Spine neck plasticity regulates compartmentalization of synapses. Nat. Neurosci. *17*, 678–685.

Toro, R., Konyukh, M., Delorme, R., Leblond, C., Chaste, P., Fauchereau, F., Coleman, M., Leboyer, M., Gillberg, C., and Bourgeron, T. (2010). Key role for gene dosage and synaptic homeostasis in autism spectrum disorders. Trends Genet. *26*, 363–372.

Trachtenberg, J.T., Chen, B.E., Knott, G.W., Feng, G., Sanes, J.R., Welker, E., and Svoboda, K. (2002). Long-term in vivo imaging of experience-dependent synaptic plasticity in adult cortex. Nature *420*, 788–794.

Tran, T.S., Rubio, M.E., Clem, R.L., Johnson, D., Case, L., Tessier-Lavigne, M., Huganir, R.L., Ginty, D.D., and Kolodkin, A.L. (2009). Secreted semaphorins control spine distribution and morphogenesis in the postnatal CNS. Nature *462*, 1065–1069.

Vadodaria, K.C., Brakebusch, C., Suter, U., and Jessberger, S. (2013). Stage-specific functions of the small Rho GTPases Cdc42 and Rac1 for adult hippocampal neurogenesis. J. Neurosci. *33*, 1179–1189.

Valiente, M., and Marín, O. (2010). Neuronal migration mechanisms in development and disease. Curr. Opin. Neurobiol. *20*, 68–78.

Waites, C.L., Craig, A.M., and Garner, C.C. (2005). Mechanisms of vertebrate synaptogenesis. Annu. Rev. Neurosci. *28*, 251–274.

Waites, C.L., Specht, C.G., Härtel, K., Leal-Ortiz, S., Genoux, D., Li, D., Drisdel, R.C., Jeyifous, O., Cheyne, J.E., Green, W.N., et al. (2009). Synaptic SAP97 isoforms regulate AMPA receptor dynamics and access to presynaptic glutamate. J. Neurosci. *29*, 4332–4345.

Walsh, T., McClellan, J.M., McCarthy, S.E., Addington, A.M., Pierce, S.B., Cooper, G.M., Nord, A.S., Kusenda, M., Malhotra, D., Bhandari, A., et al. (2008). Rare structural variants disrupt multiple genes in neurodevelopmental pathways in schizophrenia. Science *320*, 539–543.

Wenzel, A., Fritschy, J.M., Mohler, H., and Benke, D. (1997). NMDA receptor heterogeneity during postnatal development of the rat brain: differential expression of the NR2A, NR2B, and NR2C subunit proteins. J. Neurochem. *68*, 469–478.

Whitford, K.L., Dijkhuizen, P., Polleux, F., and Ghosh, A. (2002a). Molecular control of cortical dendrite development. Annu. Rev. Neurosci. *25*, 127–149.

Whitford, K.L., Marillat, V., Stein, E., Goodman, C.S., Tessier-Lavigne, M., Chédotal, A., and Ghosh, A. (2002b). Regulation of cortical dendrite development by Slit-Robo interactions. Neuron *33*, 47–61.

Wong, R.O.L., and Ghosh, A. (2002). Activity-dependent regulation of dendritic growth and patterning. Nat. Rev. Neurosci. *3*, 803–812.

Wu, G.Y., Zou, D.J., Rajan, I., and Cline, H. (1999). Dendritic Dynamics In Vivo Change during Neuronal Maturation. J. Neurosci. *19*, 4472–4483.

Xu, W. (2011). PSD-95-like membrane associated guanylate kinases (PSD-MAGUKs) and synaptic plasticity. Curr. Opin. Neurobiol. *21*, 306–312.

Xu, B., Roos, J.L., Levy, S., van Rensburg, E.J., Gogos, J.A., and Karayiorgou, M. (2008). Strong association of de novo copy number mutations with sporadic schizophrenia. Nat. Genet. *40*, 880–885.

Yang, N., Higuchi, O., Ohashi, K., Nagata, K., Wada, a, Kangawa, K., Nishida, E., and Mizuno, K. (1998). Cofilin phosphorylation by LIM-kinase 1 and its role in Rac-mediated actin reorganization. Nature *393*, 809–812.

Ye, B., Zhang, Y., Song, W., Younger, S.H., Jan, L.Y., and Jan, Y.N. (2007). Growing dendrites and axons differ in their reliance on the secretory pathway. Cell *130*, 717–729.

Yizhar, O., Fenno, L.E., Prigge, M., Schneider, F., Davidson, T.J., O'Shea, D.J., Sohal, V.S., Goshen, I., Finkelstein, J., Paz, J.T., et al. (2011). Neocortical excitation/inhibition balance in information processing and social dysfunction. Nature *477*, 171–178.

Yokota, Y., Eom, T.-Y., Stanco, A., Kim, W.-Y., Rao, S., Snider, W.D., and Anton, E.S. (2010). Cdc42 and Gsk3 modulate the dynamics of radial glial growth, inter-radial glial interactions and polarity in the developing cerebral cortex. Development *137*, 4101–4110.

Yoo, Y., Ho, H.J., Wang, C., and Guan, J.-L. (2010). Tyrosine phosphorylation of cofilin at Y68 by v-Src leads to its degradation through ubiquitin-proteasome pathway. Oncogene *29*, 263–272.

Yoshii, A., and Constantine-Paton, M. (2007). BDNF induces transport of PSD-95 to dendrites through PI3K-AKT signaling after NMDA receptor activation. Nat. Neurosci. *10*, 702–711.

Yoshii, A., Murata, Y., Kim, J., Zhang, C., Shokat, K.M., and Constantine-Paton, M. (2011). TrkB and protein kinase Mζ regulate synaptic localization of PSD-95 in developing cortex. J. Neurosci. *31*, 11894–11904.

Yu, W., Cook, C., Sauter, C., Kuriyama, R., Kaplan, P.L., and Baas, P.W. (2000). Depletion of a microtubule-associated motor protein induces the loss of dendritic identity. J. Neurosci. *20*, 5782–5791.

Yuste, R. (2011). Dendritic Spines and Distributed Circuits. Neuron *71*, 772–781.

Yuste, R., and Bonhoeffer, T. (2004). Genesis of dendritic spines: insights from ultrastructural and imaging studies. Nat. Rev. Neurosci. *5*, 24–34.

Yuzawa, S., Ogura, K., Horiuchi, M., Suzuki, N.N., Fujioka, Y., Kataoka, M., Sumimoto, H., and Inagaki, F. (2004). Solution structure of the tandem Src homology 3 domains of p47phox in an autoinhibited form. J. Biol. Chem. *279*, 29752–29760.

Zheng, C.-Y., Seabold, G.K., Horak, M., and Petralia, R.S. (2011). MAGUKs, Synaptic Development, and Synaptic Plasticity. Neurosci. *17*, 493–512.

Ziff, E.B. (2007). TARPs and the AMPA Receptor Trafficking Paradox. Neuron *53*, 627–633.

Zoghbi, H.Y., and Bear, M.F. (2012). Synaptic dysfunction in neurodevelopmental disorders associated with autism and intellectual disabilities. Cold Spring Harb. Perspect. Biol. *4*.

Statement of contribution

Stephanie Beyer and Pamela Engelbrecht provided extensive technical assistance with animal breeding and caring. Denis Lajkó, Doreen Lüdecke, Claudia Hille, Roman Wunderlich and the author performed genotyping of transgenic mice. René Jüttner performed all silverstainings by the Golgi method. Srinivas Parthasarathy performed all *in utero* electroporations. Technical assistance by Denis Lajkó, Doreen Lüdecke and Claudia Hille contributed to this work. Marta Rosario performed the representative western blot of figure 29.

Curriculum vitae

For privacy reasons the CV is not included in the online version of this dissertation.

Aus datenschutzrechtlichen Gründen ist der Lebenslauf in der Online-Version der Dissertation nicht enthalten.

Publications

Publications from the work presented in this thesis.

Rosário, M., Schuster, S., Jüttner, R., Parthasarathy, S., Tarabykin, V., and Birchmeier, W. (2012). Neocortical dendritic complexity is controlled during development by NOMA-GAP-dependent inhibition of Cdc42 and activation of cofilin. **Genes Dev.** *26*, 1743–1757.

Link: http://dx.doi.org/10.1101/gad.191593.112

Schuster, S., Rivalan, M., Strauss, U., Stoenica, L., Trimbuch, T., Rademacher, N., Parthasarathy, S., Lajkó, D., Rosenmund, C., Shoichet, S.A., Winter, Y., Tarabykin, V., and Rosário, M. (2015). NOMA-GAP/*ARHGAP33* regulates synapse development and autistic-like behavior in the mouse. **Mol. Psychiatry** 20**,** 1120-31

Link: http://dx.doi.org/10.1038/mp.2015.42

Eidesstattliche Versicherung

Hiermit versichere ich, Steffen Schuster, dass ich diese Doktorarbeit mit dem Titel „*Differential Regulation of Dendritic Structures by NOMA-GAP*“ selbständig und ohne fremde Hilfe verfasst und keine anderen als die angegebenen Hilfsmittel benutzt habe. Die Stellen der Arbeit, die dem Wortlaut oder dem Sinne nach anderen Werken entnommen wurden, sind unter Angabe der Quelle kenntlich gemacht.

Der experimentelle Teil dieser Arbeit wurde angefertigt unter der Betreuung durch Dr. Marta Rosário von Januar 2010 bis März 2015 am Institut für Zell- und Neurobiologie der Charité – Universitätsmedizin Berlin, Deutschland.

Acknowledgements

First of all, I would like to thank my supervisor Marta Rosario for sharing her knowledge and providing guidance through my PhD period. Thank you for sharing your love to science and power of endurance.

I would like to thank Prof. Stephan Sigrist for agreeing to be a reviewer of this thesis.

A big thank you to Denis Lajkó for his sacrificially endorsement during ups and down inside and outside the lab. This work would not have been possible without you.

I would like to thank all the former NOMA-GAP members, Doreen Lüdecke, Theresa Köbe and Claudia Hille for the nice working atmosphere and all the NOMA-GAP collaborators that helped to push this project forward, in particular Srinivas Parthasarathy for always had an open ear for me.

I also would like to gratitude to Jutta Schüler for advice on microscopy, Marni Pollrich for administrative assistance and all the members of the Institute of Cell and Neurobiology for providing me a delightful environment to work in.

Moreover, I would like to thank the committee for funding opportunities of the Charité - Universitätsmedizin Berlin and Victor Tarabykin for their financial support during my PhD.

Thanks to Axel, Ben, Benni, Boris, Chris, Christian, Elisa, Eva, Ingmar, Kai, Lucas, Marian, Mira, Nikola, Peter, Sascha, Smriti, Suse, Susi, Thomas, Toralf, Yehudit and all my other dear friends for all the fun time and support during dark times.

And lastly, Laura, thank you for your love and support during the last obstacles to finish my thesis.